Technische Universität Graz
Institute for Fundamentals and Theory in Electrical Engineering

NXP Semiconductors
Application and System Center Gratkorn

Diplomarbeit

Experimental and Theoretical Investigations on a Close Coupled RFID Document Tracking System

vorgelegt von:

Stefan Maier

Begutachter: Dipl.-Ing. Dr.techn., Ao.Univ.-Prof. Kurt Preis
Betreuer: Dipl.-Ing. Thomas Bauernfeind
Betreuer: Dr.-Ing. Alexey Nazarov

Graz, im September 2012

Contents

List of Figures

List of Tables

Kurzfassung

Diese Diplomarbeit beschäftigt sich mit der automatischen Erfassung von Dokumenten ('Document Tracking') mit Hilfe der Radio-Frequency-Identification Technologie (RFID). Es werden hierbei Systeme in den ISM-Frequenzbändern (Industrial, Scientific and Medical) des Hochfrequenz- (HF) und Ultrahochfrequenz-Bereichs (UHF) untersucht, wobei der verwendete Frequenzbereich als Unterscheidungskriterium herangezogen wird. Im ersten Schritt wird die Funktionalität kommerziell verfügbarer Systeme analysiert und die Grenzen ihrer Leistungsfähigkeit ausgelotet. In den jeweiligen Kapiteln wird dabei auf die verwendeten Messprinzipien und Aufbauten eingegangen. Das aus den Untersuchungen gewonnene Wissen bildet die Basis zum Aufbau eigener Systeme, wobei das Hauptaugenmerk auf die Antennen der passiven Transponder gelegt wird. Im Fokus der Untersuchungen stehen Kopplungseffekte zwischen den einzelnen Transpondern, da speziell bei Document-Tracking Anwendungen mit hohen Populationen und geringen Abständen zwischen den Transpondern zu rechnen ist. Für die Untersuchungen im HF-Bereich wird auf analytische Modelle zurückgegriffen, die UHF-Systeme werden hingegen mit Hilfe eines Finiten-Elemente Softwarepakets (HFSS) analysiert. Die aus den Analysen gewonnenen Erkenntnisse und grundlegende Design Prinzipien dienen letztlich der Realisierung einer UHF-Transponderantenne. Den Abschluss bilden umfangreiche Applikationstests, wobei die mit den entwickelten RFID-Tags erzielten Ergebnisse den Resultaten der kommerziell verfügbaren Systeme gegenübergestellt werden.

Abstract

The present diploma thesis deals with the automatic recognition of documents (Document Tracking) with the aid of Radio-Frequency-Identification technology (RFID). Systems operating in the High-Frequency (HF) and Ultra-High-Frequency domains (UHF) of the ISM (Industrial, Scientific and Medical) frequency bands are investigated whereby the operating frequency is used as distinguishing characteristics. In the first step, commercially available systems are analyzed in terms of their functionality and limitation of performance. In the specific chapters, the test setups and measurement principles used are described in detail. The knowledge gathered by the described investigations is used for the developement of in-house systems with the focus on the developement of antenna structures for the passive transponders. Here in particular on coupling effects between the passive transponder-tags, since, especially in document tracking applications, a big transponder population with small spacings between them are common. For the analyses of the HF-systems, analytic descriptions are used, whereas the investigations into the UHF-systems are carried out by means of a finite-element software tool (HFSS). The gathered knowledge as well as fundamental design principles are finally utilized to build a UHF-transponder antenna. At last, extensive tests in various applications using the developed transponders are carried out, and the gained results are compared to those of the commercial available systems.

Danksagung

Nach einer langen, schönen, anstrengenden, spannenden, nervigen und sehr lehrreichen Zeit ist nun der Punkt erreicht, an dem ich meine Diplomarbeit abgeschlossen habe. Es ist an der Zeit allen Personen die mich unterstützt haben, in fachlicher sowie in seelischer und finanzieller Hinsicht, gebührenden Dank auszusprechen.
Allen voran möchte ich Thomas Bauernfeind, meinem kompetenten und verständnisvollen Betreuer danken, der mich durch den RFID Dschungel begleitet hat und immer ein offenes Ohr für mich hatte. Zusätzlich erfuhr ich großartige Unterstützung vom gesamten Team des NXP Application and System Centers, insbesondere von Alexey Nazarov und Dariusz Mastela.
Mein Dank gilt aber auch meinen Eltern, die es mir möglich gemacht haben zu studieren, meiner Familie, meinen Freunden und vor allem meiner Freundin Mareike. Sie haben es verstanden, mich in schweren Zeiten zu motivieren und trotz etwaiger Unfreundlichkeiten meinerseits sind sie noch immer gut auf mich zu sprechen.

Eidesstattliche Erklärung

Ich erkläre an Eides statt, dass ich die vorliegende Arbeit selbstständig verfasst, andere als die angegebenen Quellen/Hilfsmittel nicht benutzt und die den benutzten Quellen wörtlich und inhaltlich entnommenen Stellen als solche kenntlich gemacht habe.

Statutory Declaration

I declare that I have authored this thesis independently, that I have not used other than the declared sources / resources and that I have explicitly marked all material which has been quoted either literally or by content from the used sources.

Graz, ...

1 Introduction

Automatic identification (Auto-ID) systems play a major role in different economic branches, such as retail, logistics, and production.
The main goal of Auto-ID systems is the allocation of information regarding different products and consumer items. To satisfy this growing market, various systems have been developed within the last years. The majority of the established systems are based on barcodes, bringing along the disadvantage of having low data storage and making it impossible to change the information on the item label. Radio Frequency Identification (RFID) systems are quickly approaching contactless ID-systems, able to replace barcode systems in a large number of applications. In the following, a short explanation of RFID systems is given.

1.1 Typical RFID system

The operating frequency used, allows one to distinguish between different types of RFID systems.

- High frequency (HF) systems operate at 13.56 MHz *(see chapter 3.2 for details)*
- Ultra High frequency systems (UHF) operate at 840-960 MHz *(see chapter 3.3 for details)*

Components of a RFID system:

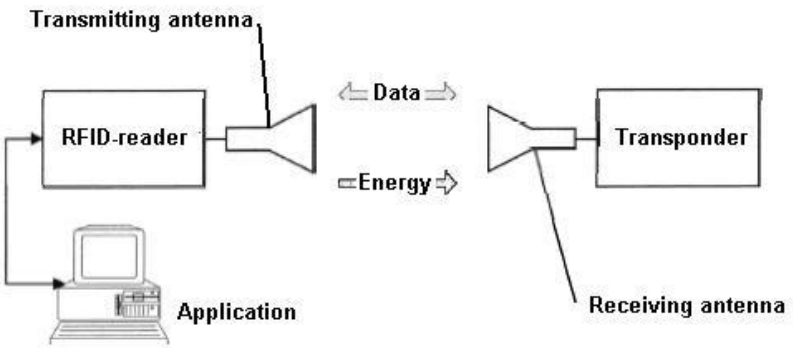

Figure 1.1: Principle of a RFID system [1]

- Reader: Contains a high frequency transmitting and receiving module. It controls the communication between transponder and its receiving unit using a transmitting protocol.
- Transmitting antenna: Represents the coupler to the transponder.
- Transponder: Consists of a coupler (receiving antenna) and an IC. Transmitting- and receiving antenna are coupled with each other using electromagnetic waves to accomplish communication between reader and transponder. The transponder is often called RFID label or RFID tag.
- Application: The reader is connected (Ethernet, USB) to a control system (PC) on which an application is running.

1.2 Motivation

RFID systems are mostly associated with the tagging of products like clothes or items. But what about documents? Large offices, hospitals, and government agencies store loads of documents in files and folders. Administration of these documents is very complex and expensive, as it is all done by handcraft. A connection between paper documents and existing electronic databases is especially time-consuming, as names or identification numbers have to be typed into a computer.
When using a RFID system all these processes can be simplified, as every document has its own RFID label and can be identified automatically.

The present diploma thesis analyzes available document tracking applications in terms of typical problems and performance. Utilizing this information own document tracking applications with the focus on label antennas have been developed. To classify the wide variety of different RFID systems, a differentiation concerning frequency regions has been done.

2 Used terms and expressions

Term	Description	Unit
$\vec{E}$	electric field intensity	$\frac{V}{m}$
$\vec{H}$	magnetic field intensity	$\frac{A}{m}$
$\vec{B}$	magnetic flux density	$T = \frac{Vs}{m^2}$
$\vec{D}$	electric flux density	$\frac{As}{m^2}$
$\vec{J}$	current density	$\frac{A}{m^2}$
ϵ_0	vacuum permittivity	$\approx 8.854 \times 10^{-12} \frac{As}{Vm}$
μ_0	vacuum permeability	$\approx 12.566 \times 10^{-7} \frac{Vs}{Am}$
L	inductance	$H = \frac{Vs}{A}$
M	mutual inductance	$H = \frac{Vs}{A}$
ψ	magnetic flux	$Wb = Vs$
ρ	charge density	$\frac{As}{m^3}$
λ	wavelength	m
c	speed of light	$\approx 3 \times 10^8 \frac{m}{s}$

Table 2.1: Used terms with description

3 RFID Theory

3.1 Electromagnetic Waves

The origin and propagation of electromagnetic waves can be described using MAXWELL's equations [2]:

1.
$$rot\vec{H} = \vec{J} + \frac{\partial \vec{D}}{\partial t}, \tag{3.1}$$

2.
$$rot\vec{E} = -\frac{\partial \vec{B}}{\partial t}, \tag{3.2}$$

3.
$$div\vec{B} = 0, \tag{3.3}$$

4.
$$div\vec{D} = \rho. \tag{3.4}$$

3.1.1 Calculation of the Magnetic Field Using the Magnetic Vector Potential

In the quasi-static consideration, the electrix flux density $\vec{D}$ from equation (3.1) is not taken into account. Due to this, the magnetizing effect of the displacement current $\frac{\partial \vec{D}}{\partial t}$ is neglected. On the other hand, the time variation of the magnetic flux density $\frac{\partial \vec{B}}{\partial t}$ from equation (3.2) will be taken into account. This quasi-static investigation holds for small antenna geometries compared to the wavelengths.

The Maxwell equations in the quasi-static magnetic case are [2]:

$$rot\vec{E} = -\frac{\partial \vec{B}}{\partial t}, \tag{3.5}$$

$$rot\vec{H} = \vec{J}, \tag{3.6}$$

$$div\vec{B} = 0, \tag{3.7}$$

$$\vec{B} = \mu\vec{H} \quad with \;\; \mu = \mu_0 \; \mu_r. \tag{3.8}$$

If μ is constant inside the problem domain, the following equation results from (3.6) and (3.8):

$$rot\vec{B} = \mu\vec{J}. \tag{3.9}$$

As $div\vec{B} = 0$, $\vec{B}$ can be determined by introducing the magnetic vector potential $\vec{A}$:

$$\vec{B} = rot\vec{A}. \tag{3.10}$$

Equation (3.9) and (3.10) lead to:

$$rotrot\vec{A} = \mu\vec{J}. \tag{3.11}$$

With the vector identity $rotrot\vec{A} = graddiv\vec{A} - \Delta\vec{A}$ and the assumption that $\vec{A}$ is free of sources ($\rightarrow \; div\vec{A} = 0$) (3.11) yields:

$$\begin{aligned} graddiv\vec{A} - \Delta\vec{A} &= \mu\vec{J}, \\ -\Delta\vec{A} &= \mu\vec{J}, \\ \Delta\vec{A} &= -\mu\vec{J}. \end{aligned} \tag{3.12}$$

A solution for (3.12), (3.13) can be found in literature [2]:

$$\vec{A} = \frac{\mu}{4\pi} \int\limits_V \frac{\vec{J}}{r} dV. \tag{3.13}$$

The calculation of the magnetic field in a linear conductor can be described by the following:

- In a linear conductor the cross section is small compared to the length. Due to this reason the volume element dV can be expressed as the product of the length element dl and the cross section Γ (with $\vec{J}$ expected to be homogenous):

$$\vec{A} = \frac{\mu}{4\pi} \oint_L \frac{J\Gamma}{r} d\vec{l} = \frac{\mu}{4\pi} I \oint_L \frac{d\vec{l}}{r}. \tag{3.14}$$

- When calculating the vector potential $\vec{A}$ with (3.14), the magnetic field $\vec{H}$ is given by [2]:

$$\vec{H} = \frac{\vec{B}}{\mu} = \frac{1}{\mu} rot\vec{A} = \frac{I}{4\pi} \oint_L rot\frac{d\vec{l}}{r}. \tag{3.15}$$

Equation 3.15 is the well-known law of Biot-Savart [2].

3.1.2 Solving the Maxwell Equations Introducing Retarded Potentials

Taking into account the displacement current $\frac{\partial \vec{D}}{\partial t}$ leads to the following Maxwell equations [2]:

$$rot\vec{H} = \vec{J} + \frac{\partial \vec{D}}{\partial t}, \tag{3.16}$$

$$rot\vec{E} = -\frac{\partial \vec{B}}{\partial t}, \tag{3.17}$$

$$div\vec{B} = 0, \tag{3.18}$$

$$div\vec{D} = \rho. \tag{3.19}$$

Again, $\vec{B}$ can be determined introducing the magnetic vector potential $\vec{A}$:

$$\vec{B} = rot\vec{A}. \tag{3.20}$$

This leads to:

$$\begin{aligned} rot\vec{E} = -\frac{\partial \vec{B}}{\partial t} = -\frac{\partial}{\partial t} rot\vec{A} = -rot\frac{\partial \vec{A}}{\partial t} \\ \rightarrow rot(\vec{E} + \frac{\partial \vec{A}}{\partial t}) = \vec{0}. \end{aligned} \tag{3.21}$$

The resulting vector $(\vec{E} + \frac{\partial \vec{A}}{\partial t})$ considers the change in time of the vector potential. As its rotation is equal to zero, it can be derived by a scalar potential (φ) and written as:

$$\vec{E} + \frac{\partial \vec{A}}{\partial t} = -grad\varphi$$

$$\rightarrow \vec{E} = -\frac{\partial \vec{A}}{\partial t} - grad\varphi. \tag{3.22}$$

As φ and $\vec{A}$ are functions of time, they can be used to determine $\vec{E}$ and $\vec{H}$. Using (3.1) together with (3.22) leads to:

$$rot\vec{H} = \frac{1}{\mu} = \frac{1}{\mu} rotrot\vec{A} = \vec{J} + \frac{\partial \vec{D}}{\partial t} = \vec{J} + \epsilon \frac{\partial \vec{E}}{\partial t}.$$

After inserting the vector identity ($rotrot\vec{A} = graddiv\vec{A} - \Delta\vec{A}$) results (3.23):

$$graddiv\vec{A} - \Delta\vec{A} = \vec{J} - \epsilon grad\frac{\partial \varphi}{\partial t} - \epsilon\mu\frac{\partial^2 \vec{A}}{\partial t^2}. \tag{3.23}$$

To have a complete definition of $\vec{A}$, its divergence has to be defined. As it can be defined arbitrarily, the Lorenz gauge [2] is used:

$$div\vec{A} + \epsilon\frac{\partial \varphi}{\partial t} = 0. \tag{3.24}$$

Inserting the divergence for $\vec{A}$ in (3.23) leads to the **inhomogenous wave equation**:

$$\Delta\vec{A} - \epsilon\mu\frac{\partial^2 \vec{A}}{\partial t^2} = -\mu\vec{J}. \tag{3.25}$$

Using (3.4) together with (3.24) leads to the equation for φ:

$$\Delta\varphi - \epsilon\mu\frac{\partial^2 \varphi}{\partial t^2} = -\frac{\rho}{\epsilon}. \tag{3.26}$$

With $\vec{J} = \vec{0}$ and $\rho = 0$, one can derive the homogenous wave equations:

$$\Delta\vec{A} - \epsilon\mu\frac{\partial^2 \vec{A}}{\partial t^2} = \vec{0} \;\; and \;\; \Delta\varphi - \epsilon\mu\frac{\partial^2 \varphi}{\partial t^2} = 0. \tag{3.27}$$

Considering an unbounded free space, [2] provides:

$$\vec{A}(x,y,z,t) = \frac{\mu}{4\pi}\int\limits_V \frac{\vec{J}(\xi,\eta,\zeta,t-\frac{r}{c})}{r} d\xi d\eta d\zeta, \tag{3.28}$$

and

$$\varphi(x,y,z,t) = \frac{1}{4\pi\epsilon}\int\limits_V \frac{\rho(\xi,\eta,\zeta,t-\frac{r}{c})}{r} d\xi d\eta d\zeta, \tag{3.29}$$

as solutions for (3.27).

Where (x, y, z) are the coordinates of the reference point P, (ξ, η, ζ) the coordinates of the source point Q, and r is the distance between P and Q.

3.1.3 Conclusion

What is the difference between the quasi-static calculation and the calculation with retarded potentials?

- Quasi-static case: The current density in a volume element (source point Q) is calculated at a reference point P. As a quasi-static consideration is used, variations in current density at point Q are treated as their effect will occur at the same time at point P. This fact can be used when exploring **HF-RFID** systems. Due to the fact that the coupling between reader and transponder occurs in the antennas near field, the propageted components of the electromagnetic wave are negligible. This allows the usage of the quasi-static consideration.
- When investigating **UHF-RFID** systems, the quasi-static considerations do not hold any more because UHF systems utilize electromagnetic waves and communicate via backscattered signals. As an electromagnetic wave in free space propagates with the speed of light (c), variations at the reference point need some time until they occur at another point in a distance (r). The term $\frac{r}{c}$ in (3.28) and (3.29) considers the time dependency.

3.2 HF RFID

3.2.1 Theory

HF-RFID systems operate at a frequency of 13.56 MHz and utilize the magnetic field in the antennas near field, as all these systems use inductive coupling. Due to this reason the reader and the transponder antennas are loops. Formulas used in this section can be found in [1] and [3]. With the magnetic flux ψ trough the loop, the inductance can be written as:

$$L = \frac{\psi}{I}. \tag{3.30}$$

For circular loops with given geometry, one gets:

$$L = N^2 \mu_0 R ln(\frac{2R}{D}), \tag{3.31}$$

where N is the number of coils, R the radius of the loop, and D the diameter of the conductor.

Assuming two loops (A1, A2)(see Fig. 3.1), some magnetic flux from A1 penetrates A2. This mutual flux assures the coupling between the loops and leads to the mutual inductance M. M can be defined analogically to the definition of L:

$$M_{21} = \frac{\psi_{21}}{I_1} = \oint_{A_2} \frac{\vec{B_{21}}}{I_1} \cdot \, d\vec{A_2}. \tag{3.32}$$

Due to symmetry reasons one can write:

$$M_{21} = M_{12} = M. \tag{3.33}$$

The mutual inductance provides information about coupling between electric circuits with the magnetic field as the transmission medium.

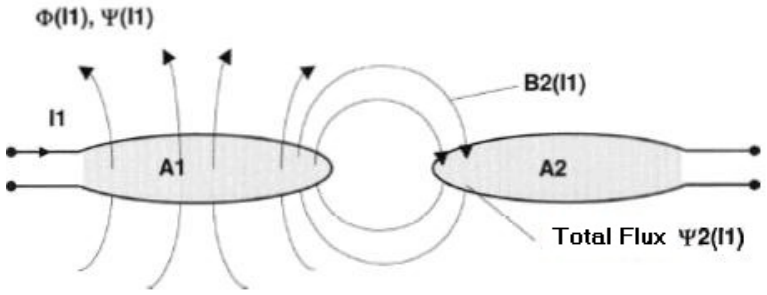

Figure 3.1: Coupling between 2 loops [1]

To get knowledge about the coupling of coils or loops without knowing the geometry, the coupling factor k has to be introduced:

$$k = \frac{M}{\sqrt{L_1 L_2}}. \tag{3.34}$$

3.2.2 Example HF-RFID System

Components of the document-tracking smart shelf HF-RFID system:

Reader antenna:	NXP ASC-loop antenna (prototype)
Reader:	Feig LR2000 [4]
Protocoll:	ISO15693 [5]
Matching:	Feig antenna tuning board [6]

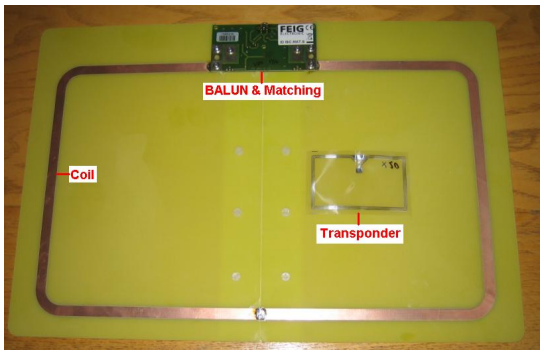

Figure 3.2: NXP loop antenna

Function:
The reader sends a signal containing a query command. A matching network prepares the signal for the transmitting reader antenna, because the antenna impedance has to be matched to the readers impedance (which is often 50Ω). The transponder antenna receives the transmitted signal and provides energy supply for the IC, which does the signal processing and applies all the information to the carrier signal using load modulation [1].

Signal Processing:
When the reader sends the query command, it expects an answer from the transponder. HF RFID ICs use load modulation for that purpose. The IC load modulator is triggered using a sub-carrier signal with frequencies 847k, 423k or 212kHz. Hence the spectrum gets an upper and a lower sideband which contain the information to transmit [1]. The reader demodulates one sideband, reclaims the baseband and with it the contained information.

3.3 UHF RFID

3.3.1 Theory

HF-RFID systems utilize inductive coupling and load modulation, whereas UHF systems show differences.
When a conductor loop produces a magnetic field beginning straight at the antenna, it converts continuously to an electromagnetic wave (due to Maxwell's law) [2].
The region surrounding the antenna where no wave propagation occurs is called the antennas NEAR-FIELD. The region from the point where the wave detaches from the antenna is called FAR-FIELD.

With the wavelength, $\lambda = \frac{c}{f}$, a boundary between near and far-field can be written as [3] :

$$r_F > 2\pi. \tag{3.35}$$

(3.35) is only valid for electrically short antennas.

Since UHF systems in general operate in the antenna's far-field region, they are also called BACKSCATTER systems.
A transmitted electromagnetic wave gets absorbed and reflected by any object in its propagation region. A part of the transmitted energy is going to be received by the transponder and gets reflected back to the reader. This backscattered part is used for data transmission between reader and transponder, as it is going to be modulated by the transponder's microchip.
The part of an electromagnetic wave that gets reflected by an object can be described using the radar-cross-section (RCS) σ [1].
When sending with a power of P_{EIRP} [1] , the radiant flux density at the transponder antenna can be written as [1]:

$$S = \frac{P_{EIRP}}{4\pi r^2}, \tag{3.36}$$

where r is the distance between sender and transponder.
The transponder antenna reflects a part of the transmitted energy. This reflected power is proportional to the received radiant flux density and the RCS [1]:

$$P_S = \sigma S. \tag{3.37}$$

When calculating the radiant flux density of the reflected wave, one can see that the radiated power of the reflected wave decreases with increasing distance from the source [1]:

$$S_{Back} = \frac{P_S}{4\pi r^2} = \frac{P_{EIRP}\ \sigma}{(4\pi)^2 r^4}. \tag{3.38}$$

[1] P_{EIRP}= Effective isotropically radiated power [7]

3.3.2 Example UHF-RFID System

- Reader [8]:

Figure 3.3: Sirit Infinity 510 UHF-reader

The reader is the head unit of any RFID system and can run up to four antennas with an internal multiplexer. It sends the modulated wave to the antenna as well as receives the backscattered signal and does the demodulation. Ethernet and USB ports are the most common choice for connecting the reader to a network or a computer.

- Transponder [9]:

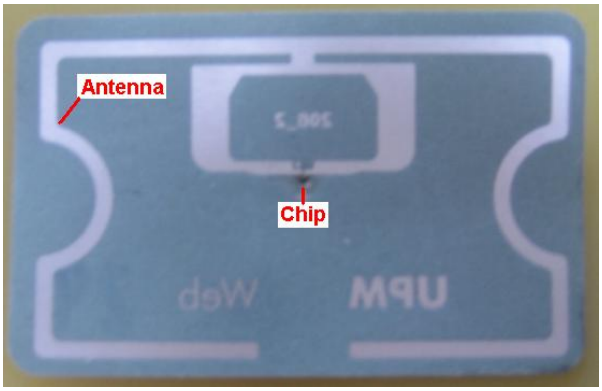

Figure 3.4: WebX label

Antenna and IC have to be matched in a conjugated and complex way to assure good energy transmission [1]. The transponder antenna receives the modulated UHF signal and provides energy for the IC to wake up. After receiving the query command, the IC modulates the answer on the UHF signal and sends it back to the reader via the transponder antenna (principle of backscattered signal).

- Reader antenna [10]:

Figure 3.5: Poynting patch antenna

The reader antenna transmits the query signal, as well as receives the transponder's answer and sends it to the reader unit.

Product	...	Poynting RFID patch antenna (Patch-A0025) [10]
Frequency range	...	860 MHz - 960 MHz
Gain	...	6.5 dBi (+-0.5 dBi)
Polarization	...	Circular

- Protocol Standard [11]:

The EPCglobal Class 1 Gen2 standard (=Class 1 Generation 2 UHF Air Interface Protocol Standard) defines the requirements for a passiv backscatter RFID system which operates in the UHF region.

4 Document Tracking Using HF Region

4.1 HF Stacking Theory

In a document tracking application, it is necessary to read multiple labels, located in the field of the reader antenna. Such an application forces label distances of 1 mm and less as they are placed on documents or similar material. Close coupling between label antennas leads to detuning and makes them difficult to read. As an example the resonance frequency could shifts outside the 13.56 MHz region. To understand and predict one of these close coupling effects (frequency shift), a mathematical analysis based on [12] has been done.

As introduced in previous chapter 3.2.1, the mutual inductance and the coupling factor can be written as:

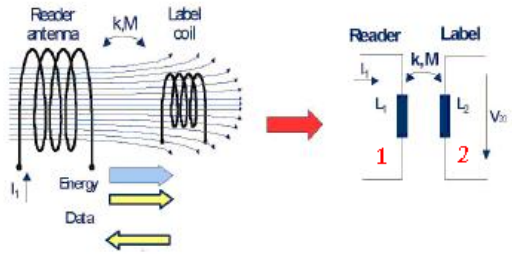

$$M_{21} = \frac{\psi_{21}}{I_1} = \oint_{A_2} \frac{\vec{B_{21}}}{I_1} \cdot d\vec{A_2}, \quad (4.1)$$

$$k = \frac{M}{\sqrt{L_1 L_2}}, \quad (4.2)$$

Figure 4.1: HF coupling system [12]

where (A_1, L_1) refer to the reader coil and (A_2, L_2) refer to the transponder coil.

Using (4.1) and (4.2), the coupling can be described as a loose coupled transformer. The connection between the loops is given by the magnetic field and can be described by previously defined values M and k.

4.1.1 Equivalent Electrical Circuit Model

To enable mathematical modeling, an equivalent electrical circuit for the label (antenna and IC) is necessary.

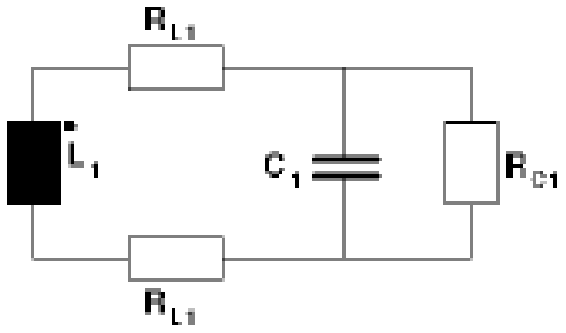

Figure 4.2: Equivalent electrical model of an inlet [12]

Where R_{L1} is the parasitic resistance, L_1 the coil inductance, R_{C1} the IC-impedance, and C_1 the IC-capacitance as well as the parasitic capacitance.

This circuit is a resonant system which is, in the optimal case, tuned to 13.56 MHz. In the resonant case, voltage for powering the IC is induced. The following calculations are simplified, as only the inductive coupling is taken into consideration. This is due to the fact that the coupling between the antennas is given by the magnetic field, thus coupling is mainly inductive.

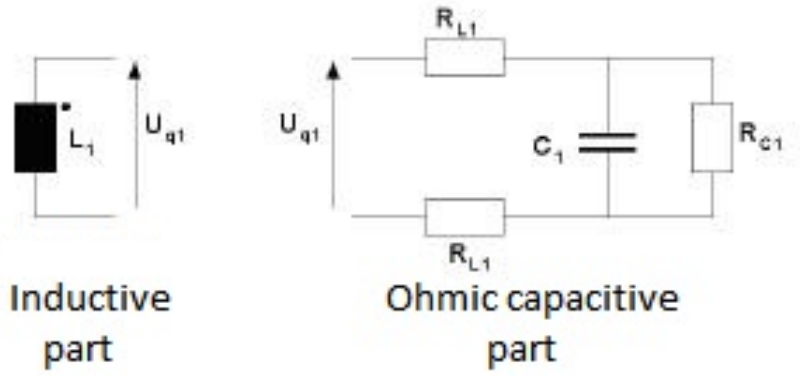

Figure 4.3: Inductive and ohmic/capacitive parts of an inlet model [12]

4.1.2 Model with Multiple Labels in the Field

Having multiple labels in the field results in more complex coupling because also the mutual inductances between the labels have to be taken into account.

Fig. 4.4 represents a system with one driver coil and two labels:

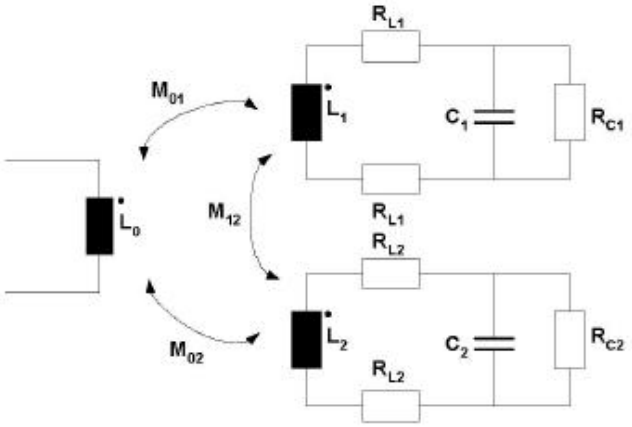

Figure 4.4: Model of a driver coil and two labels [12]

To determine the induced voltage (U_1 and U_2) in the label antennas, a common four-pole principle is used to understand the system. The Z-matrix approach (4.3) describes the common four-pole in Fig. 4.5.

$$\begin{Bmatrix} \underline{U}_0 \\ \underline{U}_1 \end{Bmatrix} = \begin{bmatrix} \underline{Z}_{00} & \underline{Z}_{01} \\ \underline{Z}_{10} & \underline{Z}_{11} \end{bmatrix} \begin{Bmatrix} \underline{I}_0 \\ \underline{I}_1 \end{Bmatrix} \tag{4.3}$$

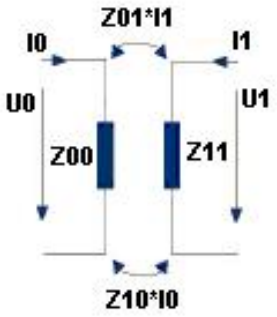

Figure 4.5: Four-pole principle

A system of one driver coil and two labels (Fig. 4.4) can be described by (4.4).

$$\begin{Bmatrix} \underline{U}_0 \\ \underline{U}_1 \\ \underline{U}_2 \end{Bmatrix} = \begin{bmatrix} \underline{Z}_{00} & \underline{Z}_{01} & \underline{Z}_{02} \\ \underline{Z}_{10} & \underline{Z}_{11} & \underline{Z}_{12} \\ \underline{Z}_{20} & \underline{Z}_{21} & \underline{Z}_{22} \end{bmatrix} \begin{Bmatrix} \underline{I}_0 \\ \underline{I}_1 \\ \underline{I}_2 \end{Bmatrix} \tag{4.4}$$

As only the induced voltages (U_1 & U_2) are of interest, the system of equations reduces to:

$$\begin{Bmatrix} \underline{U}_1 \\ \underline{U}_2 \end{Bmatrix} = \begin{bmatrix} \underline{Z}_{10} & \underline{Z}_{11} & \underline{Z}_{12} \\ \underline{Z}_{20} & \underline{Z}_{21} & \underline{Z}_{22} \end{bmatrix} \begin{Bmatrix} \underline{I}_0 \\ \underline{I}_1 \\ \underline{I}_2 \end{Bmatrix}, \tag{4.5}$$

$$\underline{U}_1 = \underline{Z}_{10}\underline{I}_0 + \underline{Z}_{11}\underline{I}_1 + \underline{Z}_{12}I_2, \tag{4.6}$$

$$\underline{U}_2 = \underline{Z}_{20}\underline{I}_0 + \underline{Z}_{21}\underline{I}_1 + \underline{Z}_{22}I_2. \tag{4.7}$$

Because the coupling is simplified and considers only the inductive parts, impedances can be replaced with inductances and mutual inductances:

$$\underline{Z}_{XX} = j\omega L_{XX} \quad and \quad \underline{Z}_{XY} = j\omega M_{XY}.$$

The equation part with I_0, which refers to the driver coil, is seperated and written as an extra term:

$$\begin{Bmatrix} \underline{U}_1 \\ \underline{U}_2 \end{Bmatrix} = j\omega \begin{bmatrix} L_1 & M_{12} \\ M_{21} & L_2 \end{bmatrix} \begin{Bmatrix} \underline{I}_1 \\ \underline{I}_2 \end{Bmatrix} + j\omega \begin{Bmatrix} M_{01} \\ M_{02} \end{Bmatrix} \underline{I}_0. \tag{4.8}$$

In the general case for n labels this can be written as:

$$\{\underline{U}\} = j\omega[\mathbf{A}]\{\underline{I}\} + j\omega\{B\}\underline{I}_0, \tag{4.9}$$

where:

$$\{\underline{U}\} = \begin{Bmatrix} \underline{U}_1 \\ \vdots \\ \underline{U}_n \end{Bmatrix} \quad and \quad \{B\} = \begin{Bmatrix} M_{01} \\ \vdots \\ M_{0n} \end{Bmatrix} \quad and \quad \{\underline{I}\} = \begin{Bmatrix} \underline{I}_1 \\ \vdots \\ \underline{I}_n \end{Bmatrix} \quad and$$

$$[\mathbf{A}] = \begin{bmatrix} L_1 & \dots & M_{1n} \\ \vdots & \ddots & \vdots \\ M_{n1} & \dots & L_n \end{bmatrix} \; with \; M_{1n} = M_{n1}. \tag{4.10}$$

Matrix [**A**] contains inductances (L_{XX}) and mutual inductances (M_{XY}). Therefore it can be predefined that [**A**] is symmetric and positive semi-definite because $M_{XY} = M_{YX}$. Due to this fact the most important properties of [**A**] are:

- The sum of eigenvalues equals the trace of the matrix. This leads to:

$$\sum_{i=1}^{n} \lambda_i = \sum_{i=1}^{n} L_i. \tag{4.11}$$

- When using (4.2) with a coupling factor $k = 1$, only one eigenvalue is equal to a nonzero value. As all the other eigenvalues are equal to zero, one can write:

$$\lambda_i = \sum_{i=1}^{n} L_i. \tag{4.12}$$

- Using (4.11) and (4.12), it can be seen that the eigenvalues are proportional to the inductance L and therefore to the resulting resonance frequency:

$$f_{res,i} = \frac{1}{2\pi\sqrt{\lambda_i C}}. \tag{4.13}$$

To prove previous theory of eigenvalue decomposition, an example for **two coupled** transponders is given.

Resonance frequency of the isolated transponder: $f_{res} \approx 25\ MHz$
Capacitance of the transponder: $C = 2\ pF$
Inductance of the transponder: $L = 20\ \mu H$

- $k = 0 \rightarrow$ No coupling at all between the transponders
  - Using (4.2): $M_{XY} = k * \sqrt{L_X L_Y} = k * L \rightarrow M_{12} = 0$
  - Matrix $[\mathbf{A}] = \begin{bmatrix} 0.00002 & 0 \\ 0 & 0.00002 \end{bmatrix}$
  - Eigenvalues $\lambda_1 = \lambda_2 = 0.00002$
  - Using (4.13): $f_{res} = 25.16\ MHz$

  Conclusion: As $k = 0$ there is no coupling between the transponders $\rightarrow$ no resonance shift $\rightarrow$ no detuning
- $k = 0,5 \rightarrow$ Transponders couple with each other
  - Using (4.2): $M_{XY} = k * \sqrt{L_X L_Y} = k * L \rightarrow M_{12} = 10\mu H$
  - Matrix $[\mathbf{A}] = \begin{bmatrix} 0.00002 & 0.00001 \\ 0.00001 & 0.00002 \end{bmatrix}$
  - Eigenvalues $\lambda_1 = 0.00001\ and\ \lambda_2 = 0.00003$
  - Using (4.13): $f_{res1} = 35.59\ MHz\ and\ f_{res2} = 20.55\ MHz$

Conclusion: Coupling leads to detuning as it can be seen when looking at the resonance frequencies f_{res1} and f_{res2}. One resonance shifts upwards to higher values, the other one towards lower values. The lower resonance peak shifts to lower values with a smaller gradient than the higher resonance moves towards higher values. Due to this fact, the lower resonance stays longer near the 13.56 MHz region and therefore is more important for the coupling to the reader antenna. In consequence of this conclusion, it is important to know the lower resonance frequency for prediction of stacking behaviour.

- $k = 1 \rightarrow$ WORST CASE, theoretical total coupling between the transponders
  - Using (4.2): $M_{XY} = k * \sqrt{L_X L_Y} = k * L \rightarrow M_{12} = 20\ \mu H$
  - Matrix $[\mathbf{A}] = \begin{bmatrix} 0.00002 & 0.00002 \\ 0.00002 & 0.00002 \end{bmatrix}$
  - Eigenvalues $\lambda_1 = 0\ and\ \lambda_2 = 0.00004$
  - Using (4.13): $f_{res1} = towards\ infinity\ and\ f_{res2} = 17.79\ MHz$
  - Conclusion: As one eigenvalue equals zero, the higher resonance strives towards infinity. The dominant lower value describes the worst possible detuning scenario.

- Following Fig. 4.6 shows the resonance trends of two coupled labels with a coupling factor sweep from $k = 0.1$ to $k = 0.99$.

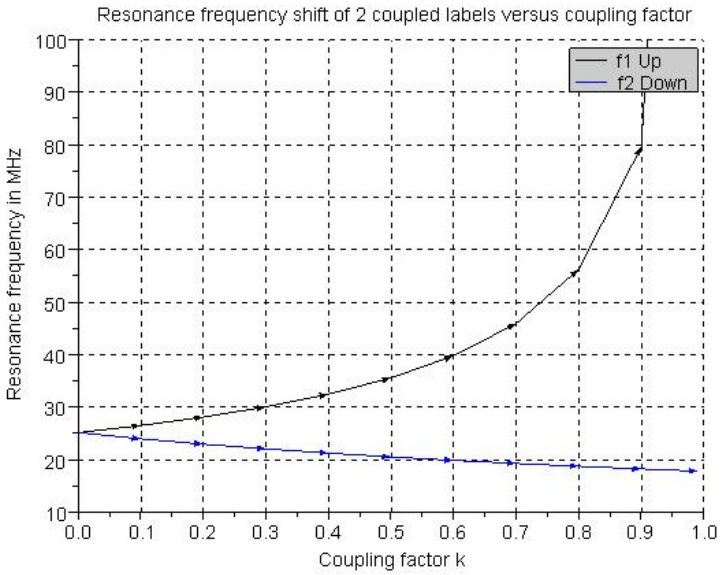

Figure 4.6: Resonance frequencies versus a coupling factor sweep

Conclusion: The theory of eigenvalue decomposition provides a strong tool for predicting the stacking behaviour of transponders. For an arbitrary number of labels, the leading resonance frequency for different stacking scenarios (coupling factors) can easily be calculated.

Calculation with a Coupling Factor Sweep

- Calculation:

  Coupling factor: k=0.1 - 0.9
  Label amount: 1-30 labels

Fig. 4.7 shows the calculated detuning for an increased stack size from 1 to 30 labels with a coupling factor variation from 0.1 to 0.9:

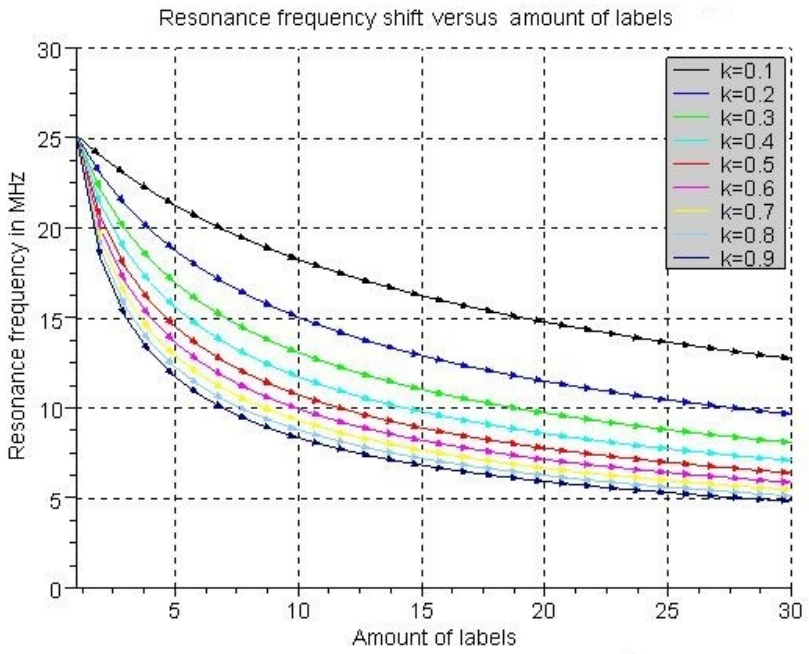

Figure 4.7: Resonance shift with increasing label amount, and coupling factor variation

The stronger the coupling between the transponders, the more detuning occurs. Hence the resonance frequency drops with a higher negative gradient to lower values at higher coupling factors. Especially label amounts up to 10 show big differences between different k-values. Higher label amounts lead to nearly constant offset values between the curves.

4.2 HF applications

A smart shelf and a document tray have been developed by NXP's team of the Application and System Center in order to cover a wide range of different document tracking use cases. The investigations deal with NXP-developed systems and with systems from a competitor company called Magellan [13]. In the following the components (reader, antenna, label) of the used document tracking solutions will be explained.

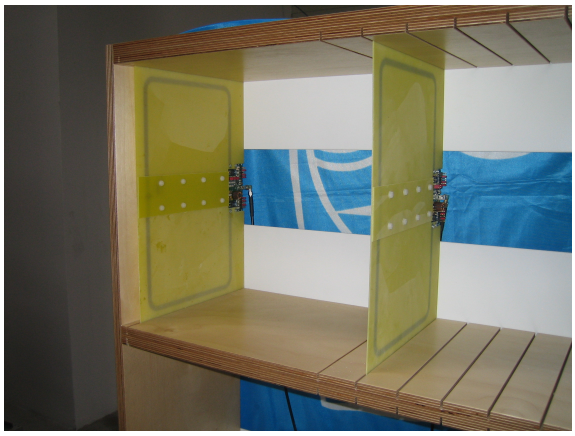

Figure 4.8: Smart shelf with NXP antennas

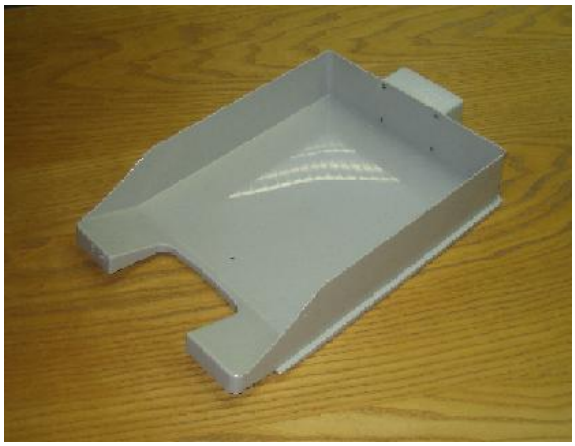

Figure 4.9: NXP document tray

- **HF smart shelf (Fig. 4.8):** Two antennas with variable distance to each other are used to read documents placed between the antennas. A multiplexer provides reader access for multiple antennas. After sending the query command, information concerning the sheets placed in the shelf can be extracted and used.
  Using the smart shelf shortens the time-consuming process of searching through loads of documents.
- **HF document tray (Fig. 4.9):**

  The document tray is placed on a desk as a tray for paper sheets, files, folders, and similar material. Not only single sheets, but stacks of documents can be placed in the tray and read simultaneously for inventory purposes.

4.2.1 Magellan's HF RFID System

Magellan [13] introduces two systems for document tracking purposes. Their operating frequencies are in the 13.56 MHz region, and they use the same transponder. Typical HF-RFID systems use amplitude shift keying [1] for the load modulation, whereas Magellan's RFID solutions utilize phase jitter modulation (PJM) [14] for that purpose.

Magellan PJM label [13]

Figure 4.10: Magellan PJM label

The first type comprising the so-called document tracking tag is shown in Fig. 4.10. The antenna of this tag has a 76 $mm \times 45$ mm format and consists of two-and-one-half turns. Being designed for extreme densely stacked tags populations, it has a high resonance frequency in the isolated mode (where no coupling between the tags occurs). The resonance frequency of the tag was determined with $f_{res} = 55$ MHz.

Magellan Mars24 [15]

Mars24 is a multi antenna-reader system.

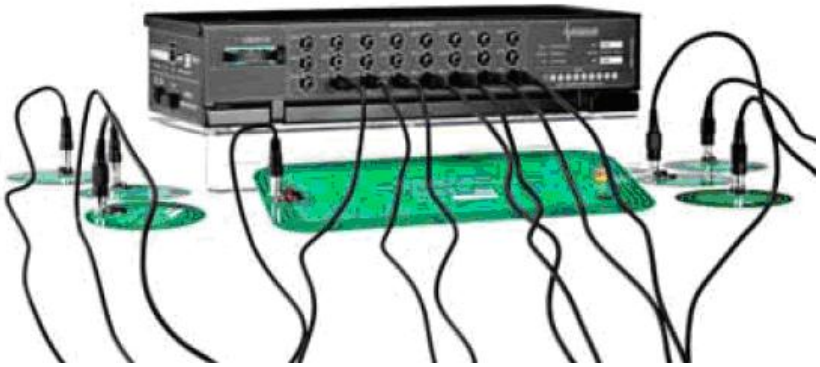

Figure 4.11: Magellan Mars24 system

Multiple antennas can be attached to the reader. As Magellan offers different reader antennas, the Mars24 system can be used for different applications. For the document tracking application, the loop antenna described in the following was selected and used together with the Mars system in the smart shelf application.

Magellan single-axis reader antenna [16]

- Antenna geometry: 202 $mm \times 352$ mm inner antenna coil

Figure 4.12: Magellan reader antenna

Figure 4.12 shows the antenna used for the HF smart shelf application.

Magellan's HF document tray [17]

With the document tray Magellan provides a stand-alone application for document tracking purposes. It is a tray for sheets with an implemented antenna and an implemented reader module. Via USB interface, the device can be attached to a computer running Magellan's software. The needlessness of external devices makes this plug & play device to a good document tracking desk solution.

Figure 4.13: Magellan document tray

4.2.2 NXP's HF RFID System

A multifunctional loop antenna and a tray for desk applications have been developed [1] to cover the same document tracking use cases as Magellan. Additionally the best fitting label for document tracking applications has been chosen.

NXP HF-label

- Standard: ISO 15693 [5]
- Format: 76 $mm \times 45$ mm
- NXP I-Code SLI IC [18]

Figure 4.14: NXP-SLI HF label

This label was the base for further investigations regarding the close coupling behavior of HF transponder antennas.

Multifunctional reader antenna

- Reader: A Feig LR 2000 reader [4] was used for testing all the developed applications. Due to the fact that this reader provides only one antenna port, an external multiplexer (Feig 8 Channel Multiplexer [19]) was used for applications with multiple antennas (smart shelf).

- Antenna:

  Antenna geometry: 205 $mm \times 350$ mm inner antenna coil

[1] Devlopement has been done by NXP's Application and System Center team.

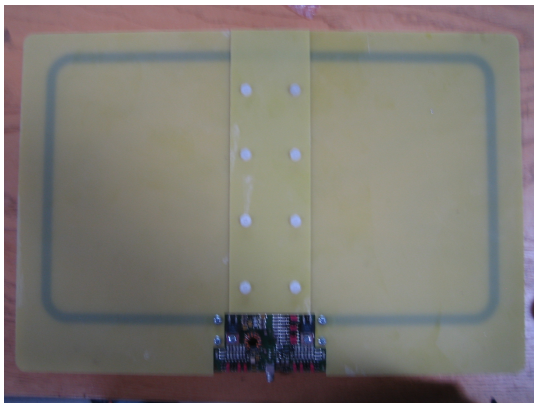

Figure 4.15: NXP multifunctional loop antenna

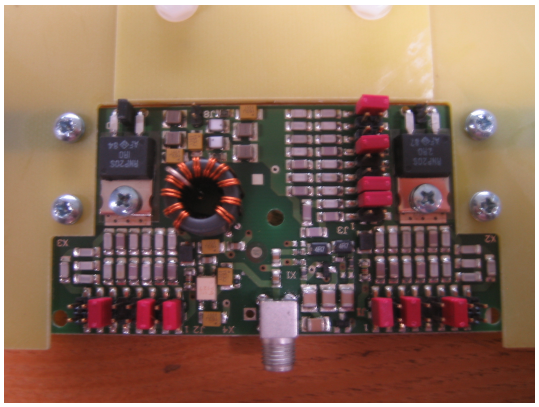

Figure 4.16: Feig matching circuit

This antenna was developed with nearly the same geometry as Magellan's antennas for the Mars system to get comparable results when measuring and testing. It has one coil with the previously described geometry and a Feig antenna tuning board (Feig OBID i-scan HF Tuning Board [6]). This Feig circuit is the matching network and assures impedance matching between reader and antenna.

NXP's HF document tray

A paper tray for a desk was extended with a loop antenna on the bottom side (see Fig. 4.9). Because there's no reader implemented, the Feig LR2000 was used again. The implemented antenna tuning board (Feig HF Tuning Board [6]) assures the matching between reader and antenna.

4.3 HF Antenna Characterization

When building up a new RFID system, as well as analyzing an available one, it is important to know the antenna's main attributes.

- How does the field look ?
- Where is the optimal label placement?
- How many antennas do I need?
- Where should the antennas be located?

To cover these questions, all used antennas have been analyzed in terms of their field power and distribution.

4.3.1 Measurement

To determine the antenna's field strength, the antenna to investigate was driven as the transmitting antenna, and the receiving antenna was a loop probe. The transmitting antenna was fed with a signal of constant power and frequency. With a robotic arm, the loop probe has been moved to scan the device under test along three axes while recording the signal power at every defined point along the axes (3-dimensional).

Measurement setup:

- Spectrum analyzer: Rhode & Schwarz [20]
- Probe: ETS Lindgren 7405 H-field probe [21]
- Scan: 3 directions (x,y,z axis)
- Transmitted signal: contineous wave @ f=13.56 MHz
- Movement: 3 axis roboter

Devices under test:

- NXP loop antenna for HF smart shelf
- Magellan Mars24 loop antenna
- NXP document tray
- Magellan document tray

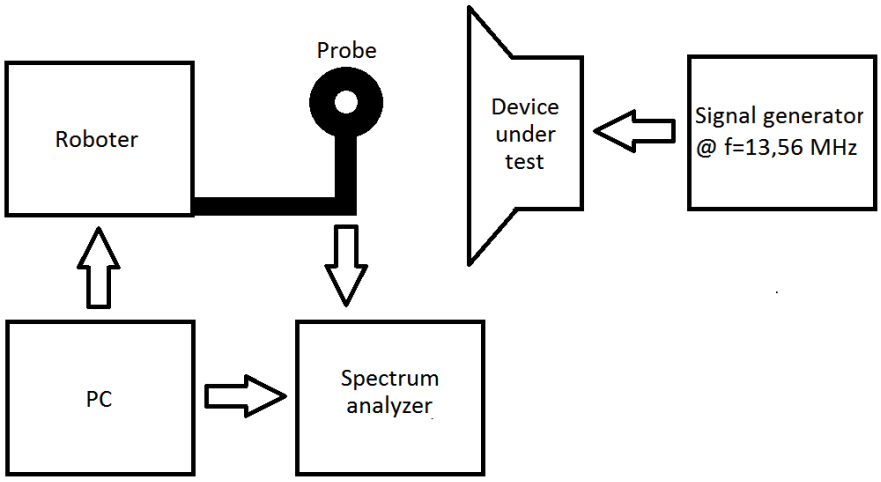

Figure 4.17: Measurement principle (block diagram) for antenna field measurements

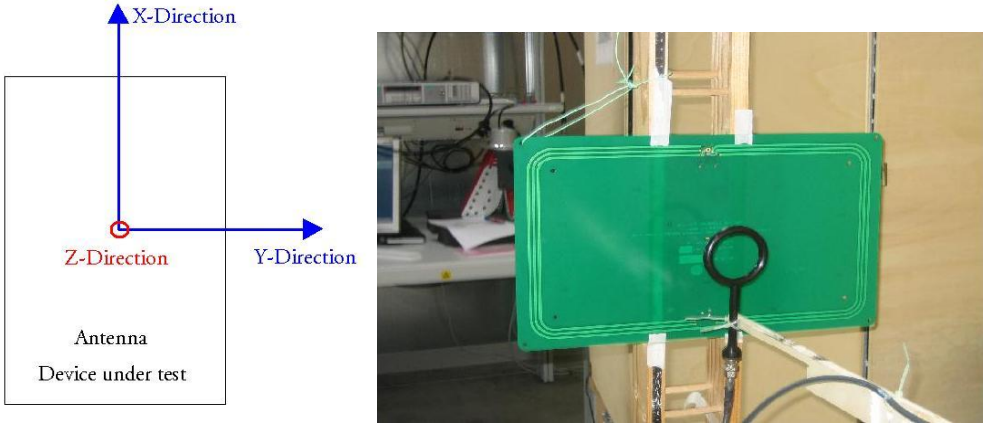

Figure 4.18: Measurement setup for antenna field measurements

All stands and holding devices are out of wood material to avoid reflections and eddy currents. Fig. 4.19 to 4.24 depict power in dBm versus distance in mm. To calculate the magnetic field intensity in $\frac{A}{m}$, one has to use the antenna performance factor of the probe [21].

4.3.2 Results

Loop antennas

Fig. 4.19 to 4.21 compare Magellan's antenna and NXP's loop antenna along 3 directions (axes).

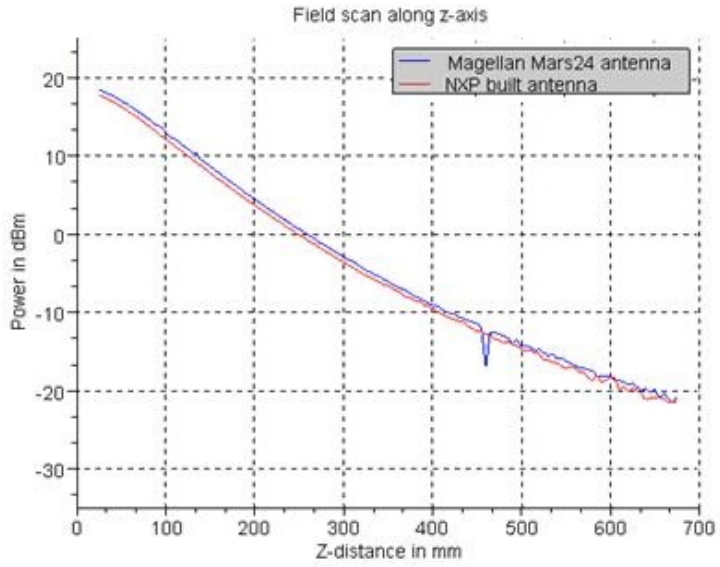

Figure 4.19: Field power along z-axis ($x = y = 0\ cm$)

Nearly similar field-power and distribution along all axes can be observed between Magellan Mars and the NXP system (Fig. 4.19-4.21). This was expected because their geometries are similar. Regarding x- and y-axis scan, the best label position can be predicted in the middle of the antennas.

The field power scan along the z-axis provides information about the labels read range, which is an important fact when building an application. In the case of our smart shelf, the antennas are arranged face to face (see Fig.4.22). The antennas distance to each other should be chosen in a way that the minimum field intensity in the middle delivers enough power to read a label.

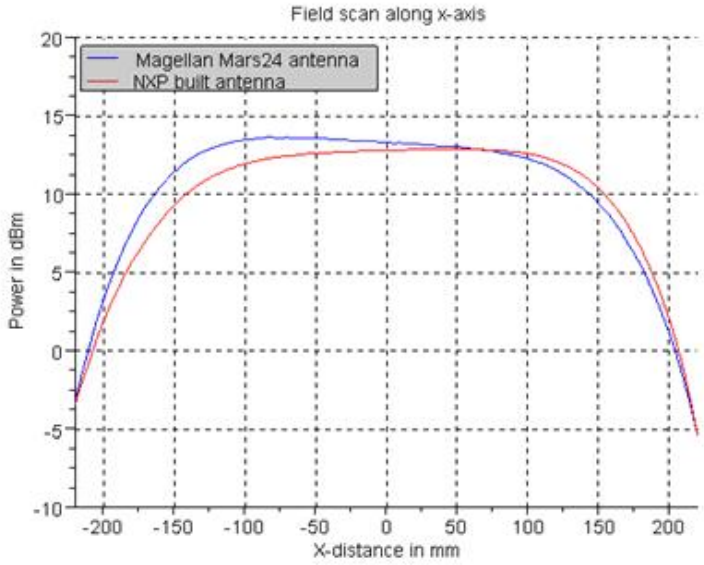

Figure 4.20: Field power along x-axis ($y = 0\ cm \quad z = 9\ cm$)

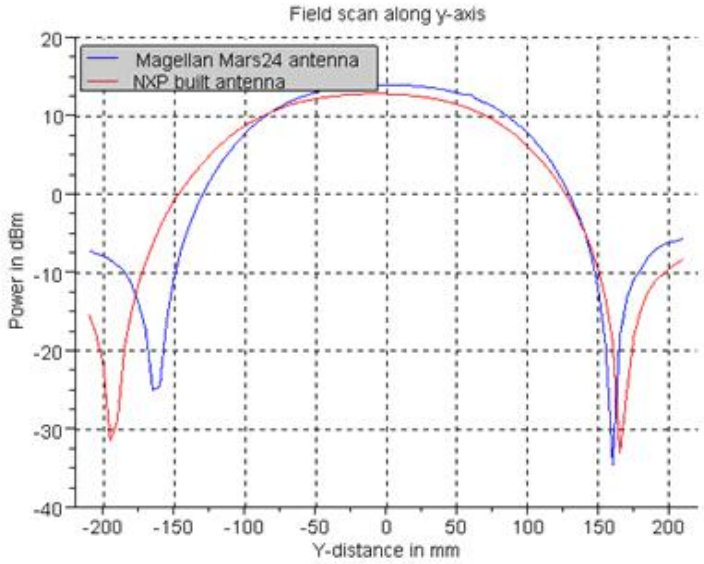

Figure 4.21: Field power along y-axis ($x = 0\ cm \quad z = 9\ cm$)

Figure 4.22 shows the expected field power in the middle of two NXP antennas with a distance of 40 cm to each other. Field power values have been determined using the z-axis scan.

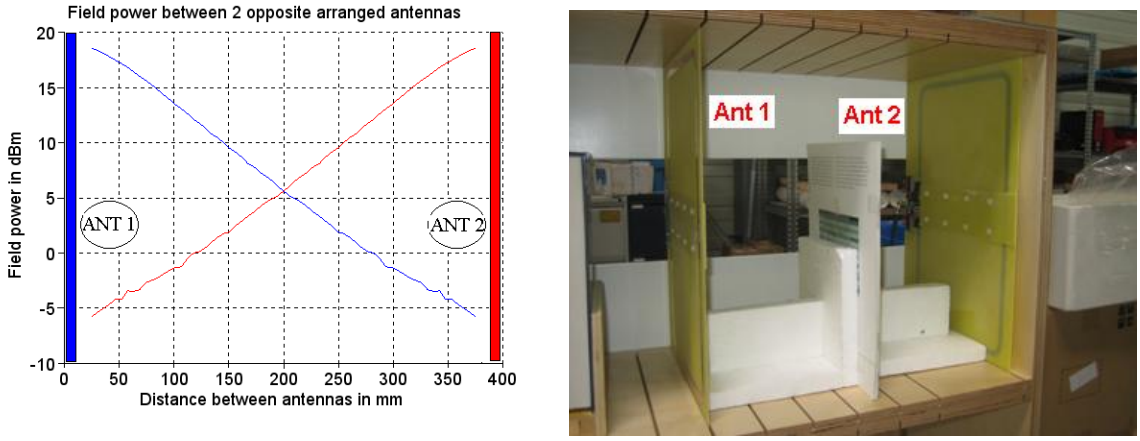

Figure 4.22: Expected field power in the middle of 2 smart shelf antennas

Document trays

Fig. 4.23-4.24 compare NXP's document tray and Magellans's document tray in terms of their field distribution and strength.

All power values are normalized. This was done because Magellan's document tray is a system with an embedded reader module, without the option to control the radiated power to the same level as used by the NXP tray. Therefore the normalization allows a comparison with different absolute power values between the systems.

Both systems show similar decreasing field power along the z-axis. When analyzing the x-axis scan, an asymmetric curve can be seen at the Magellan tray. This leads to the conclusion that the best label position when using the Magellan tray is in the rear part of the tray. NXP's system shows the best performance when the labels are placed in the middle of the tray.

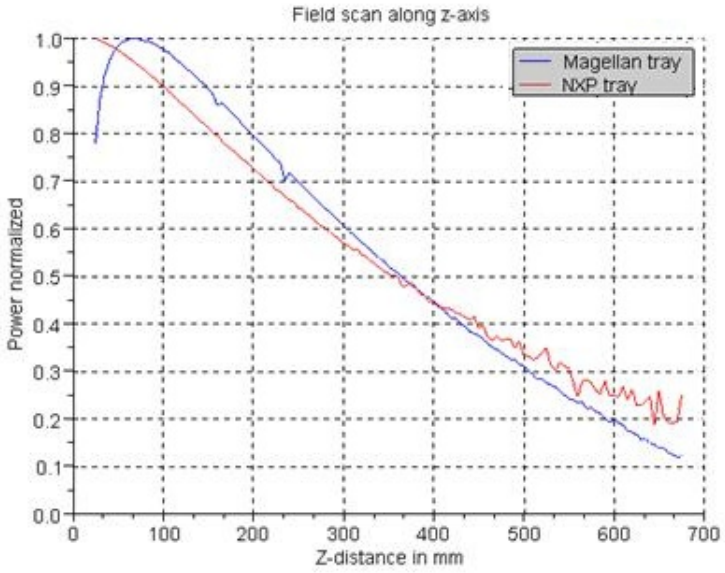

Figure 4.23: Field power along z-axis ($x = y = 0\ cm$)

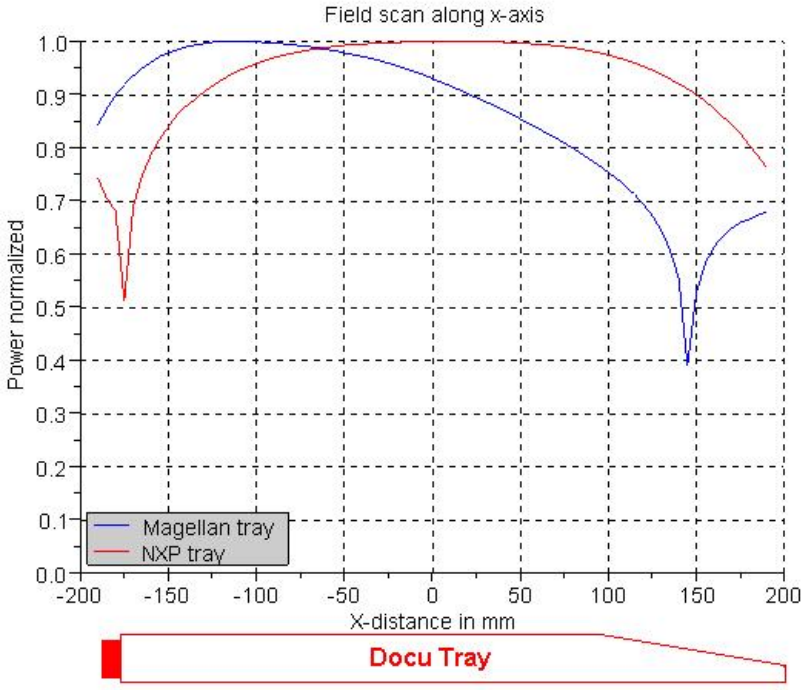

Figure 4.24: Field power along x-axis ($y = 0\ cm \quad z = 9\ cm$)

4.4 Stack Measurements

The previous mathematical approach states that label's resonance frequencies shift to lower values when they are arranged in close distances to each other. Measurements can validate this theory and are done in the following. The resonance frequencies of the stacked labels were measured using a network analyzer with a loop antenna used as a probe (Fig. 4.25). The label amount in the stack was increased successively with a spacing of 1 mm between the single tags. Material with an air-like dielectric constant was used as a spacer between them.

- Measurement:

  Label spacing: 1mm with $\epsilon_r = 1.00059$
  Label amount: 1-30 labels
  Probe: ETS Lindgren 7405 probe [21]
  Device: Agilent 8753ES network analyzer [22]

  The important, performance-influencing lower resonance value has been stored.

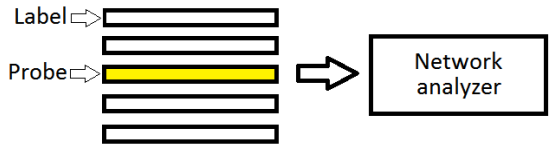

Figure 4.25: Measurement setup: f_{res} of HF labels

Fig. 4.27 shows the labels resonance frequencies versus the number of labels in the measured stack. The red line in the picture depicts the operating frequency of 13.56 MHz to illustrate the optimal operating frequency of an HF-RFID system. As predicted, increasing label amounts lead to decreasing resonance frequencies. Beginning with a single tag tuned to 25 MHz results in reaching the optimum operating frequency at a stack size of 6 tags. Adding additional labels to the stack will lead to a non-working RFID system as the label's resonances decrease.

Fig. 4.26 shows the measured curve compared to a curve, calculated with a k-value of 0.5 (see Fig. 4.7). This leads to the assumption that the transponders in the measured stack couple with a factor of 0.5, because the curves are similar and match with each other. Using this method of comparison allows the determination of unknown coupling factors occuring at real-world applications. Above all, the measurement provides a proof for the calculated detuning prediction.

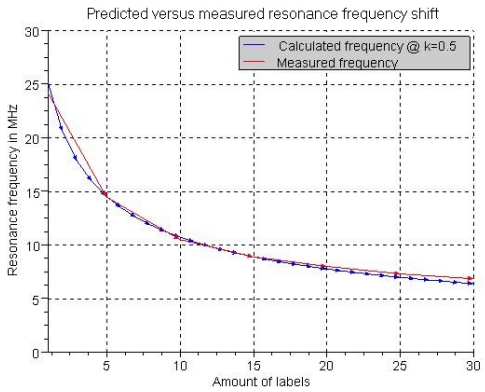

Figure 4.26: Calculated versus measured f_{res} detuning

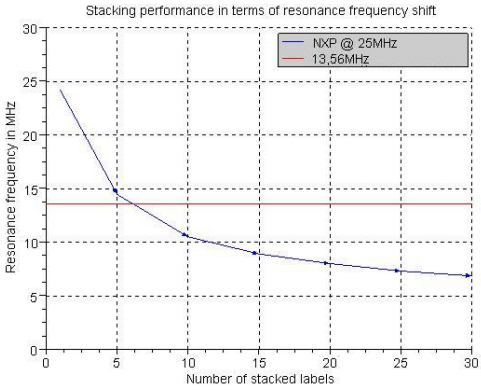

Figure 4.27: Resonance frequency versus label amount in a stack

A solution for shifting the optimal operating region to higher label amounts is a single label tuned to even higher resonance frequencies. This approach was investigated with labels tuned to 40 MHz and 50 MHz isolated resonance. Additionally Magellan's document tracking label was analyzed in terms of its stacking behavior. Fig. 4.28 illustrates the NXP labels with 40 MHz (NXP40) and 50 MHz (NXP50) resonance as well as Magellan's label in comparison.

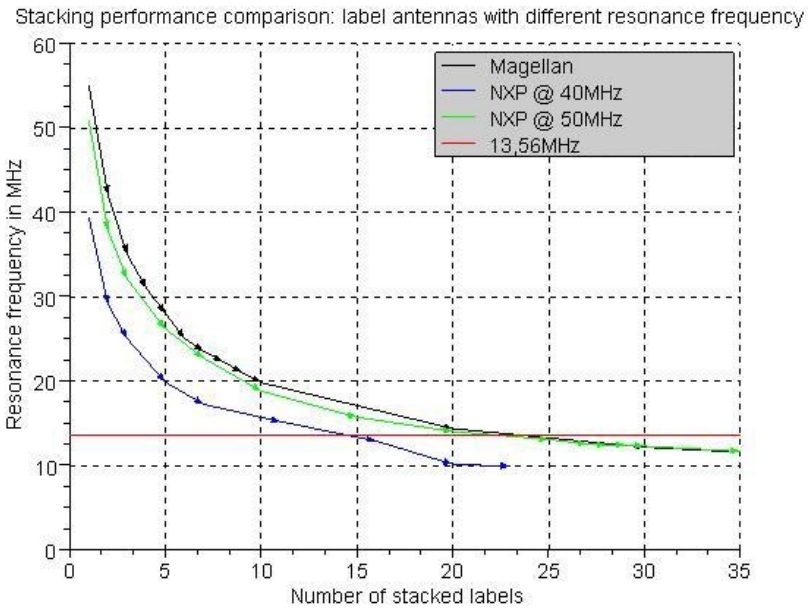

Figure 4.28: Resonance frequencies versus number of labels in the stack

Analyzing the curves in Fig. 4.28 leads to the conclusion that the resonance frequency curves do not have a constant gradient. The decrease becomes smaller at higher label amounts which means that a kind of saturation occurs. The aim of a good label for close coupling purposes is having the saturation area, where the curves are flat, near the 13.56 MHz area to get good performance at high label amounts. As the Magellan PJM label and the NXP50 label show nearly the same behaviour and cross the red line at an amount of 23 labels, good performance in stacking mode can be predicted.

Attention has to be paid to the single label's resonance frequencies also, as the system has to provide good performance, even when dealing with single labels. It is important to find a good trade-off between performance in single and in stacked mode.

A good approach to evaluate the performance of labels is measuring their read range values. The measurement has been carried out by NXP for the NXP40, the NXP50, as well as the Magellan PJM labels and is shown in Fig. 4.29.

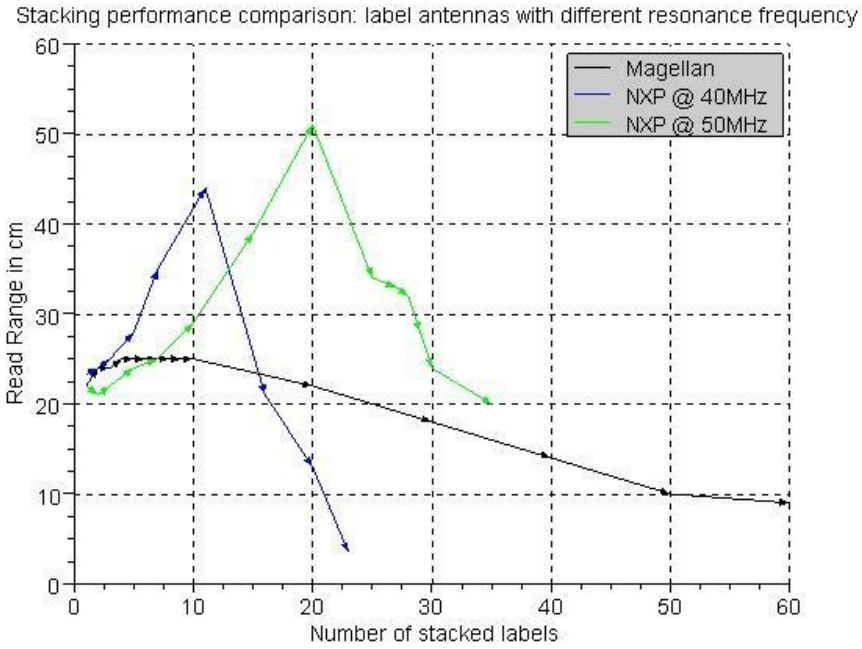

Figure 4.29: Read range distances versus number of labels in the stack (comparison)

NXP50 and PJM have shown similar behavior when comparing the curves in Fig. 4.28. Though a big difference can be observed at Fig. 4.29. NXP's labels show sharp peaks in comparison to the PJM label, which shows an overall flat curve. Sharp peaks occur when the label resonance meets the optimal operating frequency and has been designed with a high Q-value.
The NXP labels have overwhelming sensitivity in the resonance region, but a high negative gradient outside this region. This means that the performance decays fast outside

resonance. In a comparative view, Magellan's labels perform well over a wide range, but not as well as NXP's in resonance case.
Tuning a single NXP label to 50 MHz and higher may result in reaching resonance at a higher amount of labels, but for the price of reduced read ranges when operating with single labels.
The green curve stops at an amount of 35 labels because the maximum amount of testing samples was reached. Nevertheless, a forecast of approximately 40-45 read labels when using the NXP50 label in an application can be made.

4.4.1 Conclusions

- Labels' resonance frequencies shift to lower values when operating in stacked mode.
- No constant resonance decreasing → flat curve areas allow keeping resonance frequencies around region of interest (13.56MHz), even in stacked mode.
- Single labels can be tuned for stacking purposes, but there is always a trade-off between performance in single mode and stacked mode, as high single resonances lead to good stacking performance, but to bad single performance.
- NXP50 and PJM cross the red line in figure 4.28 at an amount of 23 labels. The read range graph proves good performance even with higher label amounts.
  - PJM: 10 cm read range @ 50 labels
  - NXP50: 10 cm read range @ $\approx$ 45 labels

4.5 HF Application Tests

In order to prove the predicted results from chapter 4.4, application tests with all the HF-RFID document tracking systems have been done. Analyzed systems:

- NXP smart self system
- NXP document tray
- Magellan Mars24 system
- Magellan document tray

In order to cover a wide range of different applications, the tests were executed with the labels placed on materials with different thickness.

Materials:

- Paper sheet: 0.1 mm thickness
- Flyer sheet: 0.24 mm thickness

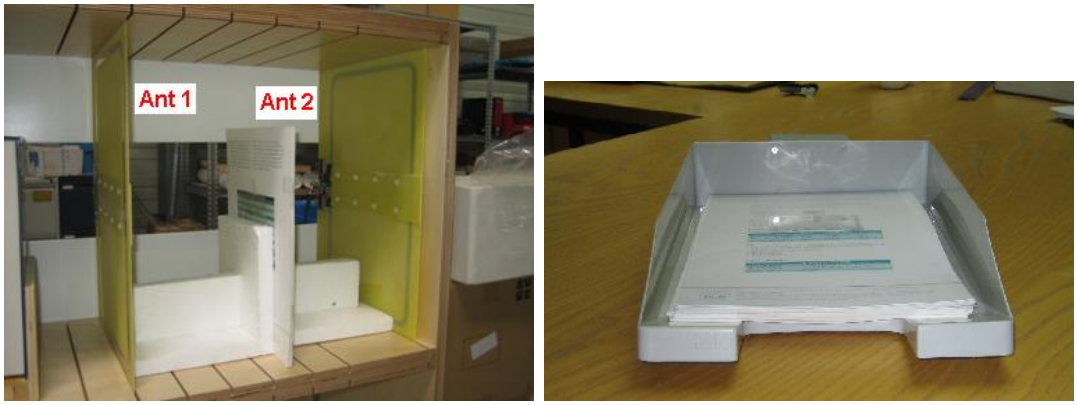

Figure 4.30: Smart shelf and document tray under application conditions

Fig. 4.30 shows the NXP document tray and the smart shelf with a stack of flyer sheets inside. This demonstrates the way the application tests were executed. As the amount of labels in the stack increased successively, read rates gave information about how many labels could be read.

A read rate of 100% means that all the labels in the stack could be read. Fig. 4.31 shows the maximum amount of labels in the stack where it was possible to reach 100% read rate. Increasing the label amount to a size bigger than shown in Fig. 4.31 leads to read rates smaller than 100%, thus not all the documents can be read by the system.

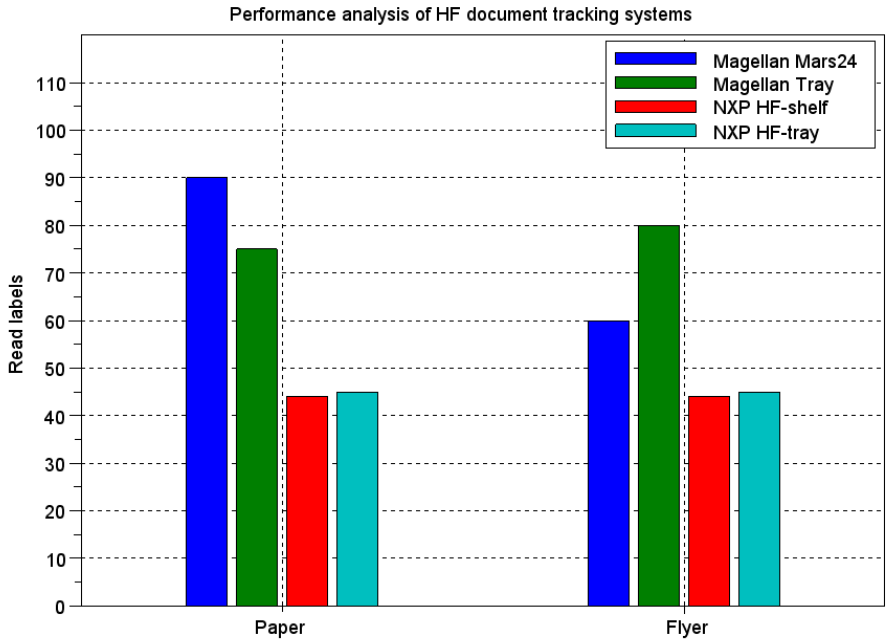

Figure 4.31: Application test results

One can see in Fig. 4.31 that NXP's shelf as well as the document tray show similar performance. Both systems show an upper limit of about 45 stacked labels as predicted in chapter 4.4. Varying material thickness (paper, flyer) leads to the same results, thus the NXP systems are not sensitive to a changed coupling factor as a result of different label spacings ($\Delta = 0.14mm$). When analyzing the Magellan Mars24 system, it can be seen that bigger label spacings lead to decreasing performance (paper: 90 labels upper limit; flyer: 60 labels upper limit). On the other hand, Magellan's tray increases its performance with bigger label spacing. Varying label spacing leads to a changed coupling factor which influences the detuning of labels.

As one can see, Magellan's systems show an overall better performance than NXP's systems when dealing with stacked transponders. This can be explained when looking at Fig.4.29 from the previous section. Magellan's design has a low Q-factor (antenna and IC), which means that the IC needs more energy to wake up in resonance case, but the slope outside resonance has a small gradient. This leads to more bandwidth and therefore better performance when dealing with stacked and detuned transponder antennas. Another difference between Magellan and NXP is the used modulation type. NXP uses amplitude shift keying (ASK) [1], whereas Magellan uses phase jitter modulation (PJM) [1]. PJM may offer some advantages over ASK in terms of spectral efficiencies, but the detection of a small phase shift also needs a more complex process followed by a higher current consumption.

Additionally, Magellan's document tray uses different power modes for optimizing its stacking performance. These power modes may be needed because too much energy may otherwise be extracted from the magnetic field by inactive transponders. Magellan describes the power modes in a whitepaper about PJM as follows [23]:
StackTags operate in two power states, a normal power state and a low power state where the tags draw only the lowest possible current. Tags move randomly but deliberately between the normal and low power states so that at any time the majority of the tags are in the low power state. This further eliminates the normal problems associated with parasitic coupling between the antennas of closely stacked tags and also provides the benefits of time division multiplexed operation with the added major advantage of frequency division.

Selling the Magellan document tray as a complete and 'closed' system provides advantages compared to a system composed of independent components (reader, antenna, software,...), because every part of the system can be optimized for the specific application (eg.: Low-Q IC, optimized for document tracking).

5 Document Tracking Using UHF Region

5.1 UHF Applications

UHF document tracking applications cover the same use cases as the HF applications discussed in chapter 4.

5.1.1 Readpoints

UHF smart shelf

The following commercial available smart shelf (Fig 5.1) concept can be used for tagged documents. The shelves material is metal, which is not used for UHF RFID applications in general. The simple slot antenna concept makes metal the material of choice and allows cost competitive solutions. The shelf consists of 5 racks, each with 5 antennas. That means that 5 slots are milled out of the metal back plane, each excited by a microstrip structure.

- Reader: Sirit Infinity 510 [8]
- Multiplexer: SkyeTek SkyePlus MXU 8-port multiplexer [24]
- Antenna: Milled slot with exciting structure (refer to section 5.2.2)

A UHF RFID reader works as the head unit and powers the slot antennas. As there are 25 slot antennas, a multiplexer is needed to supply the whole shelf with just one reader unit. Because the multiplexer powers only one slot at a time, there is no interference problem between the single slots.

Figure 5.1: UHF smart shelf

UHF patch system

To cover the use case of a desk application, a patch antenna was used to investigate the behaviour of a label stack in a document tray.

- Reader: Sirit Infinity 510 [8]
- Antenna: Feig patch antenna [25]

Figure 5.2: UHF system with a patch antenna

5.1.2 Labels

Previously described read points are one part of a good performing document tracking application. Especially when dealing with scenarios with close coupling transponders, the choice of a good label is an important, performance-influencing point. Two commercial available labels were used for testing under document tracking conditions. These measurements provided knowledge about UHF label behaviour in close coupled testing scenarios and were used as a base for the developement of a good performing document tracking UHF label.

WebX [9]

- Optimized for **fashion** application
- Aluminium antenna with directly assembled IC

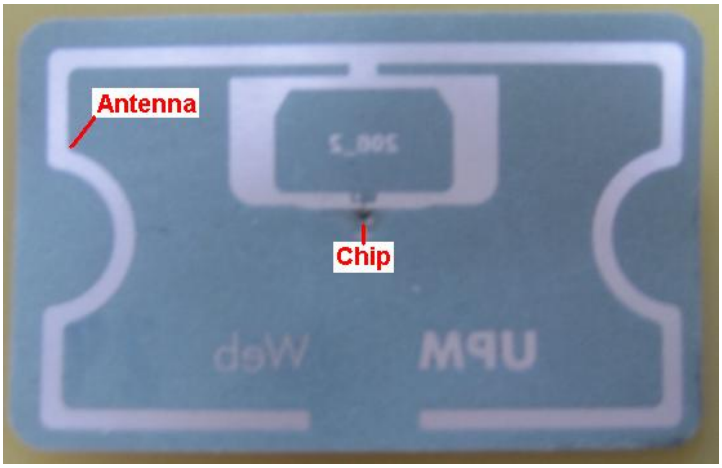

Figure 5.3: WebX label

Tagsys DocTrak [26]

- Optimized for **document tracking** application
- Aluminium antenna with a loop glued on it. The IC is directly assembled on the glued loop.

The label uses inductive coupling between the loop with the IC and the dipole antenna. This means that there is no galvanic contact between them.
The loop including the IC is sold seperately by Tagsys, as this provides a variable and

cheap solution because various autonomous label antennas can be designed and produced detached from the loop.

Figure 5.4: Tagsys DocTrak label and its loop with the IC

As Tagsys sells the DocTrak label as a label optimized for document tracking applications, its results from the performance tests were used as a reference for the newly developed document tracking label (see section 6).

5.2 UHF Smart Shelf

The UHF smart shelf readpoint was introduced in chapter 5.1.1. In the following, the shelves concept is explained and adequate theory introduced. In section 5.2.2 measurements regarding the electromagnetic field are illustrated and explained.

5.2.1 Slot Antenna Basics

To understand the basic functionality of slot antennas, Babinet's principle [3] is going to be explained in the following.

Babinet's prinicple

In optics, Babinet's prinicple says [3]: *When the field behind a screen with an opening is added to the field of a complementary structure, the sum is equal to the field when there is no screen.*

To use this principle in antenna theory, the complementaries of quantities describing the electromagnetic field are itemized in table 5.1.

Electric sources ($\vec{J} \neq 0,\ \vec{M} = 0$)	Magnetic sources ($\vec{J} = 0,\ \vec{M} \neq 0$)
$\vec{E}_A$	$\vec{H}_F$
$\vec{H}_A$	$-\vec{E}_F$
$\vec{J}$	$\vec{M}$
ϵ	μ
μ	ϵ
η	$\frac{1}{\eta}$
$\frac{1}{\eta}$	η

Table 5.1: Dual quantities describing the electromagnetic field [3]

- An electric source $\vec{J}$ in a medium produces at a point P the field described by $\vec{E}_0$ and $\vec{H}_0$.

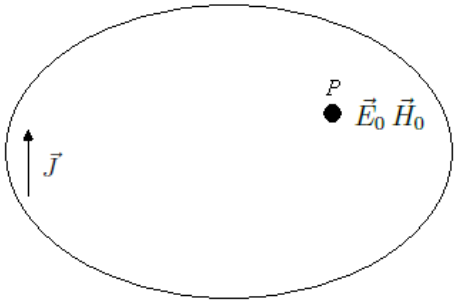

Figure 5.5: Babinet's principle (1)

- Fig. 5.6 shows the same source, but with an infinite, planar, very thin and perfect electric conductor (PEC) inside the propagation region. The PEC plane has an opening (S) and its complementary structure is depicted in Fig. 5.7.

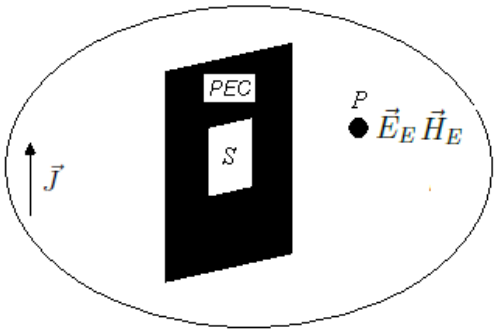

Figure 5.6: Babinet's principle (2)

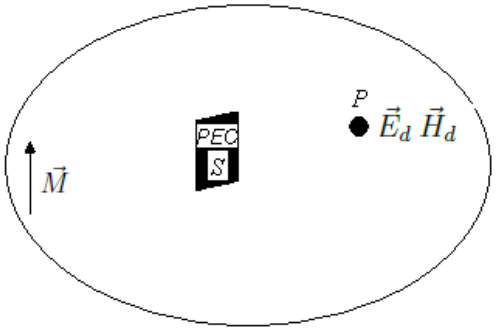

Figure 5.7: Babinet's principle (3)

Assuming Babinet's principle, the field described by $\vec{E}_0$ and $\vec{H}_0$ can also be obtained by combining the complementary structures from Fig. 5.6 and Fig. 5.7.

$$\vec{E}_0 = \vec{E}_E + \vec{H}_d \tag{5.1}$$

$$\vec{H}_0 = \vec{H}_E - \vec{E}_d \tag{5.2}$$

Conclusions

When thinking about previous explanations, one can see that a slot antenna is the complementary structure of a dipole structure. This is useful when designing slot antennas:

- The slot antenna has the same dimensions as the complementary resonant dipole.

- The radiation pattern is consistent with a dipoles pattern, except that the $\vec{E}$ and $\vec{H}$ vectors are interchanged.

Radiation pattern of a slot antenna and its complementary structure:

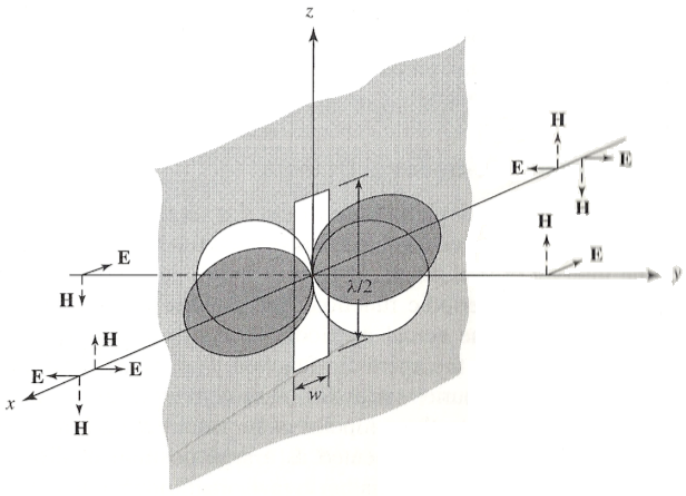

Figure 5.8: Radiation pattern of a $\frac{\lambda}{2}$ slot antenna [3]

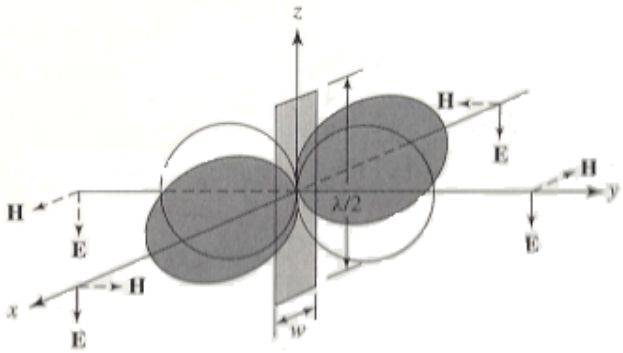

Figure 5.9: Radiation pattern of a $\frac{\lambda}{2}$ flat dipole [3]

5.2.2 Smart Shelf Antenna

Antenna dimensions

The investigated slot antenna in the UHF smart shelf application is milled out of the metal plane and its dimensions are chosen in a way that it is resonant at 865 MHz. Slot dimensions: 19.8 *cm* length and 0.3 *cm* width

Feeding structure

As the slot antenna has to be fed with high-frequency signals, the feeding structure of the smart shelves slot antennas is going to be explained in the following section.

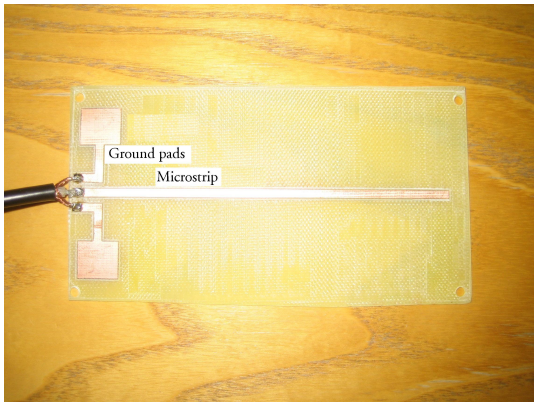

Figure 5.10: Feeding structure of the slot antenna

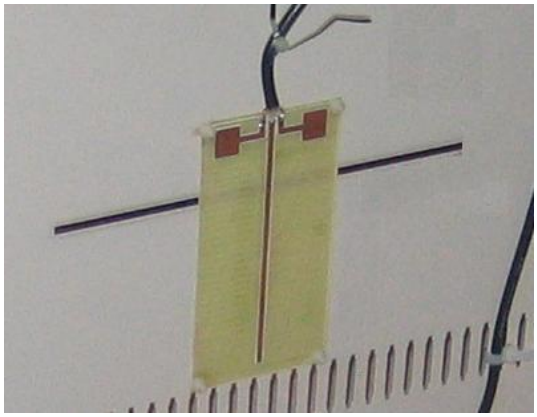

Figure 5.11: Slot antenna with feeding structure (1)

Conductor paths on FR4 material represent the slot's feeder. It is screwed on the metal plane in a way that there is no galvanic contact between metal and conductor paths.

The ground pads (see Fig. 5.10) represent a short (only valid for radio frequencies) to the ground plane, whereas the long microstrip line excites the slot. The antenna's **feed-in points** can be seen as the points where the slot crosses the long microstrip line.

Impedance and matching

Varying the feed-in points' position influences the antennas impedance, thus the matching between antenna and reader. The influence of the feeder's correct position was determined by measurements with a network analyzer.

The x-position (see Fig. 5.12) of the structure is in the middle of the slot as this allows reaching the 50 Ω point by varying the feeding structure's y-position. Shifting the feeding points in y-direction corrects the antennas impedance, as the long microstrip works

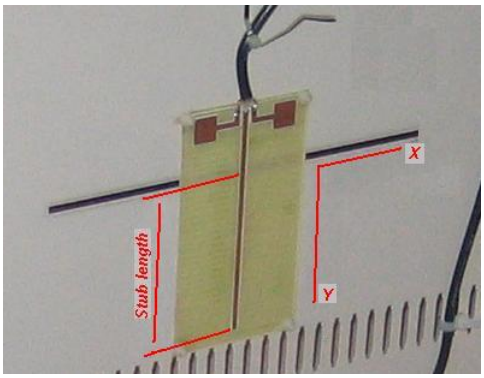

Figure 5.12: Slot antenna with feeding structure (2)

as a stub and compensates the reactive character of the structure.

The following smith chart (Fig. 5.13) plots the antennas impedance with varied stub length. The stub length can be defined as the length from the feeding points to the end of the long microstrip.

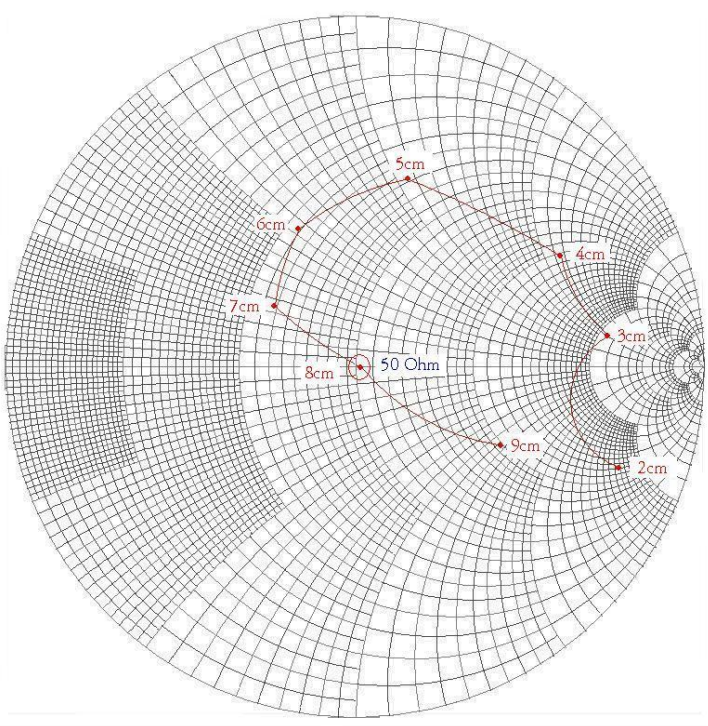

Figure 5.13: Smith chart of the antennas impedance with variation of the feeders y-position (Distance values in the chart depict the used stub length in cm .)

A stub length of 8 cm, together with the structure placed in the middle of the slot results in reaching the 50 Ω matching point.

Far-field measurement

Far-field measurements provide knowledge about the antenna's field in a distance outside the Fresnel zone. Far-field knowledge is important to detect minima and maxima in the field distribution of the antenna. The important prediction of a region where false positive reads [1] could occur is based on the knowledge of the antenna's far-field radiation pattern.

Measurement setup:

- Signal generator: Agilent E4438C (866 MHz @ 15 dBm) [27]
- Amplifier: AR 10W100C [28]
- Signal analyzer: Agilent MXA 9020A [29]
- Antennas: ETS Lindgren horn antennas [30]
- Rotary table (360° in 5° steps)

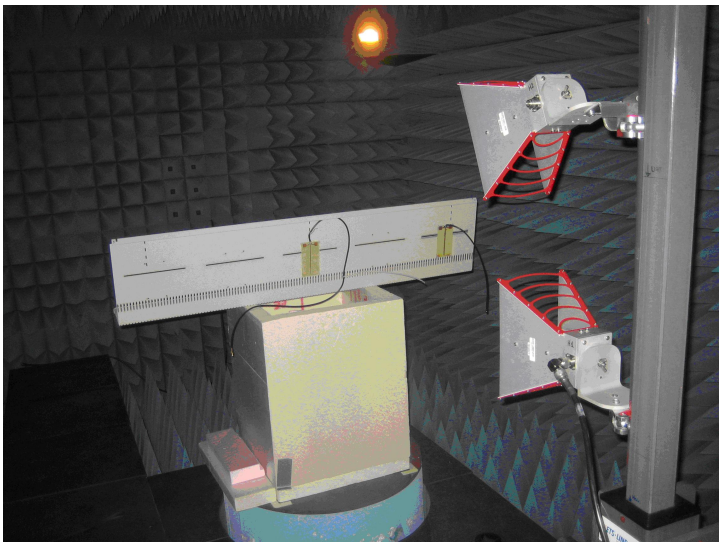

Figure 5.14: Setup for measuring the antenna's radiation pattern

The slot was used as the transmitting antenna and the horn as the receiving antenna. A rotation of the transmitting antenna results in a 360 degree radiation pattern. To cover all degrees of freedom, measurements were carried out with horizontal and vertical slot positions regarding the horn antenna. In one case the $\vec{E}$-plane, and in the other case the $\vec{H}$-plane have been measured. Additionally, separate measurements for co-polarization and cross-polarization between the antennas were carried out. The position between the

[1] Tags that have been read unintentionally by an RFID reader are called **false positives** eg.: the smart shelf detects a tag which belongs to another smart shelf positioned nearby.

transmitting antenna and the receiving antenna in Fig. 5.14 equals the 0° positions in the following pictures.

- Radiation pattern, measured in the antenna's $\vec{E}$-plane and $\vec{H}$-plane:

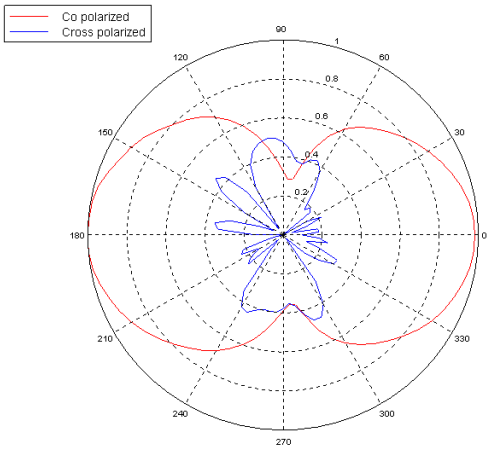

Figure 5.15: $\vec{H}$-plane measurement

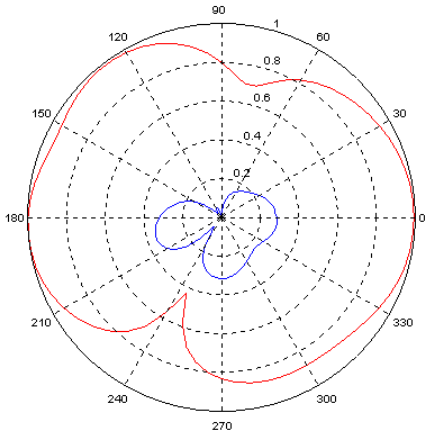

Figure 5.16: $\vec{E}$-plane measurement

When looking at Fig. 5.15 and 5.16, one can see that the minima are arranged at the small sides of the slot. The dipole-like radiation pattern is due to the previously described duality between slots and dipoles as they show the same pattern, but with interchanged $\vec{E}$ and $\vec{H}$ vectors.

Looking at Fig. 5.16, one can observe an asymmetry due to a twist of 30 degrees in the pattern. This can be explained by the shelf's L-shape. To prove this theory, a measurement with a self-built I-shaped shelf rack has been done.

- $\vec{E}$-plane measurement with self-built antenna:

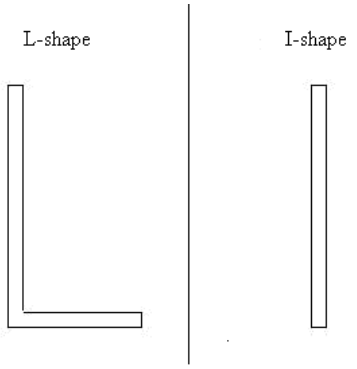

Figure 5.17: L-shaped versus I-shaped rack

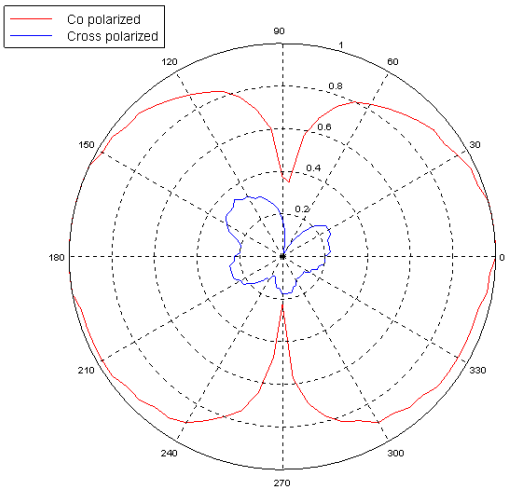

Figure 5.18: $\vec{E}$-plane pattern (I-shape)

As the pattern in Fig. 5.18 is symmetric, the L-shaped metal influences the $\vec{E}$ vector and leads to an asymmetric radiation pattern.

- Gain (see section 6.3.3) [3]:

  The gain value is a very important parameter when characterizing an antenna. It can be determined using a calibrated setup and a well-known reference antenna. A signal with defined amplitude and frequency has been sent via a transmitting antenna and detected using a receiving antenna. The measurement was carried out with the reference antenna, and the unknown antenna as sending antennas. When measuring the received power and comparing both results, the gain value of the unknown antenna can be determined.
  Using a $\frac{\lambda}{2}$ reference dipole with a gain of 2.15 dBi [3] leads to the resulting slot antenna gain value, which was determined with 5.6 dBi @ 866 MHz.

Near-field measurement

When considering a smart shelf application, the tagged items are placed in close proximity to the antenna. Due to this fact, knowledge about the occurring field on the label position, which is inside the antennas near-field, is very important. Scanning the antenna's near-field provides this information.

Again, the slot works as the transmitting antenna. It has been fed with a continuous wave signal at a frequency of 866 MHz. The receiving antenna is a dipole that looks like the Web label and is matched to 50 Ω @ 866 MHz. Using a spectrum analyzer [20] allows one to analyze and store the measured field power at defined points in a region around the slot.

Measurement distance: 2 cm from antenna to antenna.
Scan region: 300 $mm \times 220$ mm symmetric around the slot.

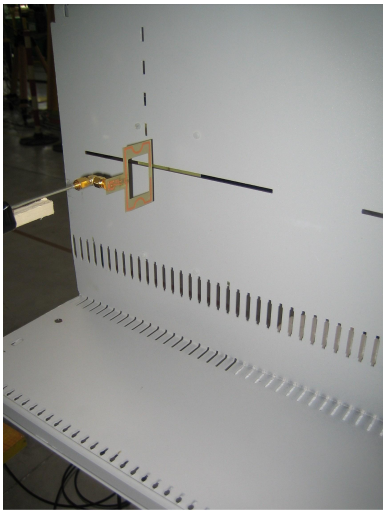

Figure 5.19: Scan setup for near-field measurement

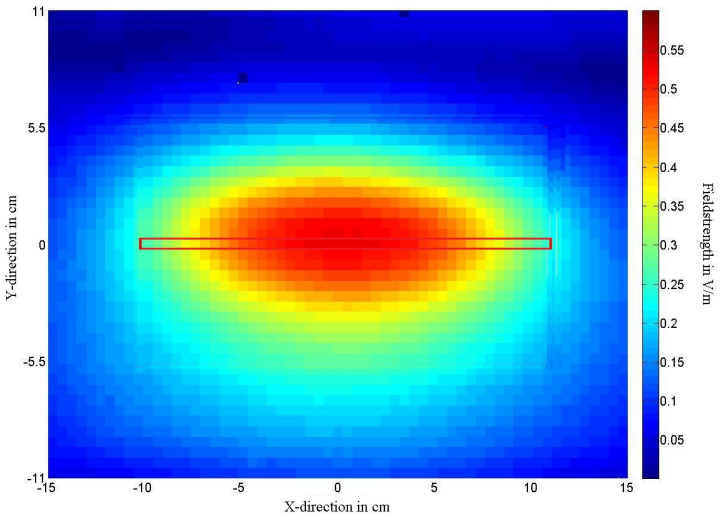

Figure 5.20: Measured field intensity

The field intensity graph shows a field distribution which can be described as a concentric ellipsoid with steadily decreasing intensity. As the field strength is concentrated in the middle of the slot, the optimal label position will be around this area. The red rectangle in Fig. 5.20 depicts the slot's position.

6 UHF Label Design

The previous chapter introduced the readpoints used for the document tracking appplications. Choosing the right label design is also important when optimizing an application for a specific Auto-ID scenario. The following sections describe the design process of the NXP document tracking label antenna.

6.1 Method of Design

A base for further investigations on a label antenna for document tracking purposes is delivered by measurements and simulations of commercially available labels.

Path to a new design

- Analysis: Build up a knowledge base
  - Measurements with established labels in single and stacked mode
  - Simulations with established labels in single and stacked mode
- Synthesis: Use acquired knowledge for the new design
  - Creation of new designs
  - Simulation provides knowledge about stacking behaviour
  - Extraction of best performing antenna designs
  - Building prototypes for measurements
  - Measurements in single and stacked mode
  - Repetition of previous steps until results are satisfying
  - **New Design**

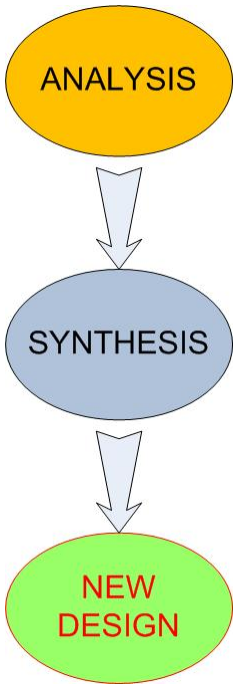

6.2 Simulation of Stacked Labels

This section explains important things when doing a simulation with a stack of labels, with the main focus on the connection between scattering parameters and impedance parameters.

6.2.1 Portload and Matching

When analyzing an antenna using numerical field simulation, an excitation source has to be specified. In the simulation program used, *Ansoft HFSS* [31] , this excitation source is called a lumped port. As an impedance value has to be assigned to the lumped port, the choice of the port impedance changes the way the simulation results have to be interpreted. To demonstrate the effects of different port impedance assignments, an antenna structure with resonance at $\approx 1.2\ GHz$ has been simulated with the port impedances shown in Fig. 6.1.

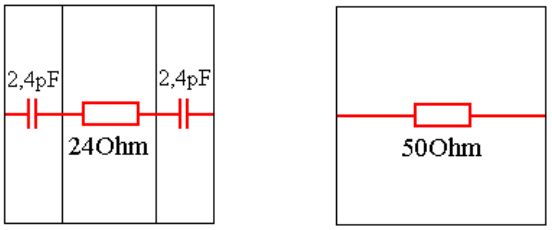

- Port load: 50 Ω
- Port load: 24 Ω *and* 1.2 *pF*
  → Realistic value for a RFID IC. [a]

[a] Real parts have been assigned to the lumped ports. The imaginary part has been realized with lumped elements connected to the lumped port.

Figure 6.1: Lumped ports with different impedance assignements

The simulated antenna's resonance frequency can be seen in Fig. 6.4. A good S_{11} value occurs when the impedance matching between antenna and IC is good, which means that antenna and IC have to have the same real parts and imaginary parts which compensate each other [1].

- $\underline{Z}_a$ ... *Antenna Impedance*
- $\underline{Z}_p$ ... *Port Impedance*

$$\underline{S}_{11} = \frac{\frac{1}{\underline{Z}_p{}^*}\underline{Z}_a - 1}{\frac{1}{\underline{Z}_p{}^*}\underline{Z}_a + 1} \tag{6.1}$$

$$C = 1.2\ pF \rightarrow \underline{X}_C = ?$$

$$\underline{X}_C = \frac{1}{j\omega C} = \frac{-j}{\omega C}\ with\ \omega = 2\pi f \tag{6.2}$$

[1] Conjugate complex matching [3].

Using (6.2) delivers the $\underline{X}_C$ value for $C = 1.2\ pF$ @ $f = 1.2\ GHz$ as

$$\underline{X}_C = -110.52427j\ \Omega.$$

Accounting a wanted resonance of 1.2 GHz, the antenna's impedance has to match $24 + j110.52\ \Omega$ to get a perfect match to the IC input impedance.

In general, simulations with different port loads lead to the same results, but different interpretations are necessary.

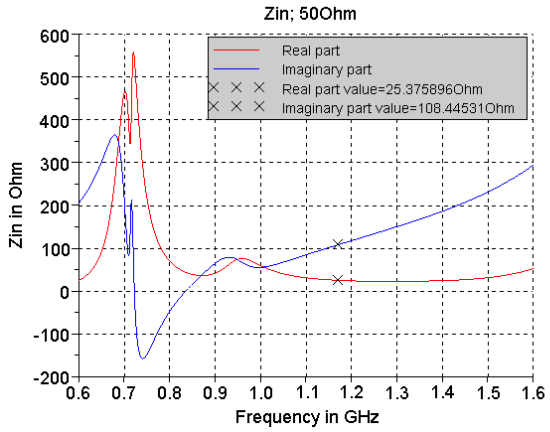

Figure 6.2: Z_{In} with 50 Ω load

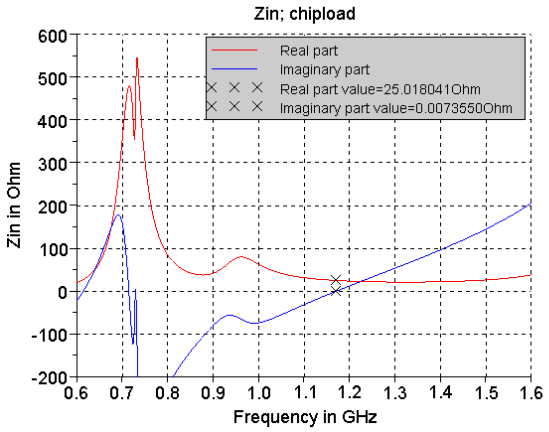

Figure 6.3: Z_{In} with IC-impedance load

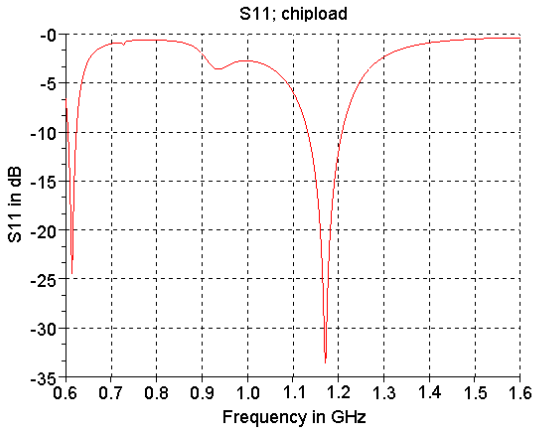

Figure 6.4: S_{11}: single label

- 50 Ω load: When simulating with 50 Ω port impedance, the best matching (peak in the S11 curve) will be at an impedance of $\underline{Z} = 50 + j0\ \Omega$. But for RFID labels, the antenna has to be designed to match to the IC impedance and therefore post-processing is necessary. To get the S_{11} related to the IC impedance one has to look for the conjugated complex value of the IC impedance using the curve of the antennas impedance created with 50 Ω port load. When comparing Fig.6.2 and

Fig. 6.4 one can see that the S_{11} peaks occurs approximately at the conjugated complex IC impedance (see crosses in Fig. 6.2). The advantage of a simulation with 50 Ω port load is the increased calculation speed.

- chip load: Loading the port with the IC impedance results in getting the correct S-curves without post processing. As one can see in Fig. 6.3, the point of best matching is at $\underline{Z} \approx 25 + j0\ \Omega$, as the imaginary parts compensate each other.

A perfect match is not possible as slight differences between IC impedance and antenna impedance are common, so the best compromise has to be found.

6.2.2 Z_{11} versus Z_{In}

When refering to Fig. 6.3 and 6.4 from section 6.2.1, one can see an obvious connection between Z_{11} and S_{11}. It can be confusing that there is no apparent connection between S_{11} and Z_{11} when there is more than a single tag in the stack. Fig. 6.5 and 6.6 show S-curves and Z-curves of a simulation that has been done with two stacked tags [2].

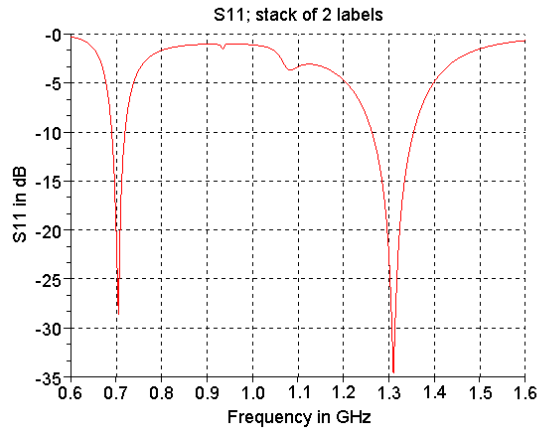

Figure 6.5: S_{11}: stack of 2 Web labels

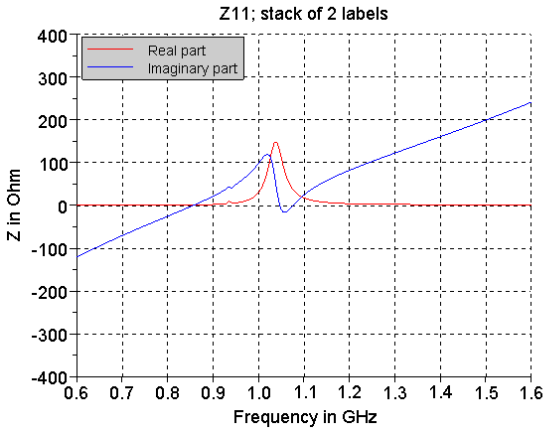

Figure 6.6: Z_{11}: stack of 2 Web labels

As one can see in Fig. 6.6, resonance should occur in a region between 1.05 GHz and 1.1 GHz. Confronting the S_{11} curve in Fig. 6.5, one can see that the resonances are located at regions around 0.7 Ghz and 1.3 Ghz.
This happens due to the S-parameter calculation when there are multiple tags in the field. As S_{11} contains influences from the other tags, a calculation refering only to Z_{11} is invalid. The S-parameter calculation has to contain all occuring impedance curves to consider influences from the other labels in the field. The expression Z_{In} concludes all Z-curves and is used in (6.5).

[2] The excitation ports have been loaded with IC impedance

Z_{In}-calculation

The following calculation is valid for a simulation with two stacked labels. Both ports were loaded with IC impedance [32].
Ohms law provides:

$$\begin{bmatrix} \underline{U}_1 \\ \underline{U}_2 \end{bmatrix} = \begin{bmatrix} \underline{Z}_{11} & \underline{Z}_{12} \\ \underline{Z}_{21} & \underline{Z}_{22} \end{bmatrix} \begin{bmatrix} \underline{I}_1 \\ \underline{I}_2 \end{bmatrix} \; with \;\; \underline{Z}_{12} = \underline{Z}_{21}, \tag{6.3}$$

$$\underline{U}_1 = \underline{Z}_{11}\underline{I}_1 + \underline{Z}_{12}\underline{I}_2 \quad and \quad \underline{U}_2 = \underline{Z}_{12}\underline{I}_1 + \underline{Z}_{22}\underline{I}_2. \tag{6.4}$$

Solving the equation system [3] (6.4) with $\underline{U}_1 = \underline{Z}_{In1}\underline{I}_1$ and $\underline{U}_2 = -\underline{Z}_{Load}\underline{I}_2$ leads to:

$$\underline{Z}_{In1} = \underline{Z}_{11} - \frac{\underline{Z}_{12}^2}{\underline{Z}_{22} + \underline{Z}_{Load}}. \tag{6.5}$$

Calculated Z_{In1} is shown in figure 6.8.

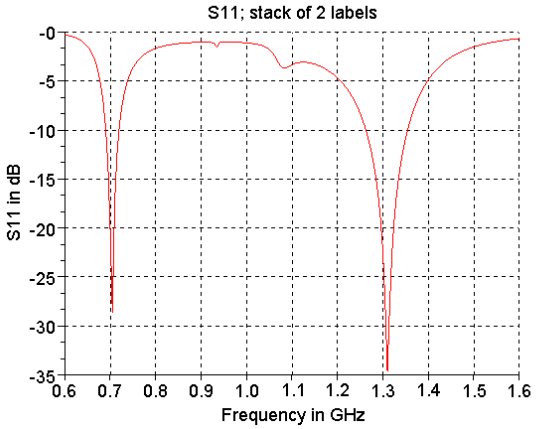

Figure 6.7: S_{11}: Stack of 2 Web labels

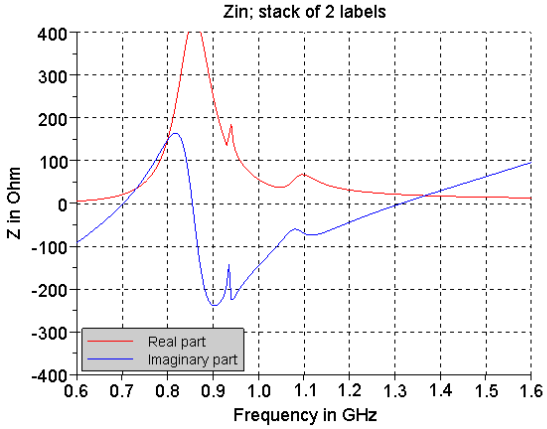

Figure 6.8: Z_{In1}: Stack of 2 Web labels

An obvious connenction between Z_{In1} and S_{11} can be seen, as zero crossings of the imaginary part mark the resonance regions found when analyzing S_{11}.

[3] The antenna of label 2 has the IC-impedance Z_{Load} across its unexcited terminals.

6.2.3 Conclusions

- Port load: Refering to section 6.2.1 all labels in the stack have to have the same port loads. The port load impedance does not effect the results, but they have to be interpreted in various ways.
- S versus Z: When simulating a stack of labels, S_{XX} refers to a Z_{InX} which has to be calculated using all Z_{XX} and Z_{XY} curves.

6.3 Analysis

Measurements and simulations of commercially available labels delivered close coupling knowledge for the new design.

6.3.1 Pmin Measurement

The minimum power (=Pmin) measurement delivers information about the lowest power value that has to occur at the tag to power up the IC.

Setup:

- Reader: Thingmagic M5e [33]
- Amplifier: AR 10W100C [28]
- Antennas: ETS Lindgren horn antennas [30]
- Software: Labview 8.5 [34]
- Frequency sweep: 840 MHz - 960 MHz
- Bistatic measurement

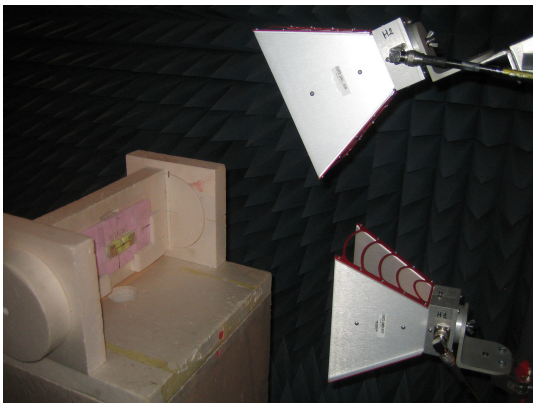

The software controls the reader unit and performs a power sweep at every defined frequency point. At every point the query signal is sent via a transmitting antenna, whereas the receiving antenna receives the backscattered signal from the tag. Decoding the backscattered signal provides information as to whether the label sends a valid answer or not. A detected label answer leads to storage of power values and frequency values, thus the minimum required power to get a label answer can be determined over a wide frequency range.
Due to calibration of the measurement system, the resulting Pmin values (Fig. 6.10 to 6.12) give information about the field power (in dBm) which has to occur at the label to power the IC. The Thingmagic reader has been used as transmitting unit and receiving unit, because using the reader allows selecting a unique Tag-ID and determining the label's Pmin curve, even when multiple labels are placed in the field.

A general equation for the received power from a transmitting antenna by a receiving antenna is known as the Friis equation [35]:

$$P_{RX} = P_{TX}\ G_{TX}\ G_{RX}\ (\frac{\lambda}{4\pi r})^2, \tag{6.6}$$

where P_{RX} is the received power, P_{TX} the transmitted power, G_{TX} the gain of the tansmitting antenna, G_{RX} the gain of the receiving antenna and $(\frac{\lambda}{4\pi r})^2$ the inverse of the free space path loss.

The Pmin value at the tag can be determined using following link budget calculation:

$$P_{min}[dB] = P_{TX}[dB] - CL[dB] + G_{TX}[dB] - FSPL[dB], \tag{6.7}$$

where P_{min} is the minimum power to activate the IC, P_{TX} the reader output power, CL the cable losses, G_{TX} the gain of the reader antenna and $FSPL$ the free space path loss.

The Pmin value is also known as the label sensitivity. When subtracting the gain of the label antenna from the label sensitivity and taking into account the mismatch losses, one can derive the power at the IC. For powering up the IC, the power at the IC has to be greater or equal the sensitivity of the IC.

Instead of the reader unit, a signal generator can be used for generating the query signal, and a signal analyzer (Agilent MXA [29]) for decoding the backscattered signal. This setup is the standard measurement setup for Pmin measurements at NXP and explained in Fig. 6.9.

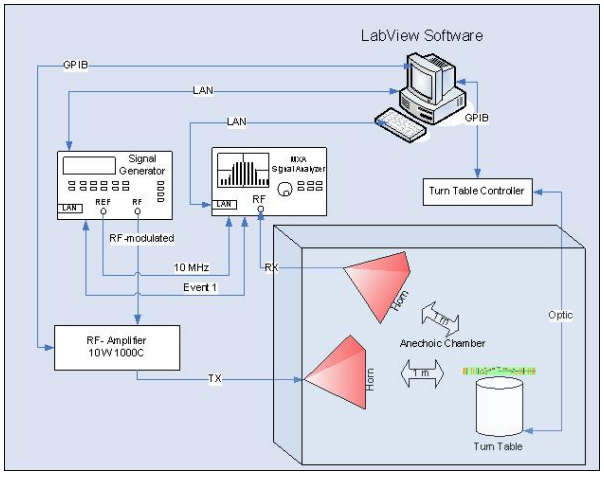

Figure 6.9: Pmin setup: Block diagram

Pmin: Tagsys DocTrak

Fig. 6.10 shows the Pmin curve of a single 'DocTrak' label:

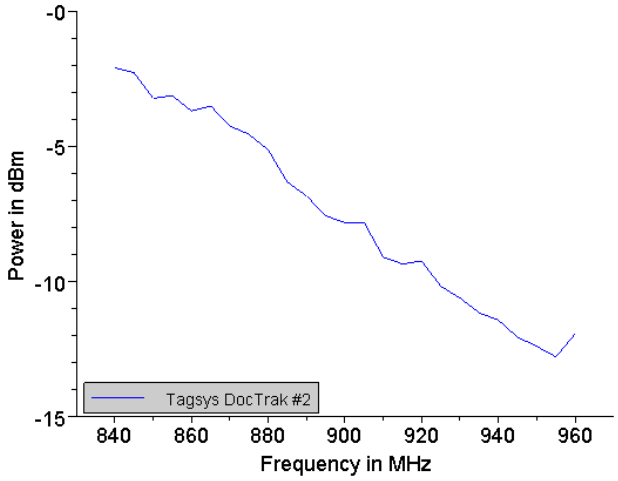

Figure 6.10: Pmin curve: Tagsys DocTrak (single label)

Fig. 6.11 and 6.12 show Pmin curves of a stack of 'DocTrak' labels [4].
The label stack was built with five and eleven labels and 1 mm spacing between them. The spacer material has an 'air-like' dielectric constant ($\epsilon_r \sim 1$).

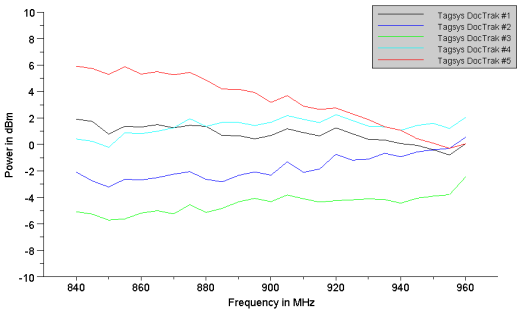

Figure 6.11: Pmin curve: Tagsys DocTrak (stack of 5 labels)

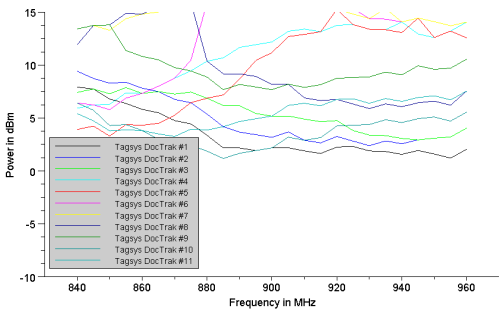

Figure 6.12: Pmin curve: Tagsys DocTrak (stack of 11 labels)

As one can see, the single label is tuned to a quite high frequency. Fig. 6.10 shows the label's resonance at 955 MHz (Pmin value = -13 dBm). When building a label stack, curves become flat, and Pmin values increase. In Fig. 6.11 and 6.12, it can be seen that the distribution between the best and the worst curve gets bigger when increasing the amount of labels in the stack.

For a better understanding of these observations, numerical field simulations of the underlying problems have been carried out.

[4] Label #1 is always the closest to the reader antenna.

6.3.2 Simulations of WebX and Tagsys DocTrak

The models of the WebX and the Tagsys label have been created using the FEM-simulator HFSS11 [31]. The excitation ports have been loaded with the IC impedance (see section 6.2.1), and spacing between the stacked labels is 1 mm.

Table 6.1 contains the assembled IC impedances which were used for the simulations.

Label	IC	IC-resistance	IC-reactance
UPM WebX [9]	NXP G2X	24 Ω	1.2 pF
Tagsys DocTrak [26]	Impinj Monza	20 Ω	1.25 pF

Table 6.1: IC impedances

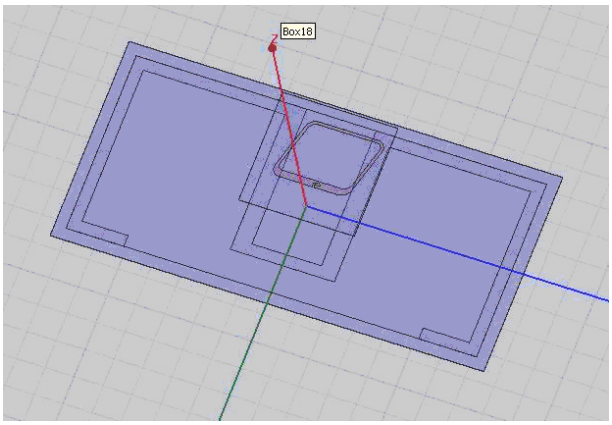

Figure 6.13: DocTrak HFSS model

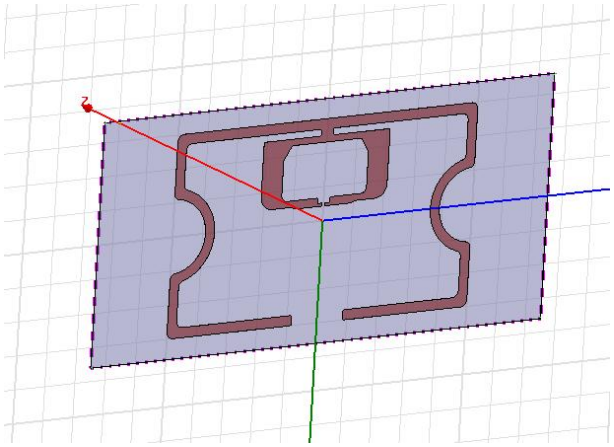

Figure 6.14: WebX HFSS model

Fig. 6.15 to 6.26 show simulated Z_{In} and S_{11} parameters of WebX and Tagsys DocTrak labels. The stack size was increased successively from one to three labels. The displayed S-curves and Z-curves always belong to the same label in the stack. Assuming the case of three stacked labels, the plotted curves belong to the label in the middle position.

Analyzing coupling effects in the UHF region is more complex than in the previously described HF region, as antenna geometry and the propagation region are different. When analyzing UHF backscatter systems, antenna geometries are different from HF-loops, and the simplification of mainly inductive coupling is not valid any more. This makes analytical calculations exceedingly difficult, though simulations provide information about UHF coupling behaviour.

- Analysis **WebX**:
  The WebX label has been developed for fashion applications. Due to this reason its resonance has been pretuned to frequencies $> 1\ GHz$. Knowledge about the stacking behaviour of the WebX label can be derived analyzing Fig. 6.15 to 6.20. With increasing stack size, the real part peak increases and shifts to lower frequency values. When looking at the imaginary part, a similar attitude can be seen. The difference between the positive and the negative peak increases as the negative peak increases its value. A movement to lower frequencies can also be observed.
  The detuning which can be seen when analyzing the Z-curves or S-curves heavily influences the label's performance, as one resonance in the frequency region of interest turns to two resonances which drift apart. Due to this reason the matching gets worse (see Fig. 6.20) which leads to difficulties when using WebX labels in document tracking applications.

- Analysis **Tagsys DocTrak**:
  As the DocTrak geometry is quite complex, the simulated frequency sweep was reduced to improve simulation speed. Comparing the S-curves leads to the conclusion that resonances do not drift apart that far and stay around the frequency region of interest, even in stacked mode. Increasing the stack size to two labels results in bigger S_{11}-curve variations than further increasing the label amount to three. Complicated Z-curve characteristics may result out of the label geometry, as the Tagsys label uses a matching loop, which provides strong coupling with other labels in the stack.

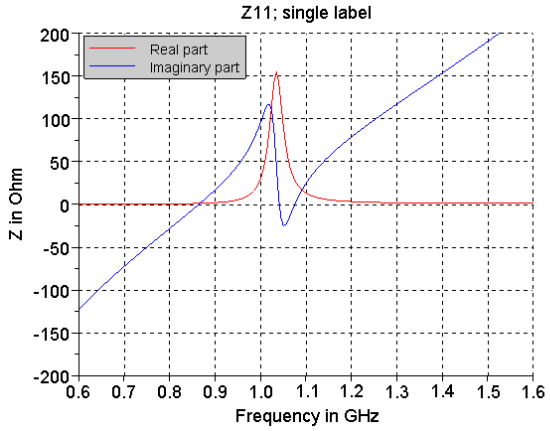

Figure 6.15: WebX: Z_{In} single label

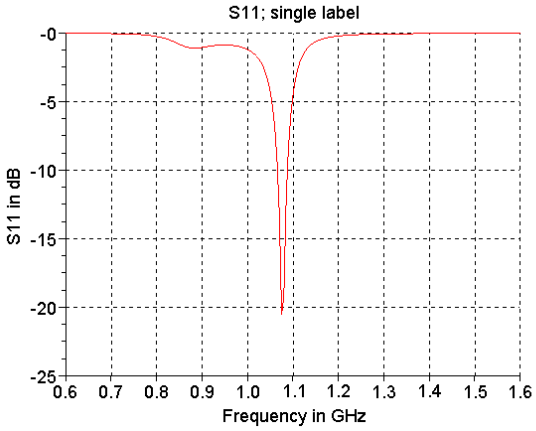

Figure 6.16: WebX: S_{11} single label

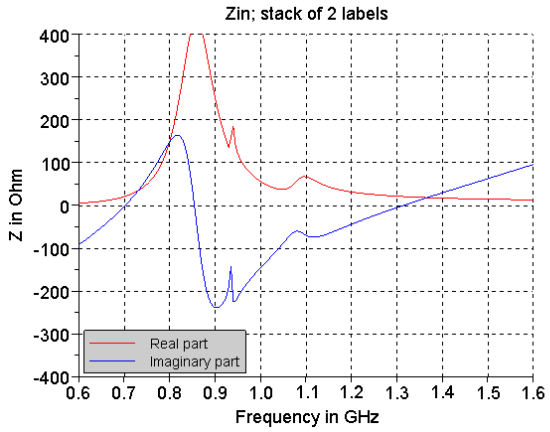

Figure 6.17: WebX: Z_{In} stack of 2

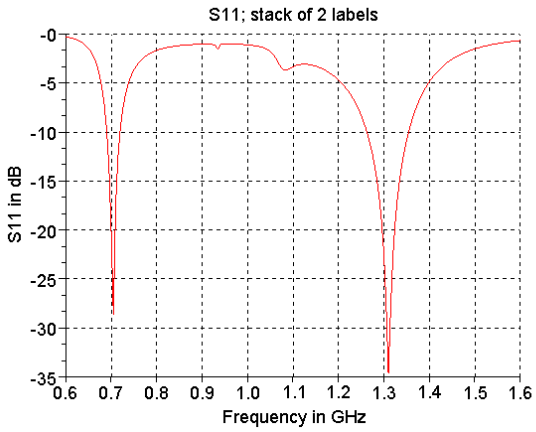

Figure 6.18: WebX: S_{11} stack of 2

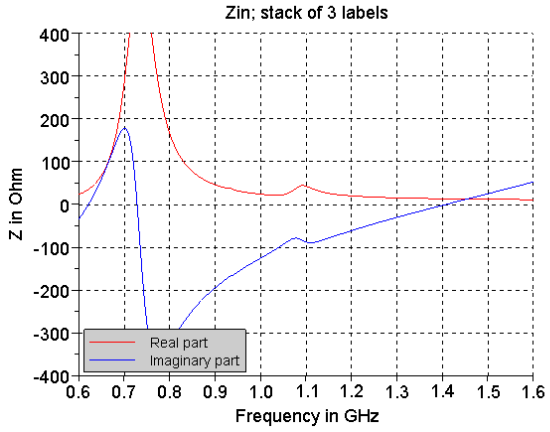

Figure 6.19: WebX: Z_{In} stack of 3

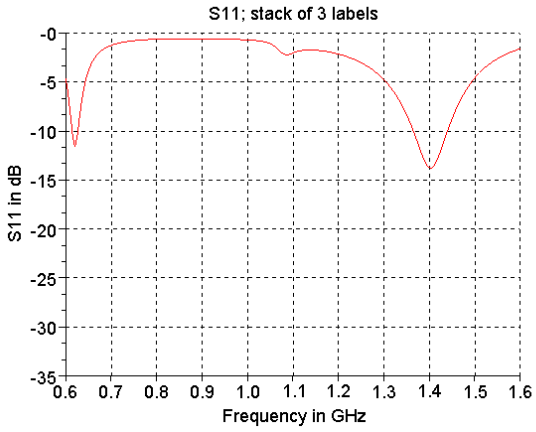

Figure 6.20: WebX: S_{11} stack of 3

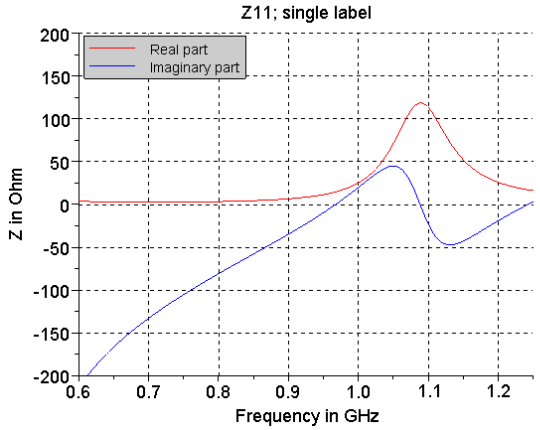

Figure 6.21: DocTrak: Z_{In} single label

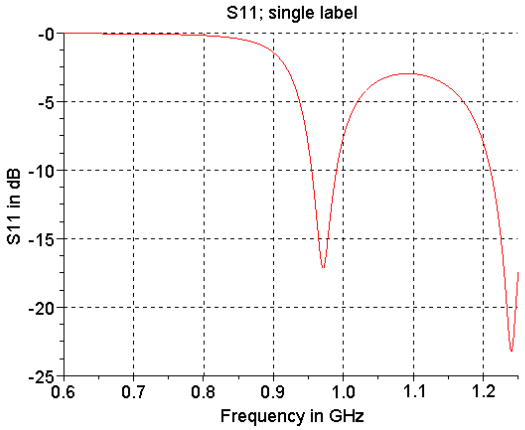

Figure 6.22: DocTrak: S_{11} single label

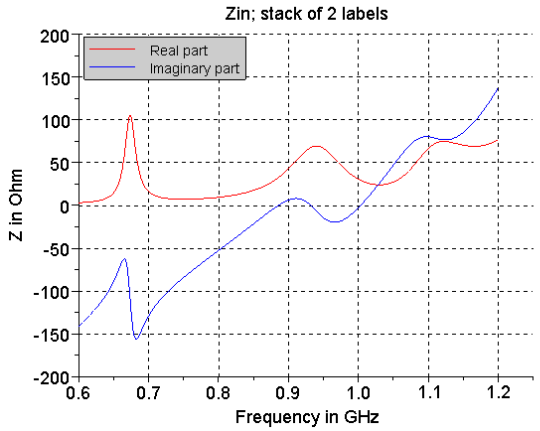

Figure 6.23: DocTrak: Z_{In} stack of 2

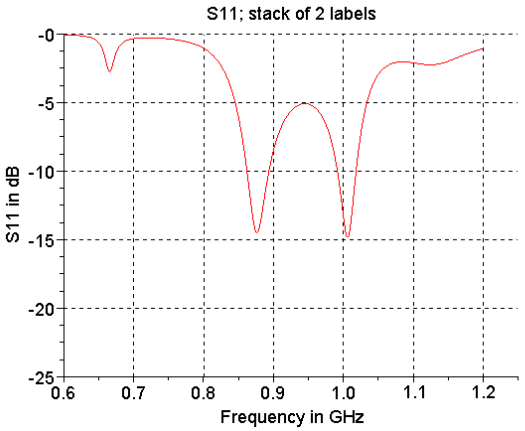

Figure 6.24: DocTrak: S_{11} stack of 2

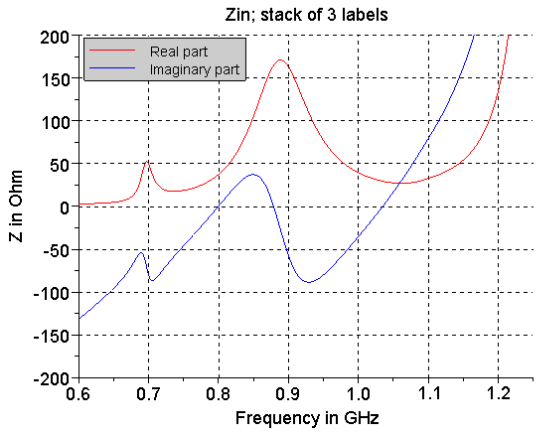

Figure 6.25: DocTrak: Z_{In} stack of 3

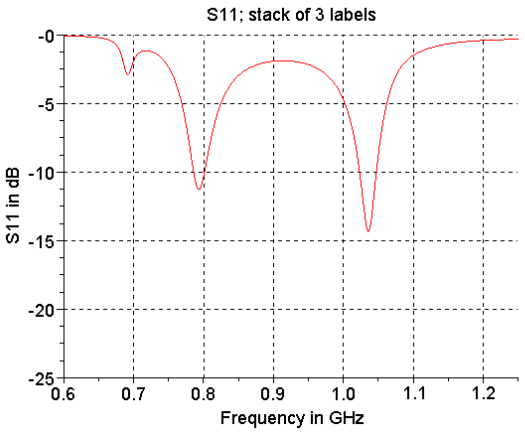

Figure 6.26: DocTrak: S_{11} stack of 3

6.3.3 Gain

Gain is an important parameter when analyzing the label's performance and is described in [3] the following way: ***The gain of an antenna (in a given direction) is defined as the ratio of the intensity, in a given direction, to the radiation intensity that would be obtained if the power accepted by the antenna were radiated isotropically.***
Due to directionality dependence, the gain value was always extracted from the HFSS simulation results at the same points ($\vartheta = 0°$, $\varphi = 0°$ see also Fig.6.69) to achieve comparable results.

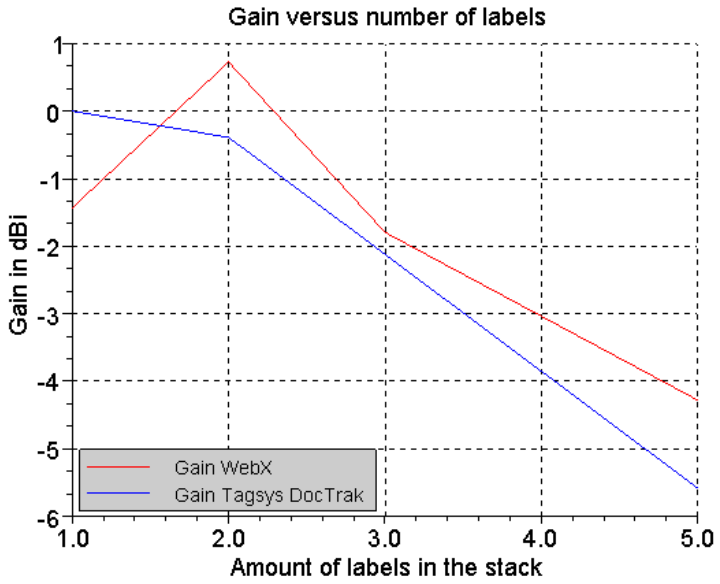

Figure 6.27: Gain value versus stacked label amount

Using RFID labels in a stacked way always leads to detuning and to losses in the gain value. Fig. 6.27 shows the gain values of WebX and DocTrak versus the number of labels in the stack. Looking at the curves, it can be seen that a negative gradient occurs with an increasing number of labels in the stack. As the gain drops to values around -5 dBi at a number of five stacked labels, serious performance losses can be assumed.
Another effect evoked by close coupling can be seen when looking at the gain curve of the WebX label. Increasing the stack size from one to two labels causes the gain value to increase. A further increase of the stack size leads to a decrease in the gain value. Due to this change in the gradient of the gain curve, one can assume directivity effects. Bringing an additional label in the field of the WebX label results in changing the radiation pattern. This leads to better gain values along the direction the beam expands.

6.4 Label Antenna Architectures

6.4.1 Dipole

The most common base for a label antenna design is a dipole [35].

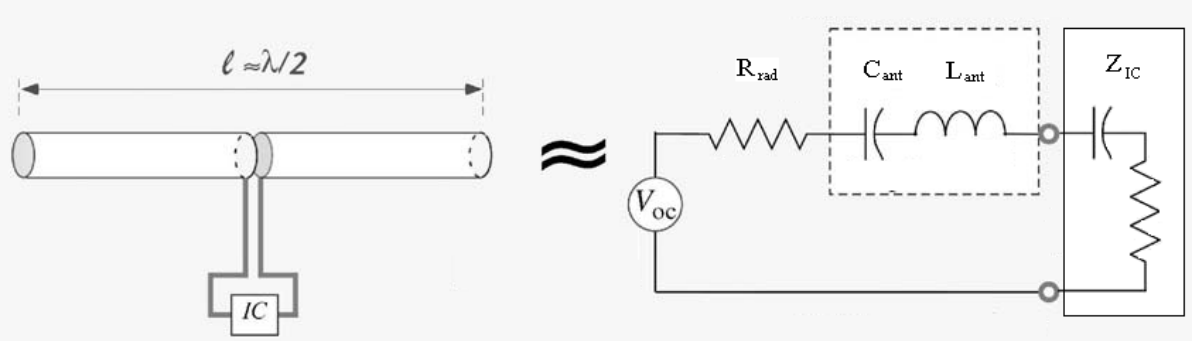

Figure 6.28: $\frac{\lambda}{2}$-dipole and its electrically equivalent form [35]

The circuit depicted in Fig. 6.28 is valid only for the first serial resonance of a dipole. The product of the dipole's inductance and capacitance is inversely proportional to the antenna's resonance frequency:

$$f_{res} = \frac{1}{2\pi\sqrt{L_{ant}C_{ant}}}, \tag{6.8}$$

thus the dipole length defines the resonance frequency. A common approach is to choose the dipole length as half the wavelength of the desired resonance frequency.

A desired resonance at 866 MHz results in a dipole length of:

$$\lambda = \frac{c}{f_{res}} \; with \; c = 3 * 10^8 \; \frac{m}{s} \; and \; f_{res} = 866 \; MHz, \tag{6.9}$$

$$\lambda = 0,346 \; m,$$

$$l = \frac{\lambda}{2} = 0.173 \; m. \tag{6.10}$$

For the conjugate matching, the imaginary part of the antenna impedance has to be near the conjugated imaginary part of the IC impedance. As a dipole antenna's impedance is $\underline{Z}_{dip} \approx 73.1 + j42.3 \; \Omega$, the imaginary part is in general too small to compensate the IC reactance. Uncompensated IC capacitance leads to a bad power-transfer coefficient, and this does not make a straight dipole the antenna of choice for a typical UHF-RFID IC. Changing the antenna length results in varying the antenna's impedance, but the price for a better matching to the IC is a shifted resonance frequency. A second disadvantage

is the length of a dipole. No form factor for a commercial RFID label will allow lengths around 17 cm. As small label sizes get more important, bending the dipole is a way to match small geometry with long antennas.

6.4.2 The Meandered Dipole

Bending a dipole leads to small label geometry at the same antenna length. These bended dipoles are also called **meandered dipoles**.

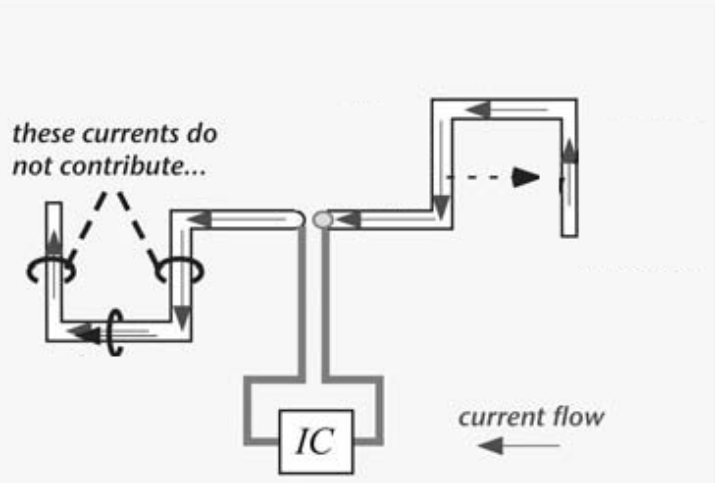

Figure 6.29: Meandered dipole: Current flow [35]

Analyzing the current flow in a meandered dipole (Fig. 6.29) shows inverted current flows in neighbored arms of the meander. This leads to the conclusion that the current in neighbored arms of the antenna approximately cancels and produces no radiation. The more narrow the meanders are, the more effective the cancellation occurs.
Only parts pointing in the direction of the original dipole produce radiated waves!

Meandering also effects the antenna's impedance. This effect is explained using Fig. 6.30, which shows one arm of a meandered dipole antenna with the red plus signs depicting charges on the wire.

- Inductance: Currents flowing in opposite directions have no effect on the magnetic vector potential, thus a meandered structure shows less inductance than a straight dipole [35].

- Capacitance: When looking at Fig. 6.30, one can see that using narrow meander wires leads to dense charge distribution. When keeping

$$Q = CU \tag{6.11}$$

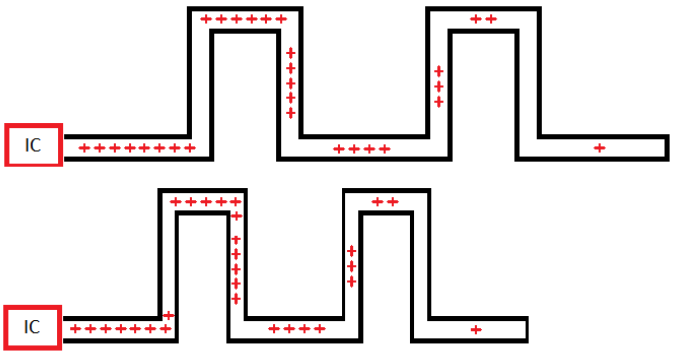

Figure 6.30: One arm of a meandered dipole

in mind, the charge Q has to stay constant. Due to the denser charge distribution the potential raises and leads to an increasing voltage on the wire. Thus the capacitance C has to decrease its value to fulfill (6.11).

Regarding (6.8), decreasing inductance and capacitance leads to an increasing resonance frequency. This inversely proportional ratio is the reason that a meandered wire has to be longer to achieve the same resonance as a straight one.
One approach (to get a better power transfer between an antenna and an RFID IC) with meandered antennas is to make the wire longer while keeping the same resonance, but this leads to even more meandering. A longer antenna is mainly inductive and therefore the capacitive IC can be compensated in a better way.

6.4.3 T-Match

Matching the antenna's impedance to the IC can also be done by using an additional matching structure. A common approach when designing UHF-RFID antennas is a so called 'T-match' depicted in Fig. 6.32.

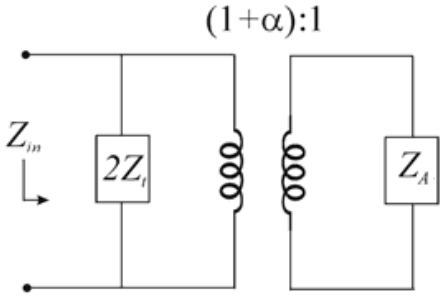

Figure 6.31: Equivalent circuit for a T-match structure [36]

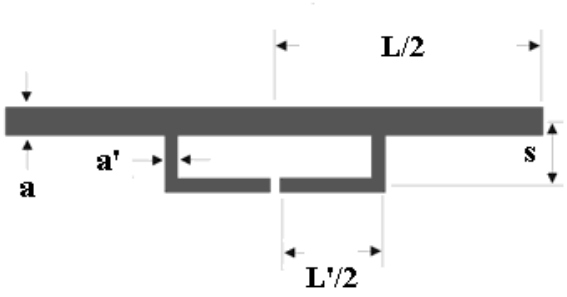

Figure 6.32: Geometry of a T-matched antenna [36]

The T-match can be seen as a second dipole with length L' and radius a', which is connected in a distance s to the large, radiating dipole with length L and radius a (see Fig. 6.32). This structure is a general form of a folded dipole, thus the T-match design procedure is similar to the design procedure of a folded dipole.
A folded dipole (Fig. 6.33) with $L = L' = \frac{\lambda}{2}$ and $a = a'$ provides a four times greater input impedance compared to an isolated dipole of the same length [3]:

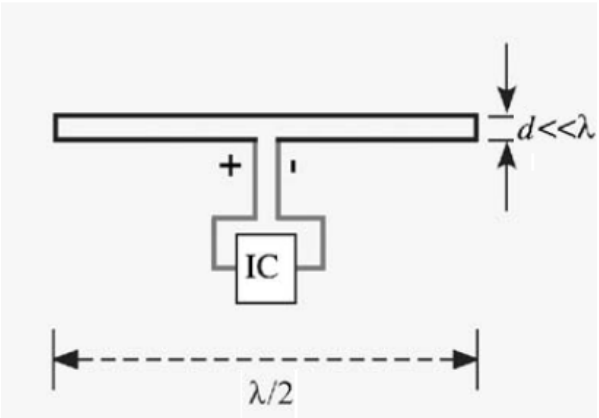

Figure 6.33: Folded dipole [35]

- The currents, flowing through the arms of the folded dipole (I_f) equal the current of the ordinary dipole (I_d):

$$2I_f = I_d. \tag{6.12}$$

- The input power values equal each other too:

$$P_f = Re\{\frac{{I_f}^2 \underline{Z}_f}{2}\} = P_d = Re\{\frac{{I_d}^2 \underline{Z}_d}{2}\}. \tag{6.13}$$

- Inserting (6.12) into (6.13) leads to:

$$\underline{Z}_f = 4\underline{Z}_d \quad for \quad d << \lambda. \tag{6.14}$$

As a T-matched dipole has different geometry ($L \neq L'$ and $a \neq a'$) than the folded dipole, the impedance step up ratio depends on the choosen values for L' and a'. When looking at the equivalent circuit (Fig. 6.31), the input impedance can be written as:

$$\underline{Z}_{in} = \frac{2\underline{Z}_T[(1+\alpha)^2 \underline{Z}_a]}{2\underline{Z}_T + (1+\alpha)^2 \underline{Z}_a}. \tag{6.15}$$

The antenna impedance Z_a is stepped up by the ratio of $1+\alpha$ and placed in parallel mode with twice the impedance of the transmission line Z_T. The resulting input impedance should provide a good match to the IC. A full design procedure can be found in [3].

6.4.4 Inductively Coupled Match

An inductively coupled matching structure consist of a loop which is placed in close proximity to the radiating part of the antenna.

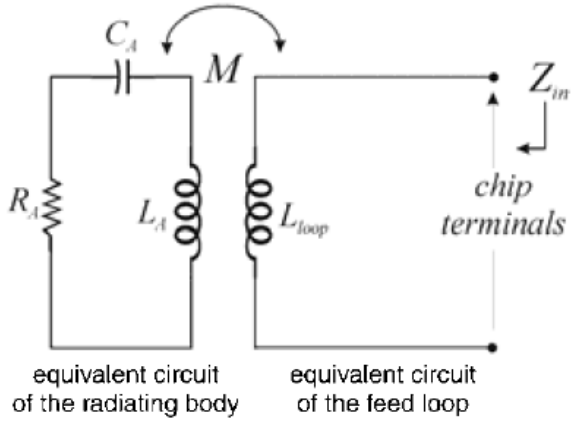

Figure 6.34: Inductive coupled antenna: Electrically equivalent form [36]

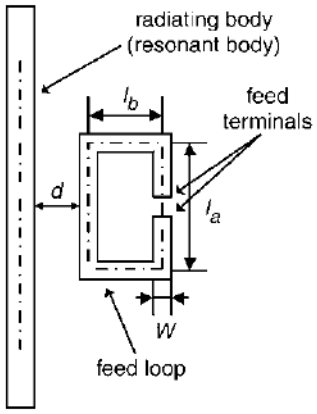

Figure 6.35: Geometry of an inductive coupled antenna [37]

The small loop is directly attached to the IC terminals, thus the loop's geometry is very important to achieve a good conjugate match. The coupling strength depends on the loop's distance to the radiating antenna as well as the loop's geometry. When looking at Fig. 6.34, one can see that the inductively coupled structure can be modeled by a transformer. The antenna's input impedance is written by [37] as:

$$\underline{Z}_{in} = R_{in} + jX_{in} = \underline{Z}_{loop} + \frac{(2\pi f M)^2}{\underline{Z}_a}, \tag{6.16}$$

where $\underline{Z}_{loop}$ is the feed loop impedance, $\underline{Z}_a$ is the antenna (radiating) impedance, and M is the mutual inductance between loop and antenna.

$$M = \sqrt{L_{loop} L_a} \tag{6.17}$$

Further calculations lead to expressions for real and imaginary parts of Z_{in} in resonance region, where $f \approx f_0$ [37]:

$$R_{in,0} = R_{in}(f = f_0) = \frac{(2\pi f_0 M)^2}{R_{a,0}}, \tag{6.18}$$

$$X_{in,0} = X_{in}(f = f_0) = 2\pi f_0 L_{loop}. \tag{6.19}$$

- (6.18) states that $R_{in,0}$ depends on the mutual inductance M. As M changes with both the loop geometry and the distance from the radiating antenna, the total input resistance is changed by varying the antenna-loop distance as well as modifying the loop's aspect ratio.

- (6.19) states that $X_{in,0}$ is only subjected to the loop's inductivity L_{loop}. But when changing L_{loop}, the value of the mututal inductance M changes, thus $R_{in,0}$ will be influenced also.

As one can see, an inductively coupled antenna design provides various possibilities to change the antenna's impedance, hence the antenna's attributes. Plenty of degrees of freedom in the design procedure make the inductively coupled match a strong tool for matching a label antenna to various RFID-ICs.
Additionaly inductively coupled matching awards wideband characteristics to the antenna, thus it can be used in various applications and frequency regions. A validation for this statement can be found in [37] or in chapter 6.5, where measurements with an inductively coupled antenna have been done.

6.5 Label Antenna Prototypes

According to previously described antenna architectures (chapter 6.4), prototypes have been designed, built, and analyzed in terms of their stacking behaviour.
Although all tested document tracking environments are near field coupled applications, the label antenna prototypes have been analyzed in terms of their far field properties. This is because the gain value, which is a very important parameter when analyzing the antenna's performance, is not defined in the near field. The gained results can be concluded to achieve knowledge about the label's near field behaviour.

6.5.1 Meander Dipole

Figure 6.36: Meandered dipole

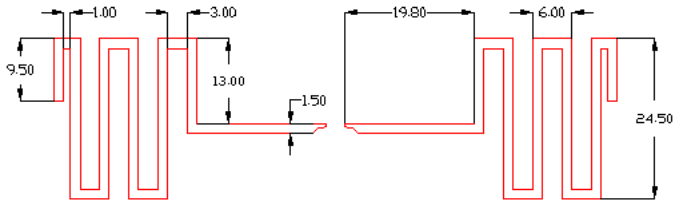

Figure 6.37: Meandered dipole: Dimensions in mm

Label facts:

- Label size: 88 $mm \times 27\ mm$
- Antenna size: 86 $mm \times 25\ mm$
- IC: *NXP-G2x (TSSOP8-housing)*
- Substrate material: *FR4* ($\epsilon_r \approx 4.3$)
- Substrate thickness: 470 μm
- Conductor material: *Copper*
- Conductor thickness: 35 μm
- Dipole length: 309 mm ($\hat{=}$*middle of conductor*)

Simulation results

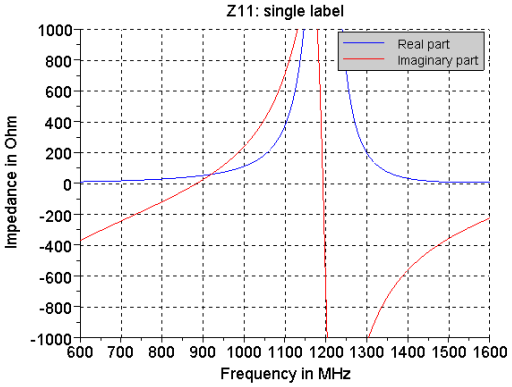

Figure 6.38: Meandered dipole: Impedance (single label)

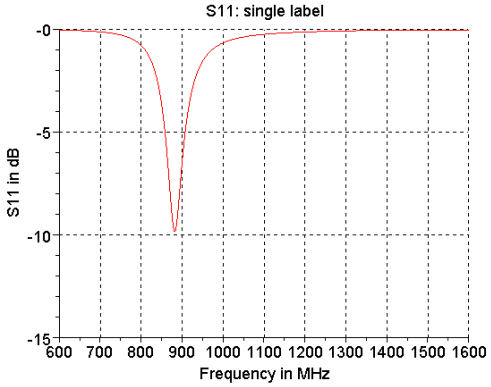

Figure 6.39: Meandered dipole: S11 (single label)

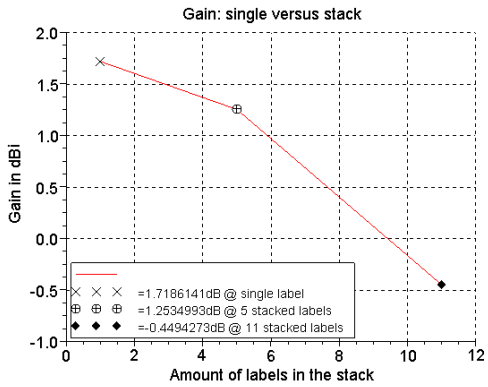

Figure 6.40: Meandered dipole: Gain values @ 865 MHz in comparison

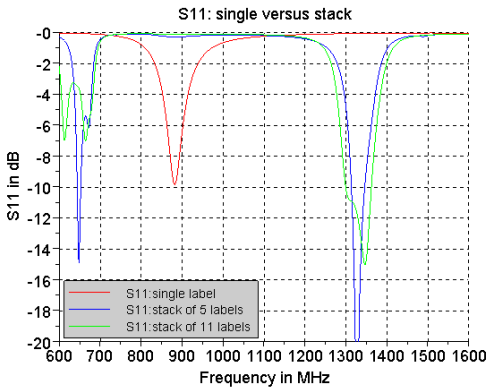

Figure 6.41: Meandered dipole: S11 curves in comparison

Regarding Fig. 6.38 and 6.39, one can see that the dipole's resonance is tuned to values between 850 MHz and 900 MHz. Its behavior when stacking five, respectively eleven labels can be seen in the simulation results depicted in Fig. 6.40 and 6.41. Comparing the S-parameter curve of the dipole label in single and stacked mode (Fig. 6.41) shows a significant drift in the resonance frequency. Increasing the label amount from one to five labels shifts the resonance about 400 MHz to higher values and 250 MHz towards lower values. As the resulting resonances lay outside our frequency of interest, the expected performance of this prototype in stacked mode is bad. Nevertheless, further increasing the label amount leads to negligible resonance shifts. It is an important fact that some kind of saturation occurs, which will be used when designing further prototypes.
A further conclusion out of this investigation is that there are losses in gain. Fig. 6.40 depicts these losses when increasing the amount of stacked labels. Chapter 6.5.4 discusses this theme.

Pmin-measurement

Simulations provide a very good approximation about a label's behavior under certain condidtions. To prove the simulated results as well as collect additional knowledge, a Pmin-measurement in an anechoic chamber has been done.
After building prototypes out of FR4-material with copper traces, the necessary power to get a backscattered answer was measured under defined conditions.

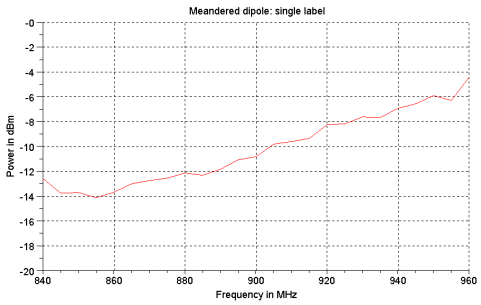

Figure 6.42: Meandered dipole: Pmin-measurement (single label)

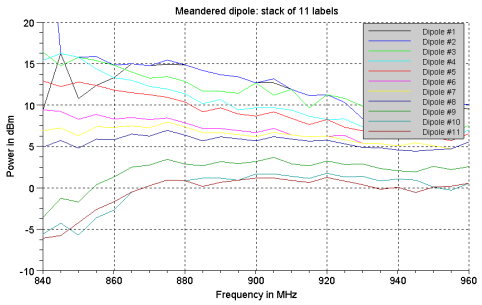

Figure 6.43: Meandered dipole: Pmin-measurement (stack of 11 labels)

With Pmin-values from $-14\ dBm$ @ 850 MHz to $-10\ dBm$ @ 910 MHz, the single label performs well at the frequencies of interest (Fig. 6.42). When stacking 11 labels, the bulk of labels cannot be read because the Pmin-value is too high. Up to spread of 20 dB in performance between the labels, within the frequencies of interest leads to bad stacking behavior. This can be explained by previously found conclusions (shifted resonances paired with losses in gain).

To get rid of these problems, another dipole prototype has been developed.

Meander dipole second version

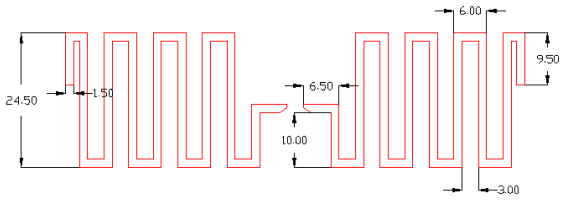

Figure 6.44: Meandered dipole v2: Dimensions in mm

Its resonance is tuned to lower values to consider the resonance shift effect when stacking the labels. More meandering affects the impedance, thus the resulting resonances lay at 750 MHz and 1520 MHz (Fig. 6.45 and 6.46). Goal of this approach is to get the shifted resonance meeting the frequency of interest.

Simulation results

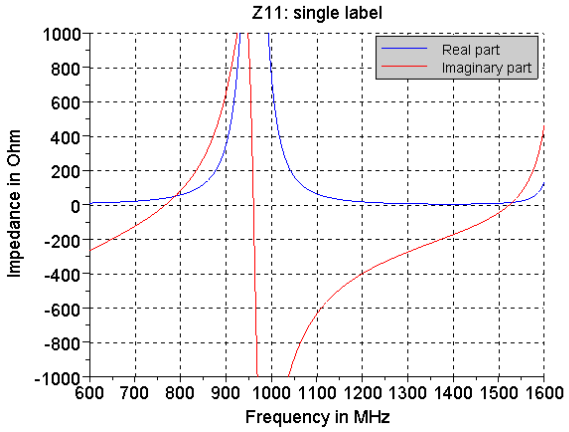

Figure 6.45: Meandered dipole v2: Impedance (single label)

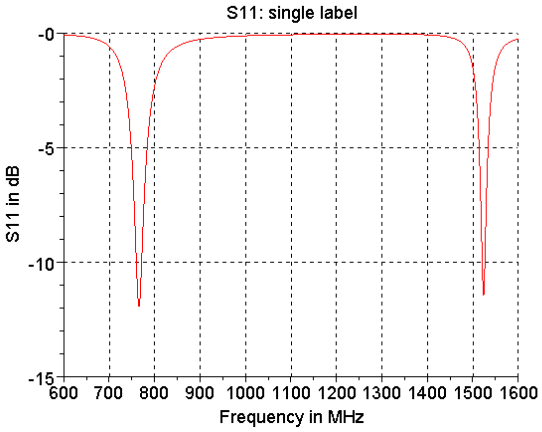

Figure 6.46: Meandered dipole v2: S11 (single label)

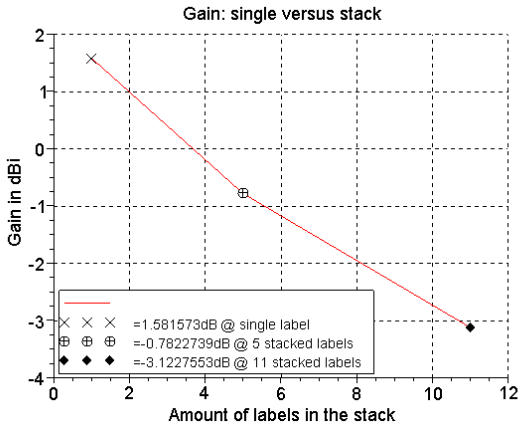

Figure 6.47: Meandered dipole v2: Gain values @ 865 MHz in comparison

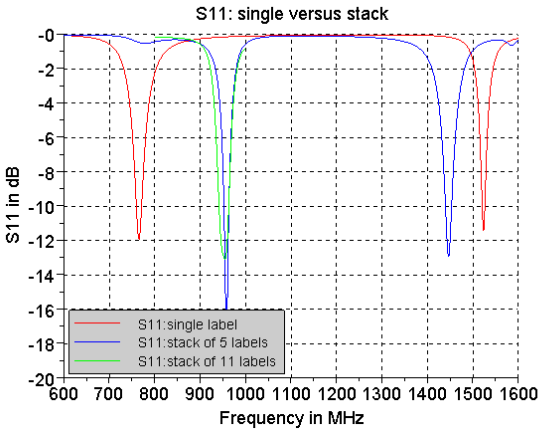

Figure 6.48: Meandered dipole v2: S11 curves in comparison

As one can see in Fig. 6.48, the resulting resonances in stacked mode are close to the region of interest, but for the price of higher losses in gain. This effect is explained in section 6.5.4.

Pmin-measurement

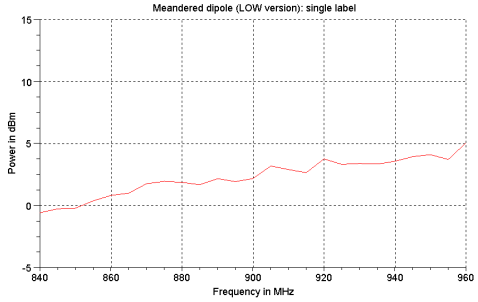

Figure 6.49: Meandered dipole v2: Pmin-measurement (single label)

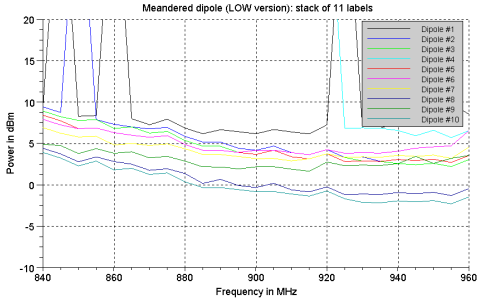

Figure 6.50: Meandered dipole v2: Pmin-measurement (stack of 11 labels)

A significant improvement in stacking behavior is shown in Fig. 6.50 at a frequency of 900 MHz. The worst performing label has a Pmin value of ≈ 7 dBm compared to a value of ≈ 13 dBm (Fig. 6.41) at the first version. Additionally, the spread between the best and the worst performing label decreased. The price for the improved stacking performance can be seen looking at Fig. 6.49. As the resonance is outside our frequencies of interest, the single label deteriorates its Pmin value from -11 dBm (first version) to 2.5 dBm (second version). For further improvement of the design, a T-matched label has been developed (section 6.5.2).
The outliers when looking at the two worst performing Pmin curves at Fig.6.50 can be explained due to the sensitivity of the measurement setup. Tags with Pmin values around +7 Bm operate at the border of the setups detecting sensitivity and this leads to outliers which can be ignored.

Conclusions

A dipole design can be tuned to provide satisfying performance for document tracking applications. As dipoles are narrow-band designs, it is very difficult to tune the single label's resonance in a way that it meets the frequency region of interest in various stacking scenarios. As controlled detuning leads to bad performance when reading single labels, the trade-off between performance in single mode and in stacked mode does not make a dipole the structure of prime selection for a document tracking application.

6.5.2 T-Matched Dipole

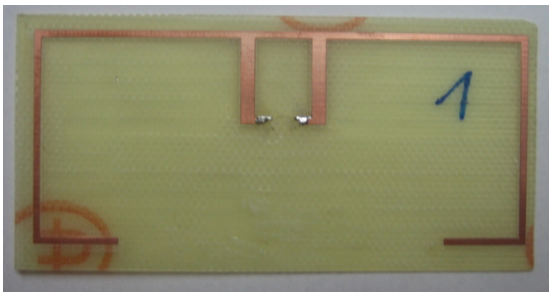

Figure 6.51: T-matched dipole

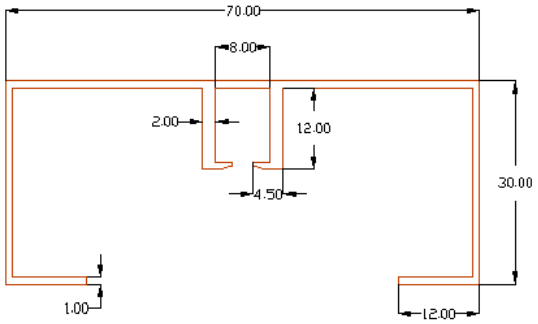

Figure 6.52: T-matched dipole: Dimensions in mm

Label facts:

- Label size: 74 $mm \times 36\ mm$
- Antenna size: 70 $mm \times 30\ mm$
- IC: *NXP-G2x (TSSOP8-housing)*
- Substrate material: *FR4* ($\epsilon_r \approx 4.3$)
- Substrate thickness: 470 μm
- Conductor material: *Copper*
- Conductor thickness: 35 μm
- Antenna length: 150 mm ($\hat{=}$*middle of conductor*)
- Loop size: 12 $mm \times 12\ mm$ (*outer edge*)

This prototype provides matching advantages as the additional loop can be used to adjust the antenna's impedance (see section 6.4.3).The remaining radiating body provides better performance as there is no meandering on it. The follwing simulation results and measurements charaterize its single and stacking behaviour.

Simulation results

As the T-matched design provides good matching in a frequency region between 850 MHz and 1 GHz, this design approach shows more broad band behavior than the dipole design (Fig. 6.54). When analyzing its stacking behavior, a $\approx$ 450 MHz resonance shift can be detected when increasing the label amount in the stack from one to five labels (Fig. 6.56). Further increasing the label amount leads to no significant resonance shifting, but alters the form of the S11 curve. Considering this behavior, similar effects occured when analyzing the dipole design. Fig. 6.55 depicts the losses in gain as a function of increased label amounts. The gain was always calculated at a frequency of 865 MHz,

so only slight losses can be seen because the regions of good matching in stacked mode are located outside the 865 MHz region (see section 6.5.4 for details).

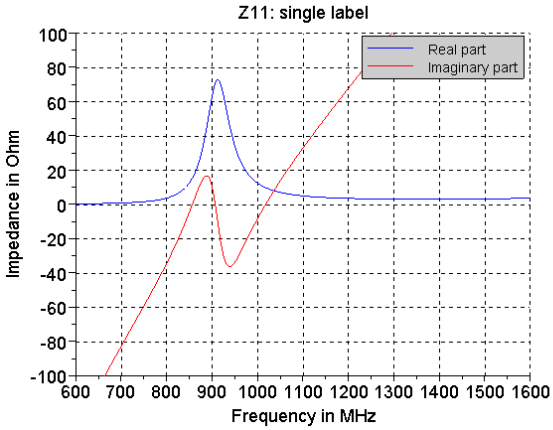

Figure 6.53: T-matched dipole: Impedance (single label)

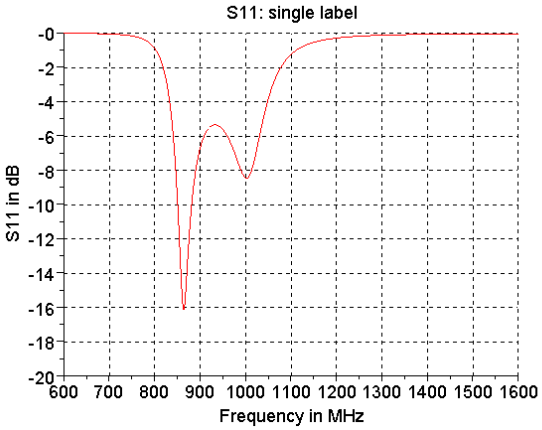

Figure 6.54: T-matched dipole: S11 (single label)

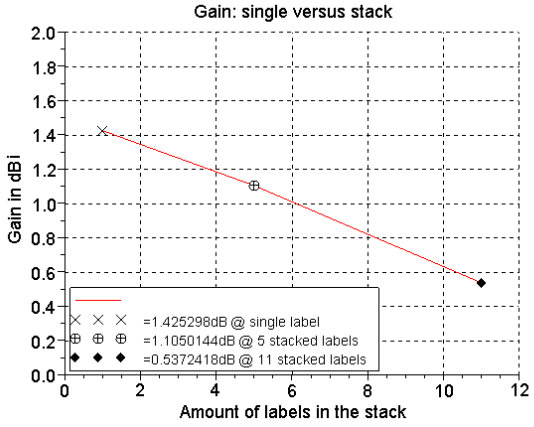

Figure 6.55: T-matched dipole: Gain values @865 MHz in comparison

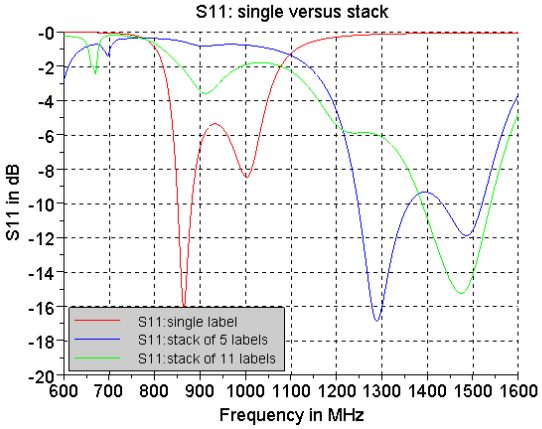

Figure 6.56: T-matched dipole: S11 curves in comparison

Pmin-measurement

- Fig. 6.57: The broad band behavior can be seen as the measured Pmin value is between -12 dBm and -14 dBm along the whole frequency axis. These values provide a good performance when using the single label in an application.

- Fig. 6.58: Savings in measurement time and prototype building time were the reasons for testing this structure with only five labels in the stack.
  The discordant values, when looking at the curve of *Label 1*, are due to the measurement setup's sensitivity and are not considered in the following.

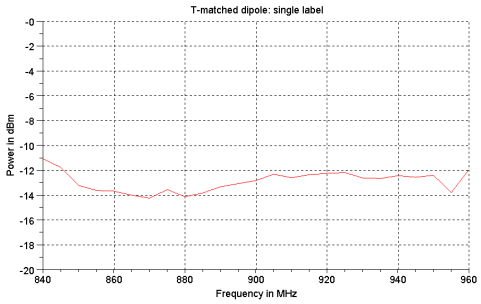

Figure 6.57: T-matched dipole: Pmin-measurement (single label)

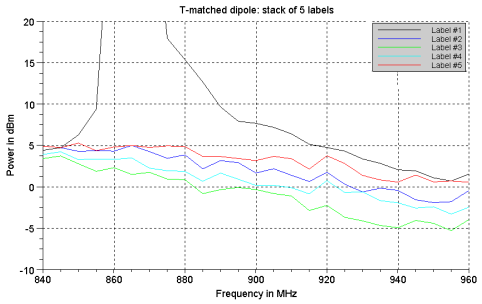

Figure 6.58: T-matched dipole: Pmin-measurement (stack of five labels)

As one can see, all curves show a negative gradient towards higher frequencies. Due to this reason better performance in stacked mode could be reached when controlled detuning, like it has been done with the dipoles, is applied to the T-matched structure. The goal would be laying the region of best performance in stacked mode near the frequency region of interest. This can be reached with pre-tuning the single label's resonance frequency.

Applying the detuning approach to the T-matched design

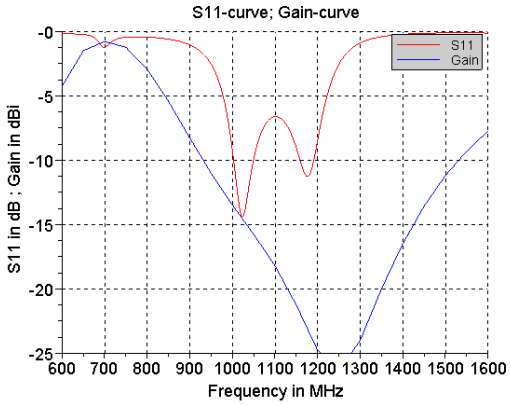

Figure 6.59: Detuned T-matched dipole: S11 curve and gain curve (stack of five labels)

Following the *Detuning* approach and tuning the single label in a way that the resonance in stacked mode lies near the frequency region of interest was unrewarding as it can be seen in Fig. 6.59. It shows the S11 curve of the middle label in a stack of five labels and its gain progression as a function of frequency.
As one can see, significant losses in gain make this approach excepted from further developement as good stacking performance cannot be reached using it.

6.5.3 DTL Design (Inductively Coupled)

D*ocu* – **T***ilt* – **L***oop* – *design* . . . *DTL* – *design*

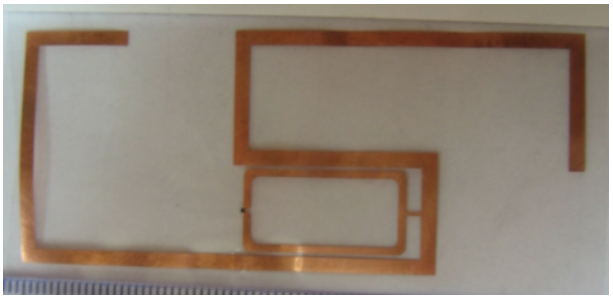

Figure 6.60: DTL design

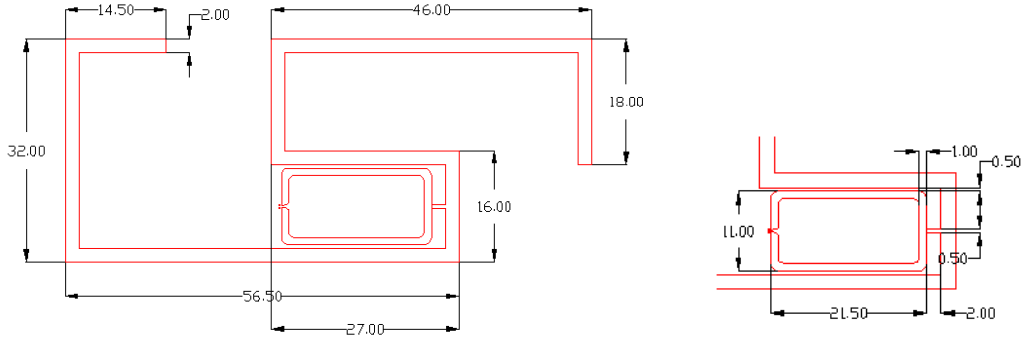

Figure 6.61: DTL design: Dimensions in mm

Label facts:

- Label size: 77.5 $mm \times 34\ mm$
- Antenna size: 75.5 $mm \times 32\ mm$
- IC: *NXP-G2il (Assembled with flip-chip package)*
- Substrate material: *PET*
- Substrate thickness: $\approx 50\ \mu m$
- Conductor material: *Copper*
- Conductor thickness: $\approx 16\ \mu m$
- Antenna length: 214 mm ($\hat{=}$*middle of conductor*)
- Loop size: 21.5 $mm \times\ 11mm$
- Tick size: 2 $mm \times 0.5\ mm$

Developing an inductively coupled design provides some advantages. A good matching to the IC can be achieved by varying the loop's geometry and leaving the radiating body nearly unaffected. This was necessary because the used IC was changed from the *NXP-G2Xl-* to the *NXP-G2il-* IC during the design process.
Tilting the design of the radiating body was done for optical and geometrical reasons.

Looking at Fig. 6.61, one can see a small stripe connecting the loop to the radiating stripe. This was necessary because inductively coupled structures are covered by a patent specification, which can be circumvented using the small stripe (which is called "tick" in the following). The tick is positioned in a way that it shows the smallest possible effects on the functionality of the label. Hence, an area for the tick placement with low current density has been chosen.

Simulation results:

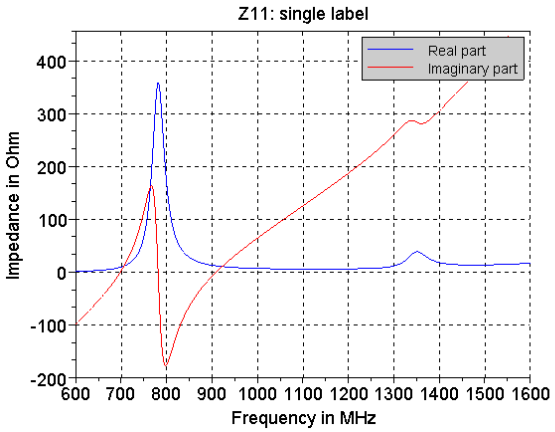

Figure 6.62: DTL design: Impedance (single label)

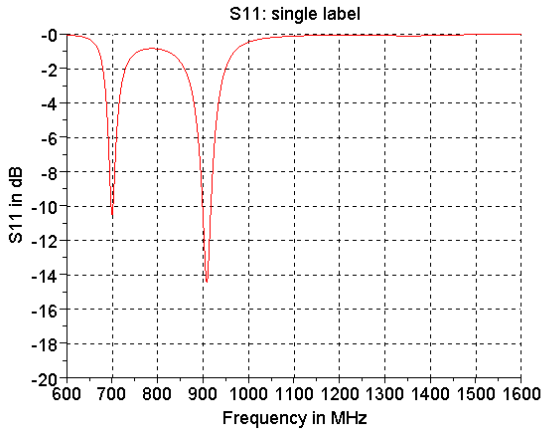

Figure 6.63: DTL design: S11 (single label)

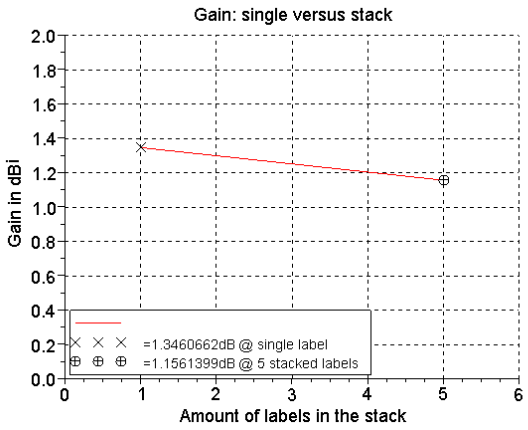

Figure 6.64: DTL design: Gain values @ 865 MHz in comparison

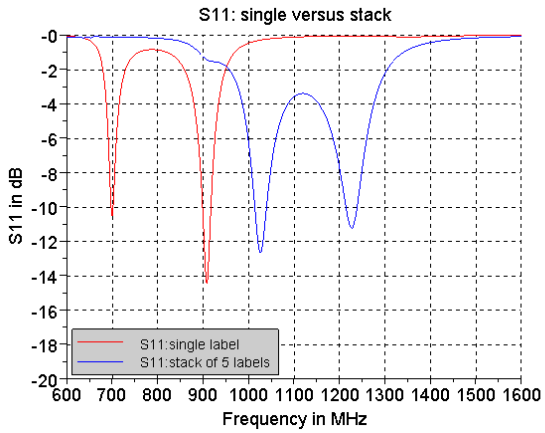

Figure 6.65: DTL design: S11 curves in comparison

This design approach leads to two resonances at $\approx 700\ MHz$ and $\approx 900\ MHz$ (Fig. 6.63). Due to this reason, good performance of the single label at 915 MHz can be forcasted. Simulating a stack of five labels results in the well-known resonance shift

(from previous simulations) with a value of ≈ 300 MHz (Fig. 6.65). Having the first peak of the S11 curve at a frequency of 1 GHz is good for the label's stacking behavior, as this provides a good trade-off between matching and gain losses (Fig. 6.64 and 6.65)(see section 6.5.4).

Pmin-measurement

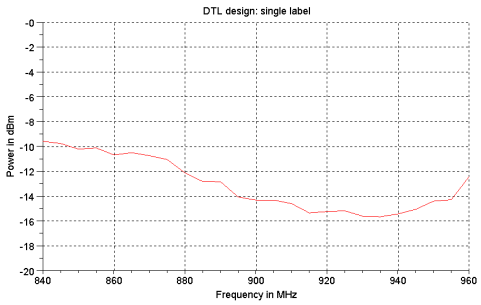

Figure 6.66: DTL design: Pmin-measurement (single label)

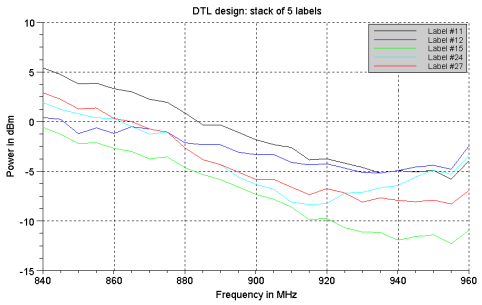

Figure 6.67: DTL design: Pmin-measurement (stack of five labels)

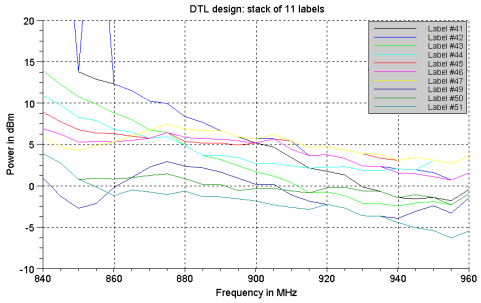

Figure 6.68: DTL design: Pmin-measurement (stack of 11 labels)

Fig. 6.66 shows the measured Pmin curve of the single label. Pmin values between -10 dBm and -16 dBm assure good performance when the single label is appointed in an application. Stacking five labels results in a Pmin value of -2 dBm @ 900 MHz of the worst performing label. This value decreases to $+6$ dBm @ 900 MHz when stacking an amount of 11 labels (The outlier, which can be seen in Fig 6.68, is again due to the sensitivity of the measurement setup). As the labels read range ($= RR$) at a Pmin value of $+6$ dBm is 82 cm (according to (6.20)), this design can be used when reading stacks of documents in a document tracking application as the smart shelf or the document tray.

$$\lambda = 0.3279\ m\ @\ 915\ MHz$$

$$Pmin_{dB} \approx +6\ dBm\ @\ 915\ MHz$$

$$P_{Reader} = 4\ W_{EIRP} \hat{=} 36\ dBm$$

$$RR = \frac{\lambda}{4\pi}\sqrt{\frac{P_{Reader[W]}}{P_{min[W]}}} = 0.825\ m \quad [3] \tag{6.20}$$

Formula 6.20 calculates the read range using the Pmin value and the radiated reader power, based on the Friis transmission equation [35].
According to the measurement and simulation results, good stacking behaviour of the DTL-design can be forcasted. Application tests to prove this forecast are given in the next chapter.

Radiation pattern

For a perfect label placement in the application, knowledge about the antenna's radiation pattern is necessary. Figure 6.69 shows a simulated 3D-plot of the antenna's radiation properties.

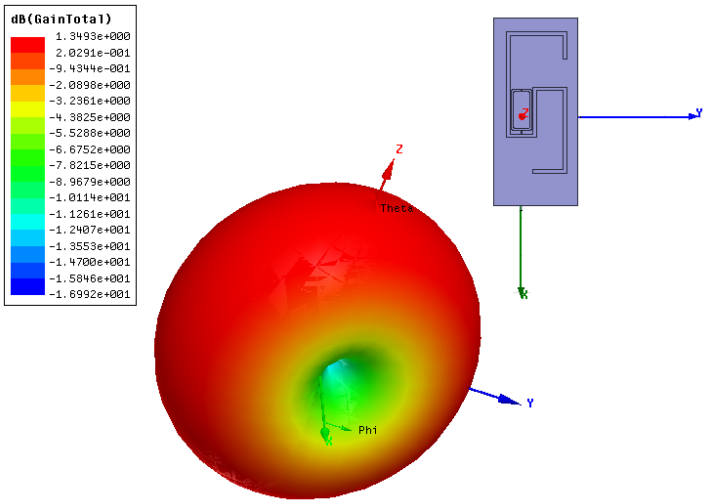

Figure 6.69: DTL design: 3D polar plot (Gain)

As one can see, the DTL-design shows a dipole-like radiation "donut". Due to this radiation properties, the labels have to be placed in a way that the long sides align with the polarization of the reader antenna. Avoiding a placement where the nulls on the small label side align with the reader antenna assures good label performance.

6.5.4 Connection between Matching and Gain Losses in Stacked Mode

Gain losses, when operating with a stack of labels, can be explained using (6.21), where the gain is defined as a product of efficiency and directivity [3]:

$$G = e_{cd}D. \tag{6.21}$$

Whereas the directivity is dependend on the antennas radiation pattern, the total efficiency e_0 [3] contains:

$$e_0 = e_r e_{cd}, \tag{6.22}$$

where e_r is the mismatch efficiency, and e_{cd} contains the conduction efficiency and the dielectric efficiency.

In (6.21) only the conduction and dielectric efficiencies are included, as this aligns with the IEEE standards. A gain value which includes the mismatch efficiency is often called absolute gain [3].

When analyzing a single antenna, the e_{cd} value depends on the conductive and dielectric antenna material and the occuring losses. But when dealing with closely coupled antennas, there are also conductive and dielectric losses due to the presence of the neighbored antennas. As a result (according to (6.21)) the gain value decreases.

Although the mismatch efficiency is not used for calculating the gain value, one can observe high losses in gain within a region of good matching when dealing with a stack of labels. As a good S11 value means a good energy transfer within the antenna, high currents are flowing through the arms of the antenna, meaning higher losses, due to the presence of the other labels in the stack, followed by a reduced gain value.

Another effect on the gain evoked by closely coupled antennas may be a change of the antenna's directivity value. Because well-matched labels in the stack have strong influence on each other's radiation patterns, the directivity values change.

6.5.5 Design Guide for a "Document Tracking" Label

Concluding the overall design process leads to some rules for designing a label, optimized for close coupling scenarios with a large amount of transponders. → *Document Tracking*

- Main effects of close coupling:
  - Resonance frequency shift
  - Losses in gain

- **Controlled detuning**: The single label should be tuned in a way that the resonances meet the frequency region of interest in stacked mode and mismatch losses stay tolerable.

- Repletion: The big shift in resonance occurs when stacking the first approximately five to ten labels. Further increasing the stack leads to an altered form of the S11 curve, but has only a slight effect on the resonance shift. This allows forcasting the resonance shift when simulating only a small amount of labels.

- Performance Trade-off: Detuning the single label in favor of good performance in stacked mode leads to decreased performance in single mode. Using broad band designs helps to keep this trade-off acceptable.

- Gain losses: To keep losses in gain minimal, the shifted resonance in stacked mode should lay beside the frequency of interest. When the slope of the peak in the S11 curve lays within the frequency region of interest, matching is still good enough, and gain losses stay tolerable.

6.6 Application Tests

Testing the developed label under real-world conditions is an important step and finishes the design process. In order to cover a wide range of document tracking applications, two test scenarios with defined conditions have been developed. Previously introduced UHF readpoints, the smart shelf, and the simulated document tray (UHF patch system), have been used for tests, for which the labels were applied to document materials with different thickness. To evaluate the developed label's performance, a competitor label was tested (Tagsys DocTrak), and the results were compared.

6.6.1 Smart Shelf Tests

These tests were executed with the *NXP DTL-design* and the *Tagsys DocTrak* design.

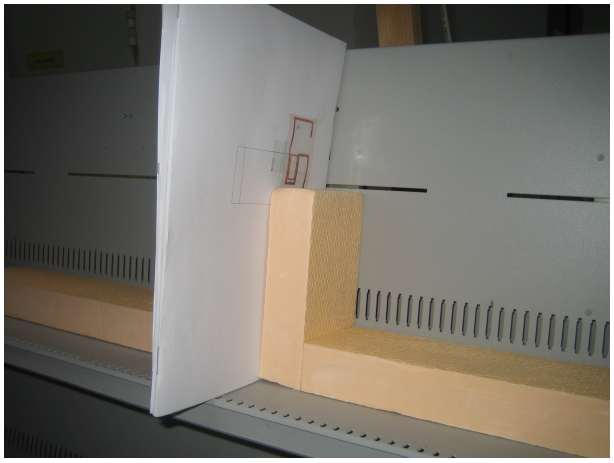

Figure 6.70: Smart shelf with tagged paper sheets

Setup:

- Reader: Sirit Infinity 510 [8]
- Multiplexer: SkyeTek MUX [24]
- Antenna: Smart shelf with four activated slots
- Software: ASC Test Suite

Documents (materials) with different thicknesses were used during the testing:

- Paper sheet: 0.1 *mm* thickness
- Flyer sheet: 0.24 *mm* thickness
- Folder: 1.34 *mm* thickness

To cover the worst case stacking scenario, all labels were aligned at the same position on the sheets, as this assures maximal coupling effects.
The tagged document stack was positioned in the shelf as shown in Fig. 6.70. Reaching a 100% read rate leads to add up five additional labels to the stack and therefore further read tries.

Labels stuck on paper sheets

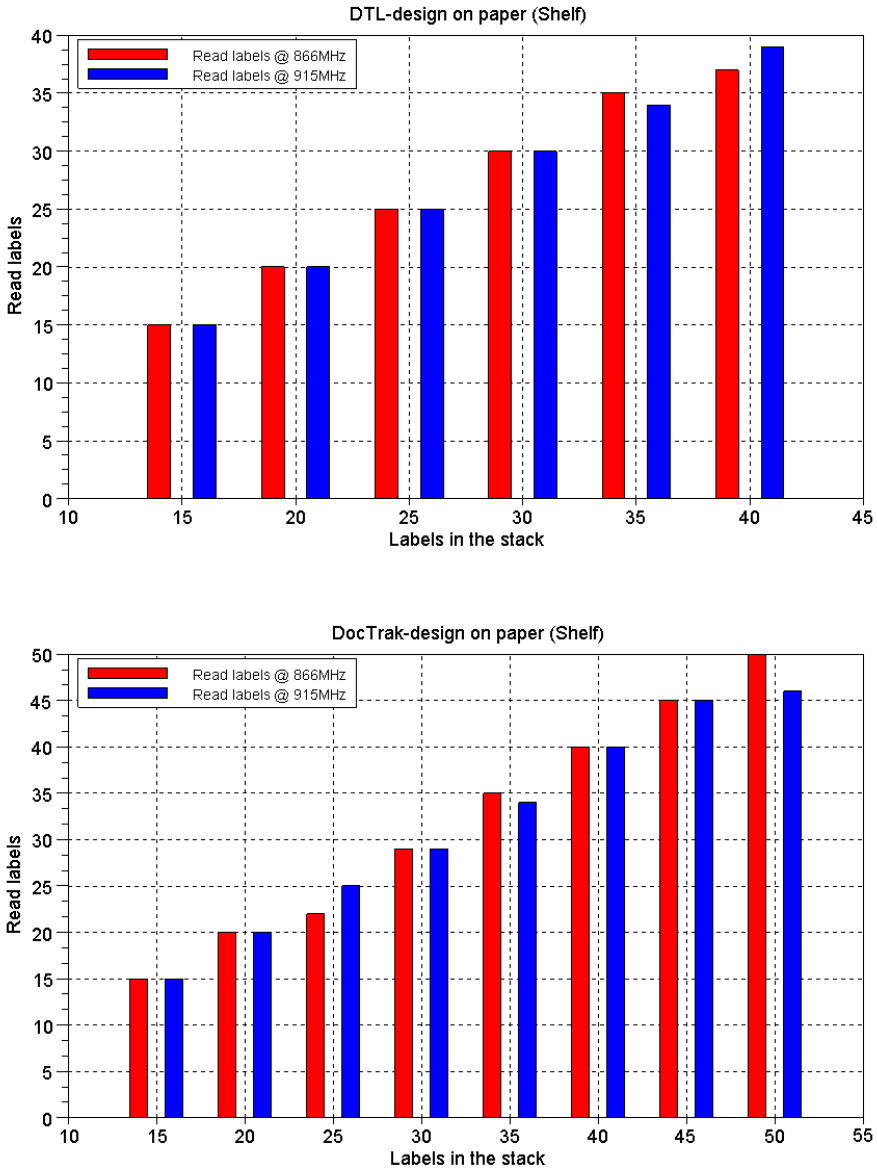

Figure 6.71: App-test results with *DTL-design* and *Tagsys DocTrak* on paper material (shelf)

- DTL-design: The DTL-design shows failsafe performance up to the label amounts between 30 and 35 sheets.
- DocTrak: At first glance, the upper borderline seems to be at an amount of 45 stacked labels. But read problems occured at a label amount of 25 stacked labels, because more than one label could not be recognised by the reader in US-frequency region.

Labels stuck on flyer sheets

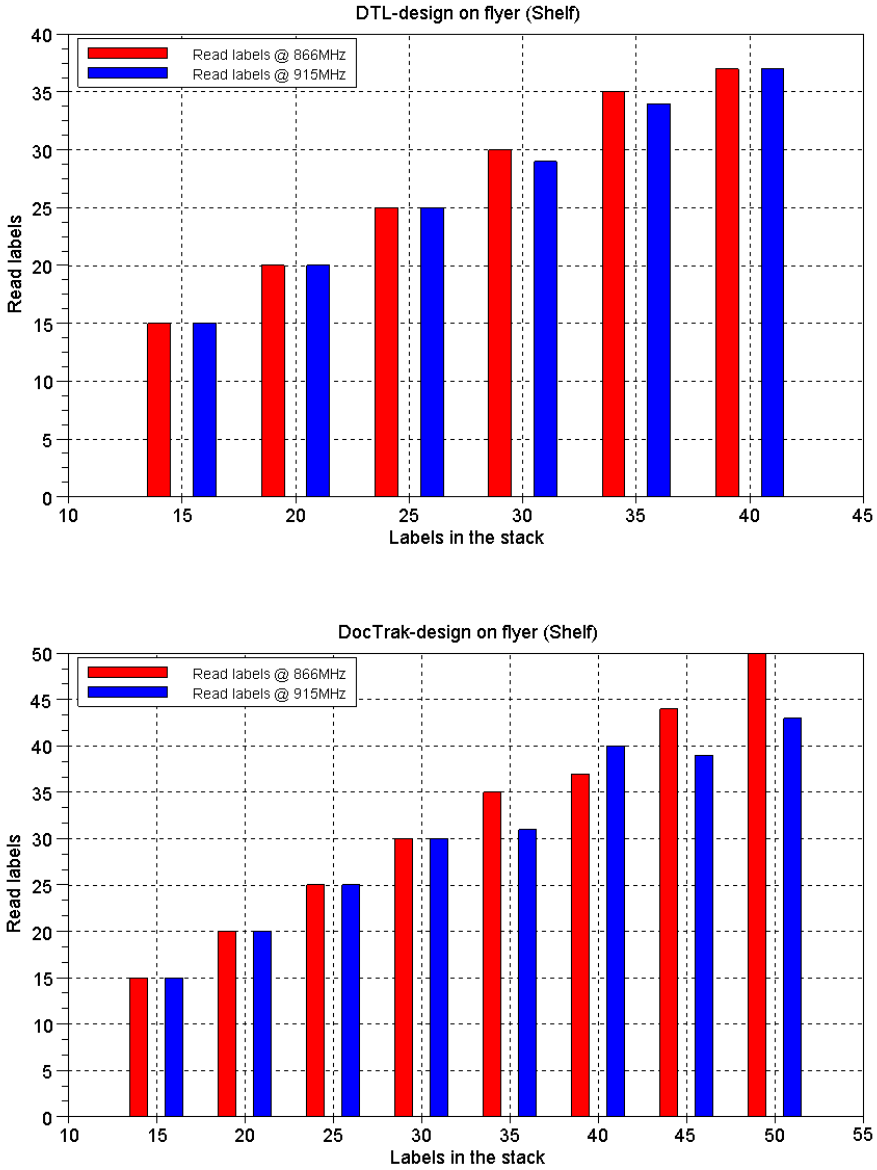

Figure 6.72: App-test results with *DTL-design* and *Tagsys DocTrak* on flyer material (shelf)

- DTL-design: Upper borderline at approximately 30 sheets
- DocTrak: Upper borderline at approximately 35 sheets

Labels stuck on folders

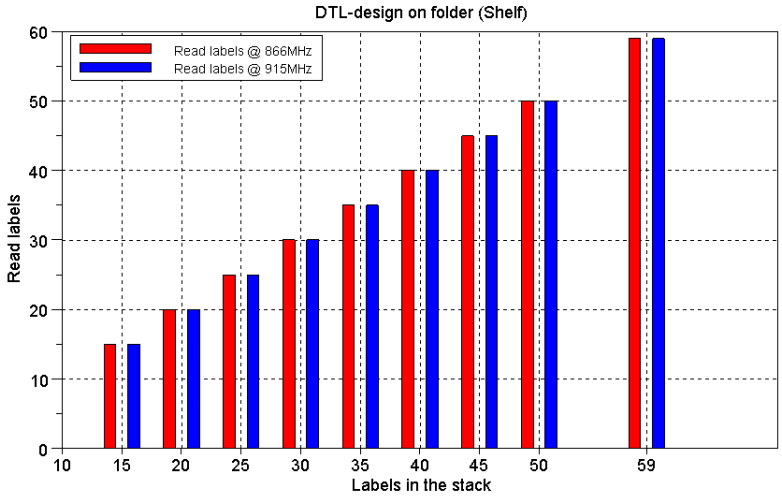

Figure 6.73: App-test results with *DTL-design* on folder material (shelf)

Fig. 6.76 shows the results achieved with the DTL-design applied on folders. The folder thickness of 1.34 *mm* reduces coupling in order that an amount of 59 labels in the stack could be read (59 labels were available). As all the simulations have been done with a spacing of 1 *mm* between the labels, they are optimized for this distance, which explains the very good results when testing with folders.

Conclusions

Due to production reasons, the performance of the single labels show a deviation, thus a read fail of one label is within the scope and should be tolerated.

- The DTL-design is optimized for label spacings around 1 *mm*, thus it shows very good performance when operating with distances near this region. → up to 59 stacked labels
- 30 read labels with a spacing of 0.1 *mm* between them makes the DTL-design a good solution when dealing with various document tracking applications.
- On average, the DocTrak design allows one to read stacks with five more labels than the DTL-design.
- Read problems at specific stack sizes may occur when using the DocTrak design.

6.6.2 Tests with a Patch Antenna

To cover also test scenarios with document trays (like in the HF-section), a simple patch antenna was used to simulate a UHF document tray.

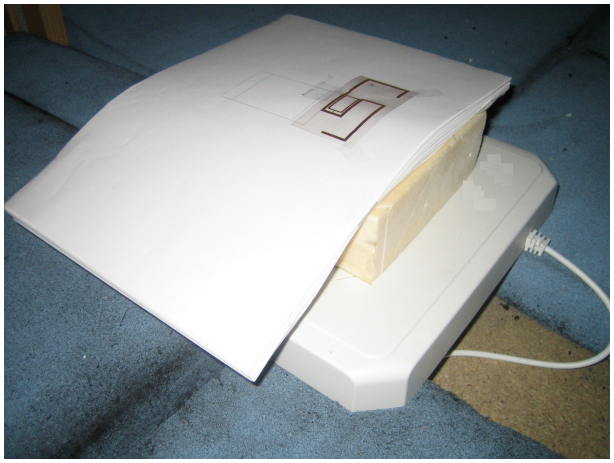

Figure 6.74: Simulated document tray with tagged paper sheets

Setup:

- Reader: Sirit Infinity 510 [8]
- Antenna: Feig patch antenna [25]
- Software: ASC Test Suite

Documents (materials) with different thicknesses were used during the testing:

- Paper sheet: 0.1 mm thickness
- Flyer sheet: 0.24 mm thickness
- Folder: 1.34 mm thickness

Fig. 6.74 explains the measurement setup. All tests were executed as described in the smart shelf section (chapter 6.6.1), but the alignment between labels and reader antenna changed. Whereas in the smart shelf application all labels have the same distance to the antenna, the distance between the document tray and the label depends on the label position within the stack, because the stack of labels is positioned on top of the patch antenna.

Labels stuck on paper sheets

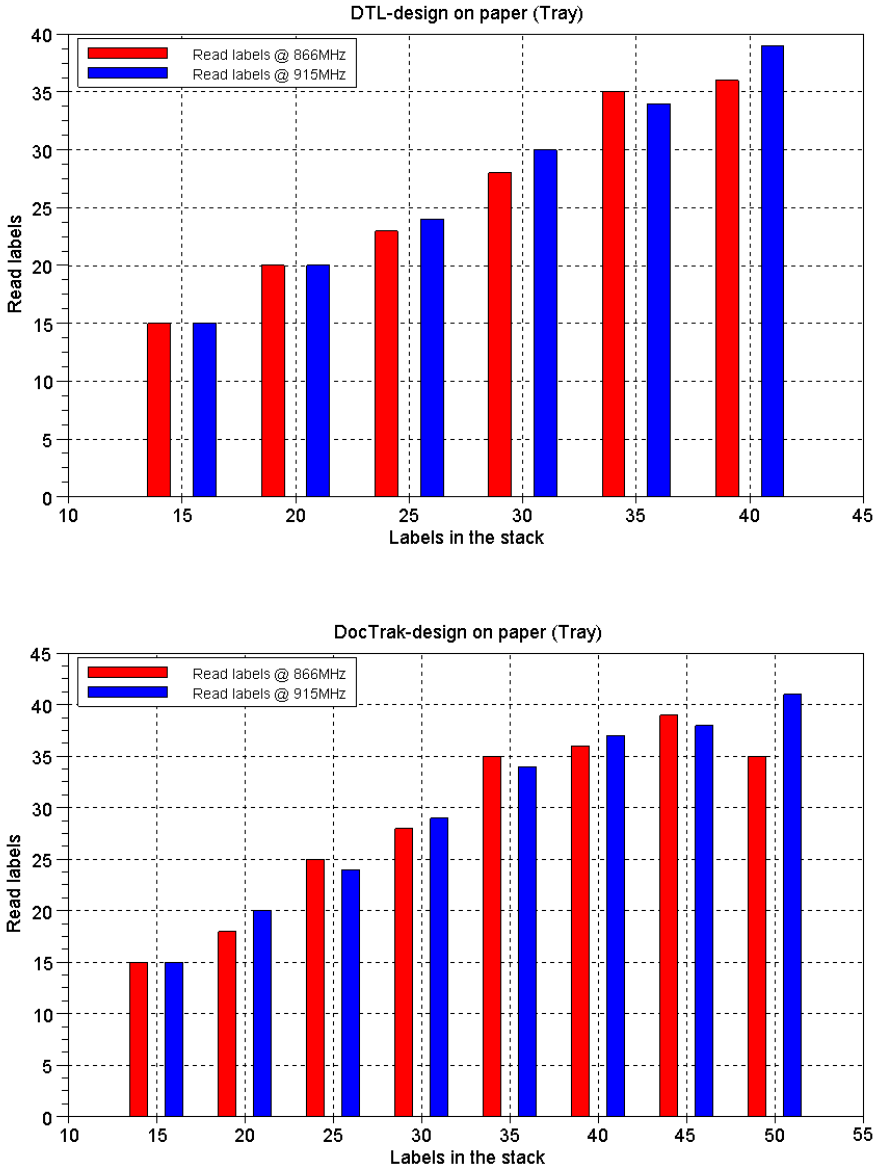

Figure 6.75: App-test results with *DTL-design* and *Tagsys DocTrak* on paper material (tray)

- DTL-design: Upper borderline between 20 and 25 sheets
- DocTrak: Upper borderline between 15 and 20 sheets

Labels stuck on folders

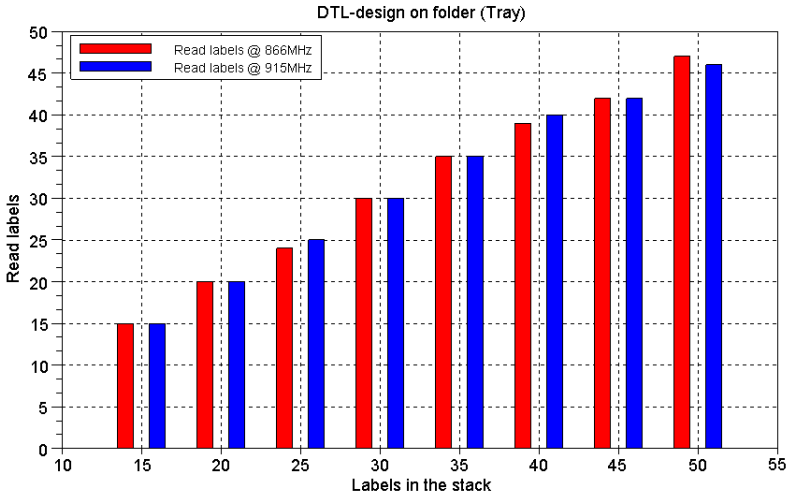

Figure 6.76: App-test results with *DTL-design* on folder material (tray)

- DTL-design: Upper borderline between 35 and 40 labels, but with read problems at a stack size of 25 sheets in EU-frequency region.

Conclusions

- This application provides more read problems than the smart shelf, as drawn by the resulting decrease of stack sizes.
- The DTL-design shows good performance when stacking sheets with spacings around 1 mm.
- The DTL-design performs better in the US-frequency region.
- The DocTrak label has more read problems due to occuring read holes at specific stack sizes.

7 Summary

7.1 HF-Domain

Two HF-demo applications from NXP, as well as two competitor systems have been under investigation. Using the NXP-HF smart shelf or the document tray allows reading up to approximately 45 tags in close proximity to each other within a stack of documents.
Knowledge about the close coupling behaviour of the labels has been acquired using electrically equivalent circuits and introducing a mathematical model. The model, together with the method of eigenvalue decomposition, provides a strong tool for predicting the resonance frequency detuning happening due to multiple labels in the field of a reader antenna. It could be observed that the leading resonance frequency peak strives towards lower values and highly depends on the number of labels in the stack as well as the coupling factor among them (Fig. 7.1). As pretuning a labels resonance frequency is necessary for achieving good performance when dealing with close coupled antennas, one has to find the best compromise between performance in single and stacked mode for the specific application.

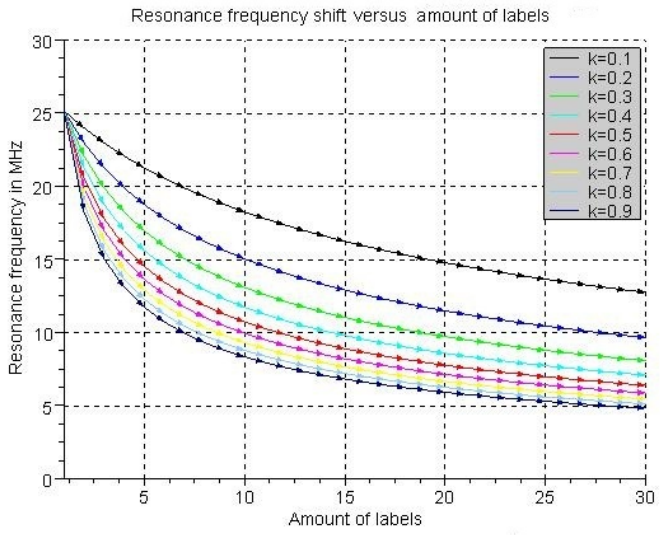

Figure 7.1: Resonance shift with label amount variation and coupling factor variation

For a good performing document tracking application, it is also necessary to place the labels on the documents in a proper way with respect to the reader antenna. For this

reason, the reader antennas of the demo systems have been analyzed in terms of their field distribution, and the best position for the labels has been determined as the point where the maximum field intensity occurs.

7.2 UHF-Domain

Testing the developed UHF document tracking label antenna together with the demo systems delivered 100% succesful reads with amounts between 25 and 59 labels in the stack. The best results have been achieved using approximately 1.34 mm spacing between the label antennas, because the developed labels have been optimized for a distance of 1 mm between them.

Measurements and simulations with commercially available UHF labels delivered knowledge about the occuring coupling effects when dealing with closely coupled UHF antennas. Two main effects, evoked by close coupling, have been detected during the investigations:

- Resonance frequency shift (Fig 7.3): The resonance frequency of a label antenna has to be pretuned to meet the frequency range of interest in the final application scenario. The frequency shift depends on the number of labels in the stack, as there is a strong shift when stacking the first one to five labels and a negligible shift when stacking amounts greater than 10-15 labels. Using this knowledge, one can design a label which is optimized for large stacking amounts with simulating just a small amount.

- Losses in gain (Fig 7.2): Stacking a large amount of antennas leads to high losses in gain due to influences on the directivity and efficiency parameters. The better the antennas' matching within the frequency region of interest, the higher the losses are in gain (in stacked mode), as good matching leads to higher current flow in the arms of the antenna.

The final document tracking UHF antenna design (DTL-design) uses inductive coupling. Simulations and measurements have shown that this structure is the optimum choice to deal with the effects mentioned above. Its broadband behavior also helped to find a good compromise between reading performance in single and in stacked mode.

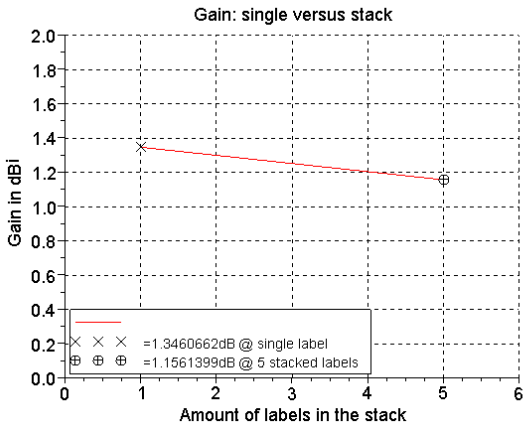

Figure 7.2: DTL design: Gain values @865 MHz in comparison

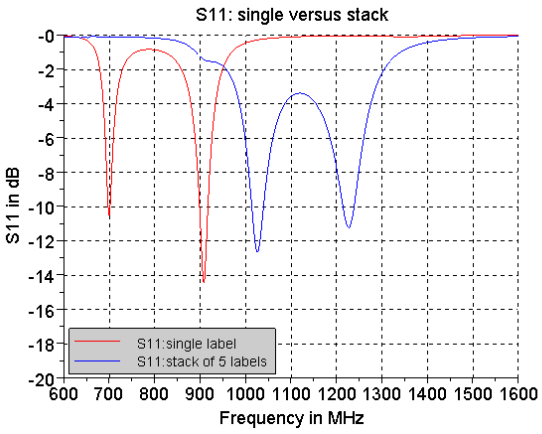

Figure 7.3: DTL design: S11 curves in comparison

For a good performing application, it is also necessary to know the optimal placing of the label stack with respect to the reader antenna. As the investigated document tracking application scenarios deal with label stacks placed within the near-fields of the reader antennas, the reader antennas' near fields have been measured in terms of distribution and intensity. Using the results of the scanned smart shelf rack, regions for optimal label placing relating to the reader antenna have been detected and can be used for further optimization of the application.

The application tests have shown comparable performance to a commercially available UHF label optimized for document tracking purposes. As the IC of the DTL-design has higher sensitivity than the IC used for the DocTrak label, the DTL-design can be further optimized to achieve much higher read rates.

8 Bibliography

[1] Klaus Finkenzeller. *RFID-Handbuch.* Carl Hanser Verlag, Kösel, 3. Auflage, 2002.

[2] Karoly Simonyi. *Theoretische Elektrotechnik.* Bad Langensalza, Johann Ambrosius Barth, 10 Auflage, 1993.

[3] Constantine A. Balanis. *Antenna Theory.* John Wiley & Sons, Third Edition, 2005.

[4] Feig LR2000 RFID reader.

. http://www.feig.de/ [Status 03.2011].

[5] ISO 15693 standard.

. http://www.iso.org/ [Status 03.2011].

[6] Feig OBID i-scan HF Tuning Board.

. http://www.feig.de/ [Status 03.2011].

[7] The Institute of Electrical and Electronics Engineers. *IEEE Std. 100 The Authoritative Dictionary of IEEE Standards Terms.* IEEE, 7th Edition, New York, 2000.

[8] Sirit Infinity 510 RFID reader.

. http://www.sirit.com/ [Status 03.2011].

[9] UPM WebX RFID label.

. http://www.upmrfid.com [Status 03.2011].

[10] Poynting Patch-A0025 antenna.

. http://www.poynting.co.za/ [Status 03.2011].

[11] EPCglobal. Class 1 Generation 2 UHF Air Interface Protocol Standard Gen 2.

. $http://www.gs1.org/gsmp/kc/epcglobal/uhfc1g2$ [Status 09.2012].

[12] J.Bruckbauer E.Merlin H.Witschnig, E.Sonnleitner. *Eigenvalue analysis of Close Coupled 13,56MHz RFID labels.* IEEE, 2006.

[13] Magellan Technology.

. http://www.magellan-rfid.com/ [Status 03.2011].

[14] Magellan Technology. About pjm technology.

. http://www.magellan-rfid.com/about-PJM/home [Status 03.2011].

[15] Magellan Mars24 system.

. $http://www.magellan-rfid.com/products-services/readers\_MARS$

[Status 03.2011].

[16] Magellan single axis antenna.

. http://www.magellan-rfid.com/products-services/antennas [Status 03.2011].

[17] Magellan MDOCR-2505 Document Tray Reader.

. $http://www.magellan-rfid.com/products-services/readers\_desktop$

[Status 03.2011].

[18] NXP Semiconductors .

. http://www.nxp.com/ [Status 03.2011].

[19] FeigID ISC.ANT.MUX 8 Channel Multiplexer.

. http://www.feig.de/ [Status 03.2011].

[20] Rhode & Schwarz. FSP spectrum analyzer.

. $http://www2.rohde-schwarz.com/en/products/test\_and\_measurement/spectrum\_analysis/FSP.html$ [Status 03.2011].

[21] ETS Lindgren near field probes 7405.

. http://www.ets-lindgren.com/pdf/7405.pdf [Status 03.2011].

[22] Agilent. 8753ES network analyzer.

. $http://cp.literature.agilent.com/litweb/pdf/5968-5160E.pdf$ [Status 03.2011].

[23] Magellan whitepaper about PJM technology.

. http://www.magellan-rfid.com/res/PDF/Brochures%20and%20Documents/White papers/PJM%20Technology.pdf [Status 03.2011].

[24] Skyetek UHF multiplexer MXU.

. $http://www.skyetek.com/Portals/0/Documents/Products/SkyePlus\_MXU\_Data Sheet.pdf$ [Status 03.2011].

[25] Feig OBID i-scan UHF antennas.

. http://www.feig.de/ [Status 03.2011].

[26] Tagsys DocTRAK UHF tag.

. http://www.blackroc-technology.com/app/public/docs/specifications/486.pdf [Status 03.2011].

[27] Agilent. Vector signal generator E4438C ESG.

. $http://cp.literature.agilent.com/litweb/pdf/5988-4039EN.pdf$

[Status 03.2011].

[28] Amplifier Research. AR 10W100C.

. $http://www.arww-rfmicro.com/post/10W1000C.pdf$ [Status 03.2011].

[29] Agilent MXA signal analyzer.

. http://cp.literature.agilent.com/litweb/pdf/5989-4942EN.pdf [Status 03.2011].

[30] ETS Lindgren. ETS Double-Ridged Waveguide Horn 3115.

. $http://www.ets-lindgren.com/pdf/3115.pdf$ [Status 03.2011].

[31] Ansys Ansoft HFSS. 3D Full-wave Electromagnetic Field Simulation:

. $http://www.ansoft.com/products/hf/hfss/$ [Status 03.2011].

[32] Gary A. Thiele Warren L. Stutzman. *Antenna Theory and Design*. John Wiley & Sons, 2nd edition, 1998.

[33] ThingMagic. Mercury5e RFID reader.

. $http://www.thingmagic.com/embedded-rfid-readers/mercury5e/1-embedded-rfid-readers/3-mercury5e$ [Status 03.2011].

[34] National Instruments. NI Labview.

. $www.ni.com$ [Status 03.2011].

[35] Daniel M.Dobkin. *The RF in RFID*. Elsevier LTD, Oxford, First Edition, 2008.

[36] Gaetano Marrocco. *The art of UHF RFID antenna design: impedance matching and size-reduction techniques*. IEEE,Antennas and Propagation Magazine, Vo.50, N.1, Jan.2008.

[37] H.-W. Son and C.-S. Pyo. *Design of RFID tag antennas using an inductively coupled feed*. IEEE-Electronic letters, Vol41/18, Sep.2005.